

國立交通大學
光電工程研究所
碩士論文

利用無色散間隔器
探討雙向光纖傳輸系統

Study of bidirectional transmission system
using novel four-port interleavers

研 究 生：林 擇 雨

指 導 教 授：祁 姓 老師
：陳 智 弘 老師

中 華 民 國 九 十 五 年 七 月

利用無色散間隔器
探討雙向光纖傳輸系統

Study of bidirectional transmission system
using novel four-port interleavers

研 究 生 : 林擇雨

Student : Tse-Yu Lin

指 導 教 授 : 陳智弘 老師

: Assistant Prof. Jyehong Chen

: 祁 姓 老師

Advisor

: Emeritus Prof. Sien Chi

國 立 交 通 大 學

光 電 工 程 研 究 所

碩 士 論 文

A Thesis

Submitted to Institute of Electro-Optical Engineering
College of Electrical Engineering and Computer Science

National Chiao Tung University

In Partial Fulfillment of the Requirements

For the Degree of Master In

Department of Photonics

July 2006

Hsinchu, Taiwan, Republic of China

中 華 民 國 九 十 五 年 七 月

致謝

ACKNOWLEDGEMENT

完成這篇論文，我由衷感謝師長的指導與學長、同學們的鼎力相助。回顧這兩年來攻讀碩士，過程中的飛鴻麟爪、點點滴滴，不僅充實我在學識方面的視野，也習得了待人處事的涵養。在此，我特別感謝一路上提攜我的良師益友：謝謝祁姓老師提供我自由研究的機會，不論是研究所初期在工研院實習或是後來回到光纖通訊實驗室做實驗；感謝陳智弘老師指導我光電研究，陳老師提供一個有效率且和樂融融的研究環境，也鼓勵大家在研究之餘多作運動 - 因為擁有強健的體魄是做研究的基礎；明芳學姐在我做實驗時大力相助，也耐心的聽我分析複雜的模擬系統並與我討論模擬結果；嘉建學長在我對理論感到困惑或是模擬遇到瓶頸時，總是能深入淺出的點出解決之道；一同共事的重佑學長，教導我做實驗的技巧與要點。除此之外，也要謝謝同實驗室伙伴，昱璋學長、炫涵學長、蔡昇祐同學、周森益學長、五樓光纖通訊實驗室的學長同學們及六樓工研院光通訊實驗室的學長們，對我的包容，為大家寧靜的研究生生活帶來些許噪音。還有，謝謝柏元同學，從推甄研究所到碩士班畢業，一直以來的扶持和鼓勵。最後，我要感謝我的爸爸、媽媽，由於他們從小到大的栽培，而且始終對我有信心，得以讓我無後顧之憂的在求學路上奮鬥。總歸來說，因為有這麼多人的相助，點點滴滴的累積，才有今日的我。

擇雨 2006/07/21

利用無色散間隔器 探討雙向光纖傳輸系統

學生：林擇雨

指導教授：祁 姓 教授

陳智弘 教授

國立交通大學光電工程研究所碩士班

摘要

在一個光纖鏈結中執行雙向傳輸為一吸引人的架構。雙向傳輸不僅可減少一半的基礎設施—例如傳輸光纖，光學分光器和光纖放大器—，還可增加頻寬的使用率。然而，要實現雙向放大和阻絕雷利後散射是雙向傳輸系統中所需要克服的困難。因此我們提出了利用間隔器組成一個單向放大路徑的結構用以達成雙向傳輸的效果。

在本論文中，先研究間隔器的相關原理和數學模型的建立，並且附上實際元件量測與間隔器在單向放大路徑的結構之操作。我們架設了兩個雙向傳輸系統(直接雙向傳輸架構與雙向迴路架構)，實驗測試以間隔器為基礎的雙向放大器的可行性。且由這兩個實驗的結果所啟發，我們利用 VPI 這一模擬軟體模擬比較直接雙向傳輸架構與雙向迴路架構。總的說來，由實驗結果和模擬結果展露出一項訊息：若使用雙向迴路架構評估長距離雙向傳輸系統，將會獲得一過於樂觀的系統效能評估。

Study of bidirectional transmission system using novel four-port interleavers

Student : Tse-Yu Lin

Advisor : Dr. Sien Chi

Dr. Jyehong Chen

Institute of Electro-Optical Engineering

National Chiao Tung University

Abstract

Bidirectional transmission over a single fiber link is an appealing architecture. Not only could it reduce the infrastructure -- such as fibers, optical splitters and optical amplifiers -- by a factor two, but it also increases the potential of bandwidth utilization. However, realization of bidirectional amplification and Rayleigh backscattering are the difficulties among bidirectional transmission. Therefore, we proposed a unidirectional amplification scheme which facilitates bidirectional transmission by using an interleaver.

In this thesis, the principle and mathematical model of the interleaver are studied first, where the experimental measurement and operations of an interleaver are included as well. In a bidirectional transmission system, we installed two bidirectional transmission systems (i.e., straight line and re-circulating loop configurations) to demonstrate the feasibility of such interleaver-based bidirectional amplifier. Afterward, inspired by the experimental results, we simulated both the loop and the straight line bidirectional transmission systems. All in all, both experimental and simulation results reveal that it is over-optimistic to estimate long distance bi-directional transmission performance using a re-circulating loop.

CONTENTS

Acknowledgement	i
Chinese Abstract	ii
English Abstract	iii
Contents	iv
List of Figures	vi
List of Tables	x

CHAPTER 1 Introduction

1.1 Bi-directional transmission system.....	1
1.2 Motivation of research.....	2
1.3 Structure of this thesis.....	3

CHAPTER 2 Characteristics of interleaver

2.1 Introduction.....	5
2.2 Digital Concepts for Optical Filters.....	5
2.2.1 Discrete Signals and Z-transform.....	6
2.2.2 Poles and Zeros.....	8
2.2.3 Magnitude Response and Group Delay.....	9
2.3 Interleaver.....	12
2.3.1 Interleaver technology approaches.....	12
2.3.2 Lattice Interleaver.....	12
2.3.3 Mathematical Derivation.....	16
2.3.4 Interleaver Simulation Results & Practical Device Measurement.....	17
2.4 Application of using an Interleaver in bi-directional amplification.....	22

CHAPTER 3 Experiment of bi-directional straight line transmission

3.1 Bidirectional Optical Amplifier Configurations.....	25
3.2 Nonlinear effects.....	27
3.2.1 Stimulated Brillouin scattering.....	27
3.2.2 Rayleigh backscattering.....	29
3.3 Experimental setup & results of bidirectional straight line transmission.....	31

CHAPTER 4 Experiment of bi-directional loop transmission

4.1 Re-circulating loop transmission.....	38
4.1.1 Loop time control.....	39
4.1.2 Dispersion management.....	41
4.2 Experimental Setup & results of bidirectional loop transmission.....	43

CHAPTER 5 Simulation of bidirectional transmission systems

5.1.1 Analysis of bidirectional loop transmission system.....	48
5.1.2 Analysis of bidirectional straight transmission system.....	51
5.2 Simulation setup.....	52
5.2.1 Simulation setup of bidirectional loop system.....	54
5.2.2 Simulation setup of bidirectional straight system.....	56
5.3 Simulation results of bidirectional transmission.....	58
5.3.1 Case I: Bidirectional loop system.....	58
5.3.2 Case II: Bidirectional straight line system.....	61
5.3.3 Comparison of the “Loop” and “Straight Line” cases.....	64
5.4 Simulation of modified straight line transmission.....	66
5.5 Discussion.....	70

CHAPTER 6 Conclusions

REFERENCE	74
------------------------	----

LIST OF FIGURES

- Fig. 2.1 Illustrations of single-stage (a) MA digital filter and (b) AR digital filter.
- Fig. 2.2 Pole-zero diagram showing the unit circle, one pole, and one zero.
- Fig. 2.3 Pole-zero diagram showing a maximum- and a minimum-phase zero.
- Fig. 2.4 Phase response of maximum and minimum phase MA filters.
- Fig. 2.5 Brief configuration of an L-2L interleaver
- Fig. 2.6 The periodic rectangular function
- Fig. 2.8 Transmission responses of the even and odd channels.
- Fig. 2.9 The bandwidth estimations of -0.1dB and -0.5dB for L-2L interleaver.
- Fig. 2.10 Detail configuration of an L-2L interleaver
- Fig. 2.11. Measured amplitude response of the interleaver for even and odd channels
- Fig. 2.12(a). Amplitude response and the corresponding group delay of the interleaver for odd channels (type II)
- Fig. 2.12(b). Amplitude response and the corresponding group delay of the interleaver for even channels (type I)
- Fig. 2.13. Passband of the interleaver for even and odd channel
- Fig. 2.14. Transmission of Interleaver
- Fig. 2.15. Wavelength re-routing scheme for bidirectional transmission
- Fig. 2.16 (a) In-band group delay for two types of interleaver, (b) group delay of cascading Type I and Type II.
- Fig. 3.1 (a) Bidirectional amplification with unidirectional optical amplifier (b) Bidirectional amplifier with optical isolation (c) double optical amplifier with shared pump laser.
- Fig. 3.2. Scheme of crosstalk due to single- and double-amplified RB of signal as well as ASE. P_{ASE} is the power of ASE noise from the EDFA. E_s^d is the downstream signal, and E_s^u is the upstream signal. E_{RB}^d and E_{RB}^u are the Rayleigh backscattered

signals of E_s^d and E_s^u , respectively.

Fig. 3.3. Experimental setup of a bidirectional transmission

Fig. 3.4(a). Received optical spectrum of the east-even traffic after 160-km transmission

Fig. 3.4(b). Received optical spectrum of the west-odd traffic after 160-km transmission

Fig. 3.5. Primary reflection path

Fig. 3.6. BER curves and corresponding Eye diagrams after 210-km transmission @

CH. 6

Fig. 3.7. Power penalty of each channel

Fig. 3.8. Noise figure and net gain of the proposed bidirectional amplifier

Fig. 3.9. Optical spectrum before the receiver

Fig. 3.10. BER curves and corresponding Eye diagrams after 210-km transmission @

CH. 6

Fig. 3.11. Power penalty of each channel for 210km transmission

Fig. 3.12. Net gain and noise figure of each channel for 210km transmission

Fig. 4.1. loop transmission block diagram

Fig. 4.2. (a) load state (b) loop state

Fig. 4.3. pulse signaling for loop time control

Fig. 4.4. Dispersion map (fully compensated @ 1553.2 nm, Max ΔD in CH 1 equals to 95.5 ps/nm)

Fig. 4.5. Experimental setup of bi-directional loop transmission

Fig. 4.6. Received optical spectrum after 500 km bidirectional transmission

Fig. 4.7. Power penalty after 500 km bidirectional loop transmission

Fig. 4.8. BER curves of Channel seven after 0 km, 100 km, 300 km, 500 km traffic

Fig. 4.9(a)~(d). Corresponding eye diagrams of Channel 7 after 0 km, 100 km, 300

km, 500 km

Fig. 4.10. Accumulated Errors after 100 km and 500 km bidirectional transmission at $BER = 2.46 \times 10^{-9}$

Fig. 5.1(a) Uni-directional loop and corresponding round trip analysis (b) loop time control

Figure 5.2. (a) Configuration of original bidirectional loop (b) Loop time control of original bidirectional loop

Fig. 5.3(a) adjusted bidirectional loop configuration (b) loop time control

Fig. 5.4 Bidirectional Loop System

Fig. 5.5 Bidirectional Straight Line System

Fig. 5.6 Dispersion map used in simulation

Fig. 5.7 Decomposed bidirectional loop system

Fig. 5.8 Decomposed bidirectional straight line system

Fig. 5.9 Simulated bidirectional straight line system

Fig. 5.10. Received optical spectrum after 800 km bidirectional loop transmission

Fig. 5.11 BER curves @ ch.10 after 0, 200, 400, 600 and 800-km bidirectional loop transmission

Fig. 5.12. Power penalty distribution of bidirectional loop transmission

Fig. 5.13 (a)~(f) Correspond eye diagrams after 0 km, 100 km, 200 km, 400 km, 600 km and 800 km bidirectional loop transmission

Fig. 5.14. Received optical spectrum after 800 km bidirectional transmission (straight line)

Fig. 5.15 BER curves @ ch.10 after 0, 200, 400, 600 and 800-km bidirectional transmission (straight line)

Fig. 5.16 Power penalty distribution of bidirectional transmission (straight line)

Fig. 5.17. (a)~(f) Correspond eye diagrams after 0 km, 100 km, 200 km, 400 km,

600 km and 800 km bidirectional transmission (straight line)

Fig. 5.18 BER curves and corresponding eye diagrams @ ch.10 for “Loop” and “Straight Line” cases after 0 km and 800 km bidirectional transmission.

Fig. 5.19. Penalty distribution for “Loop” and “Straight Line” cases.

Fig. 5.20 Modified Bidirectional Straight Line System

Fig. 5.21. Received optical spectrum after 800 km bidirectional transmission (modified straight line)

Fig. 5.22 BER curves @ ch.10 after 0, 200, 400, 600 and 800-km bidirectional transmission (modified straight line)

Fig. 5.23 Power penalty distribution of bidirectional transmission (modified straight line)

Fig. 5.24. (a)~(f) Correspond eye diagrams after 0 km, 100 km, 200 km, 400 km, 600 km and 800 km bidirectional transmission (modified straight line)

Fig. 5.25 BER curves and corresponding eyes @ ch.10 for case “Loop”, “Straight Line” and “Modified Straight Line”

Fig. 5.26 Penalty distribution for case “Loop”, “Straight Line” and “Modified Straight Line”

LIST OF TABLES

Table 1. Parameters of dispersion map for bidirectional loop experiment

Table 2. Power penalty of bidirectional transmission experiments

Table 3. Parameters used in bidirectional loop architecture.

Table 4. Parameters used in bidirectional straight line architecture.

Table 5. Simulation and experimental results

Chapter 1

Introduction

1.1 Bi-directional transmission system

In future communication network, besides dense wavelength-division- multiplexing (DWDM) scheme, bidirectional transmission over a single fiber link is also an appealing architecture. The main motivation for considering bidirectional transmission over a single optical fiber instead of “two-times unidirectional” is the reduction of the infrastructure (fibers, optical splitters and optical amplifiers) by a factor two and the potential of bandwidth utilization. As economical aspect, bidirectional wavelength-division-multiplexing (WDM) transmission system is an attractive scheme. Not only could it avoid building another new construction of fiber link, but also reduce the number of passive and active components, such as splitters and EDFAs, concurrently. Moreover, transmitting bi-directionally over a single fiber link can increase the capacity of twice as an installed unidirectional link. [1].

Rayleigh backscattering is one of the fundamental mechanisms in optical fiber that may cause crosstalk by the reverse channel [2]. It can be considered as an unavoidable background reflection level. In bidirectional networks employing optical amplifiers, signals are bi-directionally transmitted over a single fiber path. If optical isolators are not used to prevent multiple reflections, Rayleigh backscattering (or many small reflections) can significantly degrade the receiver sensitivity. Therefore, system performances are severely deteriorated on account of multiple reflections. It has been observed that due to multiple reflections along a fiber path, the laser phase noise is converted to intensity noise, which may cause performance degradation in high speed lightwave system. Even if discrete reflections are carefully suppressed by using non-reflective connector facets, the multi Rayleigh backscattering (RB) in fibers give rise to the phase-to-intensity noise conversion. Moreover, the interferometric noise from multiple RB increases proportionally with the optical amplifier gain. Thus, the

maximum gain of inline optical amplifiers without optical isolator is limited to 19 dB [3] because the additive intensity noise induced by RB.

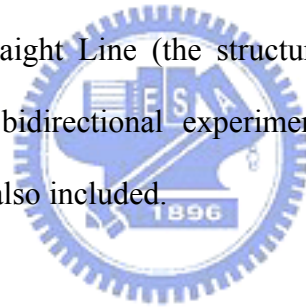
Brillouin scattering is another fundamental mechanism in optical fiber that may cause bidirectional crosstalk. It results in two new backward-propagating waves at 11 GHz optical frequency difference (at 1550 nm) above and below the input signal. Brillouin scattering is a non-linear effect. The lower frequency wave may grow exponentially with input power, for powers above a few mW. However, Brillouin scattering could be alleviated by choosing proper optical frequency and controlling maximum transmitted power in fiber.

In recent years, there has been an ongoing effort to develop bidirectional transmission system architecture with various bidirectional amplification methods. Interleaved bidirectional transmission is one of the popular manners that it offers effective means for four-wave mixing (FWM) suppression; however, they generate the coherent (in-band) crosstalk and incoherent (out-of-band) crosstalk at an amplification node. In addition, bidirectional amplification nodes are susceptible to the occurrence of self-oscillation [4]. Distributed Rayleigh mirrors are forming an optical cavity with the enclosed amplifier gain and providing the necessary conditions for a node lasing. To overcome these problems, some efforts are required to suppress the effect of RB, such as the implementation of RB-suppressed erbium-doped fiber amplifiers (EDFAs) for bidirectional transmissions. To date, the best record of bidirectional transmission is 16×10 Gb/s full-duplex capacity over 5000 km in a fully bidirectional recirculating loop [5].

1.2 Motivation of research

In this thesis, we propose a novel structure for bidirectional transmission system which utilizes only one four-port interleaver and one dual-stage EDFA. The channel spacing of this interleaver is 50 GHz for multiplexing/de-multiplexing odd and even channels in a WDM system. This function of this four-port interleaver could lead bidirectional signals passing

through the dual-stage EDFA in uni-direction amplification so as to reduce the need of additional EDFA for bidirectional operation. Better still, the RB could be eliminated significantly. Finally, this structure is applied to bidirectional transmission system. First, we demonstrate the 210 km bidirectional transmission using a novel four-port interleaver; afterward, we continue studying the feasibility of bidirectional transmission applying in long distance system using a recirculating loop. Both works experimentally manifest the applicability of such innovative structure in bidirectional transmission. Furthermore, a perspective is revealed in the results of the bidirectional experiments that bidirectional loop system is unequal to actual bidirectional system (straight line bidirectional system). To verify this concept, we ought to construct a real bidirectional system, especially the long distance architecture; however, it's an uneconomic approach. Therefore, simulation software, VPI, is utilized to simulate the “Loop” and “Straight Line (the structure employed in actual circumstance)” architectures. After the two bidirectional experiments and simulations, discussions and comparisons of the results are also included.



1.3 Structure of this thesis

The main purpose of this thesis is to experiment the bidirectional transmission systems and to discuss the feasibility of bidirectional transmission in real application. This thesis comprises six chapters. Chapter 1 is an introduction of bidirectional DWDM systems. In chapter 2, the theory and characteristics of a four-port interleaver will be described, as well as the experimental measurement and its application in bidirectional amplification. Experiments of 160-km and 210-km bidirectional transmissions using novel four-port interleavers will be presented in chapter 3. Furthermore, in chapter 4, a bidirectional loop transmission with novel four-port interleaver utilization in a recirculating loop scheme will be proposed and experimentally demonstrated. In chapter 5, a concept is proposed that a bidirectional loop configuration may be inadequate to represent a bidirectional transmission thoroughly.

Therefore, the simulations, which based on the bidirectional transmission and bidirectional loop system, for comparing the performances of the two systems will be included. Finally, in chapter 6, a brief conclusion and discussion for experimental and simulation results will be given.



Chapter 2

Characteristics of Interleaver

2.1 Introduction

An interleaver is a periodic optical filter that combines or separates a comb of dense wavelength-division multiplexed (DWDM) signals. The periodic nature of the interleaver filter reduces the number of Fourier components required for a flat passband and high-isolation rejection band. As a functional block, interleavers come in many varieties. The original design separates (or combines) even channels from odd channels across a DWDM comb. The filter function of an interleaver and its period are separable. Interleavers have been demonstrated that resolve a comb of DWDM frequencies on 100, 50, 25, and 12.5 GHz centers. The period is governed by the free-spectral range of the core elements, where narrower channel spacing is achieved by a longer optical path. [6]

There are three categories of interleaver filter technologies: lattice filter (LF), Gires-Tournois (GT) based Michelson interferometer, and arrayed-waveguide router (AWG). This chapter will focus on the detail of the theory and design process of the LF interleavers which we used in our experiments. Moreover, the measurement of the interleaver will be shown to compare with the simulation results. [7]

2.2 Digital Concepts for Optical Filters

Digital filter, or discrete time filter [8], has been widely used in digital electronic circuit. The advantages of relating digital and optical filters are that numerous algorithms developed for digital filters can be used to design optical filters. Borrowed from the electronic world, optical engineer follows the same concept and uses optical delay line to create the desired filter function. Depending on whether the transfer function has poles, an optical filter can be classified as a finite impulse response filter and an infinite impulse response filter. Before

describing the design process of the interleaver filter, the basic knowledge about the representations of digital signals, the Z-transform, the zeros, and the poles were needed to be introduced in followed sub-sections.

2.2.1 Discrete Signals and Z-transform

A similar set of properties applied for discrete signals. A discrete signal can be obtained by sampling a continuous time signal $x(t)$ at $t = nT$ where the sampling interval is, T and n is the sample number. For a digital filter, T is the unit delay associated with the discrete impulse response. The impulse response of an optical filter, where each stage has a delay that is an integer multiple of the unit delay, is described by a discrete sequence [2.4]. The Fourier transform of a sequence has a sum instead of an integral as follows:

$$X(f) = \sum_{n=-\infty}^{\infty} x(nT)e^{-j2\pi fnT} \quad (1)$$

where f denote the absolute frequency. A normalized frequency is defined as $\nu \equiv fT = f / FSR$, where the free spectral range (FSR) is the period of the absolute frequency response. The normalized angular frequency is given by $\omega = 2\pi\nu$. A discrete signal is often represented by $x(n)$, leaving T implied. The discrete-time Fourier transform (DTFT) is defined as

$$X(\nu) = \sum_{n=-\infty}^{\infty} x(n)e^{-j2\pi\nu n} \quad (2)$$

The Z-transform is an analytic extension of the DTFT for discrete signals, similar to the relationship between the Laplace transform and the Fourier transform for continuous signals. The Z-transform is defined for a discrete signal [9] by substituting z for $e^{j\omega}$ in Eq. (2) as follows:

$$H(z) = \sum_{n=-\infty}^{\infty} h(n)z^{-n} \quad (3)$$

where $h(n)$ is the impulse response of a filter or the values of a discrete signal, and z is a complex number that may have any magnitude. For the power series to be meaningful, a region of convergence must be specified, for example $r_{\min} \leq |z| \leq r_{\max}$ where r_{\min} and r_{\max} are radii. Of particular interest is $|z|=1$, called the unit circle, because the filter's frequency response is found by evaluating $H(z)$ along $z = e^{j\omega}$. The inverse Z-transform is found by applying the Cauchy integral theorem to Eq. (3) to obtain:

$$h(n) = \frac{1}{2\pi j} \oint H(z) z^{n-1} dz \quad (4)$$

The convolution resulting from filtering in the time domain

$$y(n) = x(n) * h(n) = \sum_{m=-\infty}^{\infty} x(m)h(n-m) \quad (5)$$

reduces to multiplication in the Z-domain.

$$Y(z) = H(z)X(z) \quad (6)$$

Equation (6) shows that a filter's transfer function, $H(z)$, can be obtained by dividing the output by the input in the Z-domain.

$$H(z) = \frac{Y(z)}{X(z)} \quad (7)$$

A fundamental property of the Z-transform relates $h(n-1)$ to $H(z)$ as shown in Eq. (8)

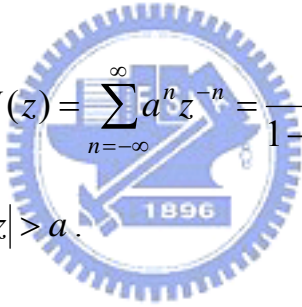
$$\sum_{n=-\infty}^{\infty} h(n-1)z^{-n} = z^{-1} \sum_{n=-\infty}^{\infty} h(n)z^{-n} = z^{-1}H(z) \quad (8)$$

The impulse response is assumed to be causal so that $h(n)=0$ for $n < 0$. One delay results in multiplication by z^{-1} in the Z-domain, and a delay of N units results in multiplication by z^{-N} .

The Z-transforms are introduced for two examples here. First, let the output of a filter be

the sum of the last $N + 1$ inputs: $y(n) = x(n) + x(n-1) + \dots + x(n-N)$. Such a filter contains N delays, which are feed-forward paths. The impulse response is $h(n) = \delta(n) + \delta(n-1) + \dots + \delta(n-N)$.

The transfer function is $H(z) = 1 + z^{-1} + \dots + z^{-N} = (1 - z^{-(N+1)}) / (1 - z^{-1})$. There are N roots of $H(z)$ which all occur on the unit circle. For second example, let the output of a filter be given as $y(n) = ay(n-1) + x(n)$, where a is a real number satisfying $0 \leq |a| < 1$ and $n \geq 0$. This filter contains one delay, which is a feedback path. Its Z-transform is $Y(z) = az^{-1}Y(z) + X(z)$, which gives the transfer function $H(z) = Y(z) / X(z) = 1 / (1 - az^{-1})$. The transfer function is equivalent to the infinite sum



$$H(z) = \sum_{n=-\infty}^{\infty} a^n z^{-n} = \frac{1}{1 - az^{-1}} \quad (9)$$

The region of convergence is $|z| > a$.

2.2.2 Poles and Zeros

A discrete linear system with a discrete input signal in Eq. (10) as follows:

$$y(n) = b_0 x(n) + b_1 x(n-1) + \dots + b_M x(n-M) - a_1 y(n-1) - \dots - a_N y(n-N) \quad (10)$$

The weights are given by the a and b coefficients. The Z-transform results in a transfer function that is a ratio of polynomials.

$$H(z) = \frac{\sum_{m=0}^M b_m z^{-m}}{1 + \sum_{n=1}^N a_n z^{-n}} = \frac{B(z)}{A(z)} \quad (11)$$

$A(z)$ and $B(z)$ are M th and N th-order polynomials, respectively. The expression for $H(z)$ can also be written in terms of the roots of the polynomials as follows [10]:

$$H(z) = \frac{\Gamma z^{N-M} \prod_{m=1}^M (z - z_m)}{\prod_{n=1}^N (z - p_n)} \quad (12)$$

The zeros of the numerator are represented by z_m . A zero that occurs on the unit circle, $|z_m|=1$, results in zero transmission at that frequency. The roots of the denominator polynomial are designed by p_n . The Γ has a maximum value determined by $\max\{|H(z)|_{z=e^{j\omega}}\} = 1$.

Digital filters are classified by the polynomials defined in Eq. (11). A moving average (MA) filter has only zeros and also belongs to a finite impulse response. It consists only of feed-forward paths. A single stage MA digital filter is shown in Figure 2.1(a). An autoregressive (AR) filter has only poles and contains one or more feedback paths as shown in Fig. 2.1(b). A pole produces an impulse response with an infinite number of terms in contrast to the finite number of terms for MA filters.

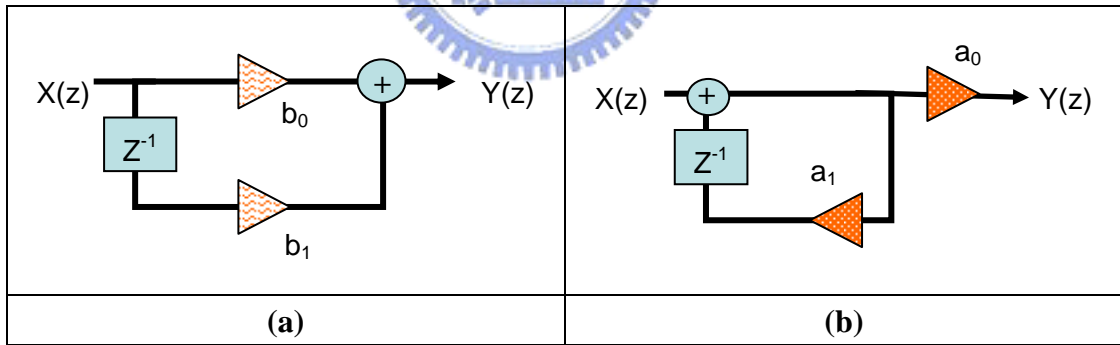


Fig. 2.1 Illustrations of single-stage (a) MA digital filter and (b) AR digital filter.

2.2.3 Magnitude Response and Group Delay

A filter's magnitude response is equal to the modulus of its transfer function, $|H(z)|$, evaluated at $z = e^{j\omega}$. Based on the pole/zero representation of $H(z)$, only the distance of each pole and zero from the unit circle affects the magnitude response, i.e. $|e^{j\omega} - z_m|$ or

$|e^{j\omega} - p_n|$. One trip around the unit circle is equal to one FSR. A convenient graphical method for estimating a filter's response is shown in Fig. 2.2. Zeros with a magnitude >1 are called maximum-phase, and those with magnitude <1 are called minimum-phase. A pole-zero diagram with a pair of zeros that are located reciprocally about the unit circle is shown in Fig. 2.3.

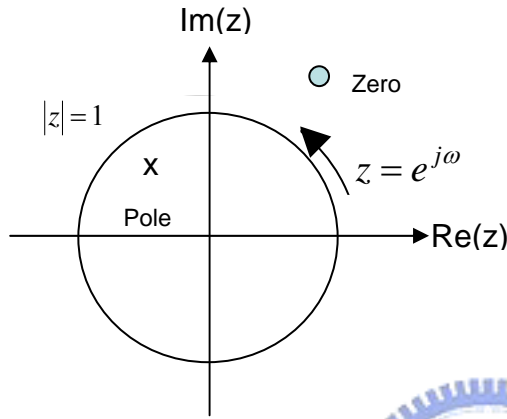


Fig. 2.2 Pole-zero diagram showing the unit circle, one pole, and one zero.

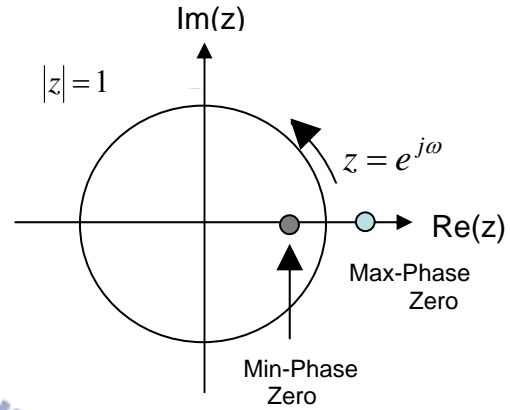


Fig. 2.3 Pole-zero diagram showing a maximum- and a minimum-phase zero.

The group delay of the filter is defined as the negative derivative of the phase of the transfer function with respect to the angular frequency as follows:

$$\tau_g = T \times \tau_n = T \times \left[-\frac{d}{d\omega} \tan^{-1} \left(\frac{\text{Im}\{H(z)\}}{\text{Re}\{H(z)\}} \right) \right]_{z=e^{j\omega}} \quad (13)$$

where τ_n is normalized to the unit delay, T. The absolute group delay is given by

$\tau_g = T \times \tau_n$. To obtain the group delay for a single zero, considering the transfer function

$H_{1-zero}(z) = 1 - re^{j\phi}z^{-1}$ where r and ϕ are the magnitude and phase of the zero. By

substituting $z = e^{j\omega}$ in $H_{1-zero}(z)$, the phase is derived in terms of r , ϕ , and ω as

follows:

$$\Phi_{1-zero} = \tan^{-1} \left[\frac{r \sin(\omega - \phi)}{1 - r \cos(\omega - \phi)} \right] \quad (14)$$

$$\frac{d \tan^{-1}[g(x)]}{dx} = \frac{g'(x)}{1 + g^2(x)} \quad (15)$$

where Φ_{1-zero} is the phase of $H_{1-zero}(z)$. From Eq. (15), the group delay simplifies to

$$\tau_{1-zero}(r, \phi) = \frac{r[r - \cos(\omega - \phi)]}{1 - 2r \cos(\omega - \phi) + r^2} \quad (16)$$

Afterwards, consider the transfer function, $H_{1-zero}(z) = re^{-j\phi} - z^{-1}$, with the reversed path, the group delay is

$$\tau_{1-zero}\left(\frac{1}{r}, \phi\right) = \frac{[1 - r \cos(\omega - \phi)]}{1 - 2r \cos(\omega - \phi) + r^2} = 1 - \tau_{1-zero}(r, \phi) \quad (17)$$

The sum of the group delays is a constant value indicating that the filter has linear phase with the same magnitude response as shown in Fig. 2.4.

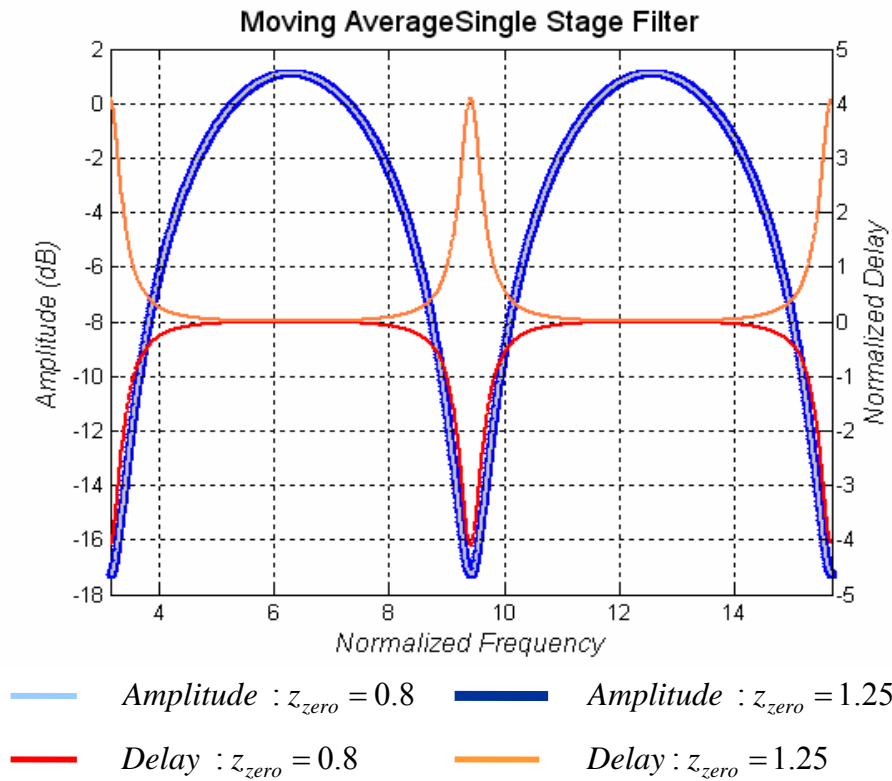



Fig. 2.4 Phase response of maximum and minimum phase MA filters.

2.3 Interleaver

2.3.1 Interleaver technology approaches

There are three broad classes of interleaver filter technologies: lattice filter (LF), Gires-Tournois based Michelson interferometer, and arrayed-waveguide router (AWG). Within the lattice filter class there is the birefringent filter, employing birefringent crystals and classically known as a Lyot or Solc filter; the glass-based filter which substitutes an artificial polarization-dependent delay for the birefringent elements of the preceding type; and the Mach-Zehnder filter, which is the analog to the Lyot filter and is generally made with planar waveguides. Within the Gires-Tournois (GT) class there is the interference filter and the birefringent analog (B-GT). Arrayed-waveguide routers have designs for single-channel and banded filters.

2.3.2 Lattice Interleaver



Lattice filters are made from a cascade of differential-delay elements where the differential-delay of each element is an integral multiple of a unit delay and power is exchanged across paths between the elements. There are three issues to address in the study of lattice filters: the realization of the unit cell that generates the differential delay; the number of unit cells and associated intermediate power exchange; and the cascade of multiple filters.

Figure 2.5 shows the configuration of the interleaver consisting of the birefringent crystals. The basic principle is based on interference between polarized light, which depends on phase retardation between the components of light polarized parallel to the slow and the fast axes of the crystal. Consequently, birefringent crystal is used to perform as optical delay, and half-wave plates are used to change the polarization direction between the delay components. An optical FIR digital filter can, thus, be made by cascading delay lines and controlling the angle of rotation between half-wave plates. The half-wave plates can also be considered to be rotated to generate require Fourier frequency components.

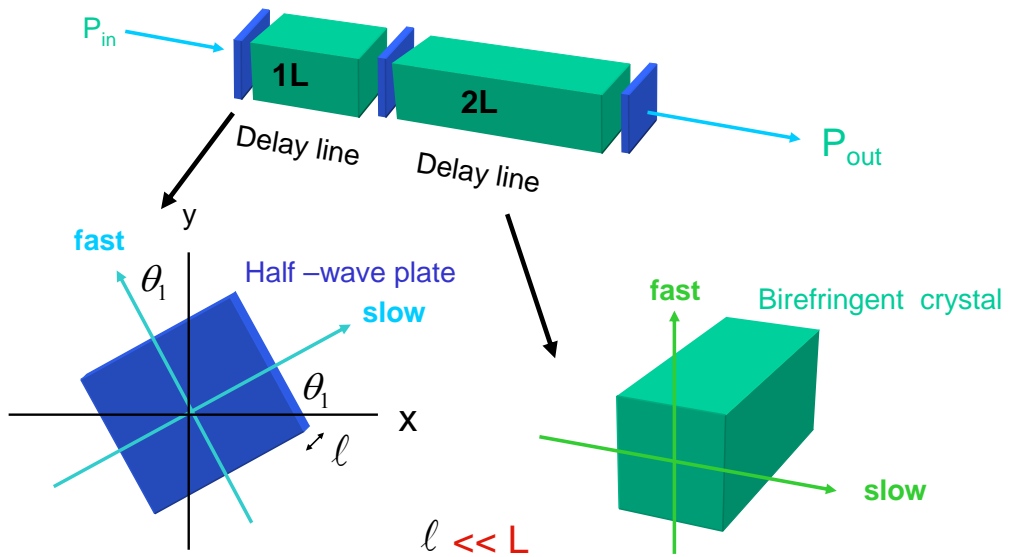


Fig. 2.5 Brief configuration of an L-2L interleaver

Actually, the design goal is to generate a periodic rectangular function as displayed in Fig. 2.6.

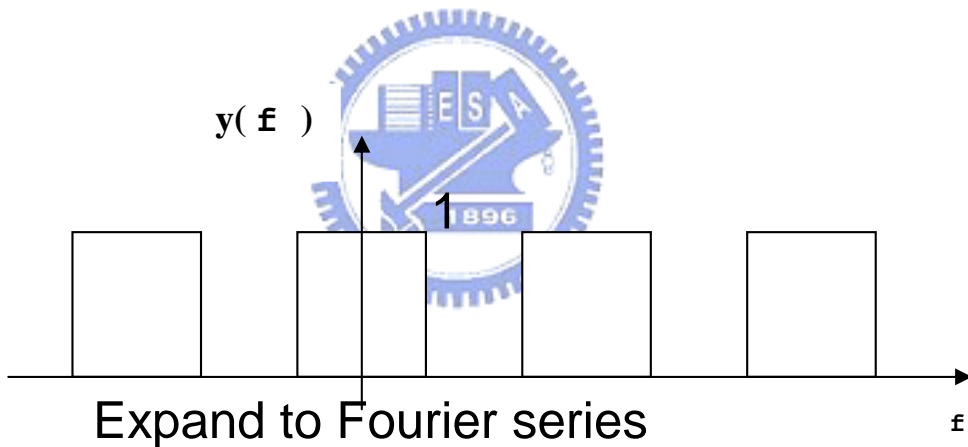


Fig. 2.6 The periodic rectangular function

The function could be defined as

$$y(f) = \begin{cases} 0 & , -50 < f < -25 \\ 1 & , -25 < f < 25 \\ 0 & , 25 < f < 50 \end{cases} \quad , \quad y(f) = y(f + 100) \quad (21)$$

Expand it to Fourier series; there is no even function term. The constant a_0 and a_n is retained.

$$\begin{aligned}
a_0 &= \frac{1}{200} \int_{-50}^{50} 1 \cdot df = \frac{1}{2} \\
a_n &= \frac{1}{100} \int_{-50}^{50} 1 \cdot \cos(n2\pi f) \cdot df = \frac{2}{n\pi} \sin\left(\frac{n\pi}{2}\right), n = 1, 2, 3 \dots
\end{aligned} \tag{22}$$

Therefore, the final rectangular function could be written as Eq. (23)

$$y(f) = \frac{1}{2} + a_1 \cdot \cos(2\pi f) - a_3 \cdot \cos(3 \times 2\pi f) + \dots \tag{23}$$

Here we know that the square-wave amplitude function has only odd Fourier frequency components with appropriate Fourier coefficients.

According to the Jones matrix theory [12], a half-wave plate has a phase retardation of $\Gamma = \pi$, and the thickness of $\ell = \lambda/2(n_e - n_o)$. The Jones matrix for the half-wave plate is obtained by using Eq. 24.

$$W_{hp} = \begin{bmatrix} 0 & -i \\ -i & 0 \end{bmatrix} \tag{24}$$

We can write the Jones matrix for the delay line as

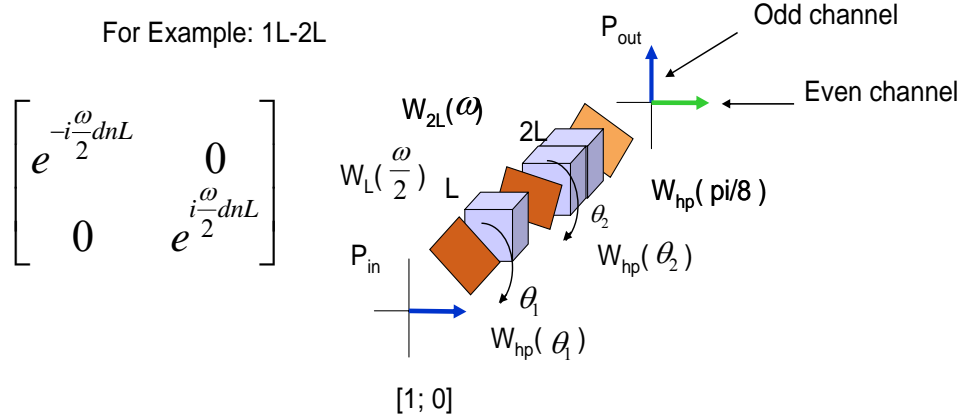
$$W_{delay} = \begin{bmatrix} e^{-i\frac{\omega}{2}dnL} & 0 \\ 0 & e^{i\frac{\omega}{2}dnL} \end{bmatrix} \tag{25}$$

where L is the length of the delay-line crystal and dn is the difference between the n_e and n_o (the indices of the ordinary and extraordinary axes).

In the figure below, the Jones matrix for the incident beam can be written as $[1;0]$ to specify the input light is linearly polarized on the x axis. By adjusting the angles of the half-wave plates appropriately, we can get the odd channels and even channels lying the x and y axes, respectively, at the output port.

Change the angle of the two half-wave plates to fit the Fourier series

For Example: 1L-2L



$$P_{out} = W_{hp}(22.5^\circ) \cdot W_{2L}(\omega) \cdot W_{hp}(\theta_2) \cdot W_L(\omega/2) \cdot W_{hp}(\theta_1) \cdot P_{in}$$

By combining all Jones matrices of the birefringent crystals, we can write the transmission as

$$E_{out} = W_{hp}(22.5^\circ) \cdot W_{delay}(2L) \cdot W_{hp}(\theta_2) \cdot W_{delay}(L) \cdot W_{hp}(\theta_1) \cdot E_{in} \quad (26)$$

where $W_{delay}(2L)$ and $W_L(L)$ are the Jones matrices of the two crystals

Nevertheless, how to get the angles to fit the Fourier coefficients in Eq. (22) is the critical point. Utilizing the optimization tools in Matlab programs is the solution. The goal is to minimize the error function by sweeping the half-wave plate angles as

$$\begin{aligned} error &= \max |y(w) - x(w)| \\ error &= \int_{w_1}^{w_2} |y(w) - x(w)| dw \\ error &= \int_{w_1}^{w_2} |y(w) - x(w)|^2 dw \quad w_1 = w_c - \frac{FSR}{2}, w_2 = w_c + \frac{FSR}{2} \quad (27) \\ error &= \int_{w_1}^{w_2} \left| \log_{10}^{y(w)^2} - x(w) \right|^2 dw \end{aligned}$$

where $x(w)$ is the target or ideal square periodic function and the $y(w)$ is real transmission function. The transmission function is periodic, so the errors are only summed over one FSR at the central frequency, w_c [13]. The last three approximation criteria include errors at all points of frequency in the interval; therefore, they include more error data

than the first for each $y(w)$ considered. We choose the last approximation criterion because it is the energy in the error signal. [14]

2.3.3 Mathematical Derivation

Here we use the easiest case: one stage interleaver includes a delay line and two half-wave plates in which the second plate is determined to 22.5 degree. Assume that there

is an incident beam $V_x (= \begin{bmatrix} 1 \\ 0 \end{bmatrix})$ injected to the first half-wave plate, then the Jones matrix

M_1 at the output can be written as

$$\begin{aligned}
 M_1 &= \begin{bmatrix} \cos \theta_1 & -\sin \theta_1 \\ \sin \theta_1 & \cos \theta_1 \end{bmatrix} \cdot \begin{bmatrix} e^{-j\frac{\pi}{2}} & 0 \\ 0 & e^{j\frac{\pi}{2}} \end{bmatrix} \cdot \begin{bmatrix} \cos \theta_1 & \sin \theta_1 \\ -\sin \theta_1 & \cos \theta_1 \end{bmatrix} \cdot \begin{bmatrix} 1 \\ 0 \end{bmatrix} \\
 &= \begin{bmatrix} e^{-j\frac{\pi}{2}} \cos^2 \theta_1 + e^{j\frac{\pi}{2}} \sin^2 \theta_1 & \\ e^{-j\frac{\pi}{2}} \cos \theta_1 \sin \theta_1 - e^{j\frac{\pi}{2}} \cos \theta_1 \sin \theta_1 & \end{bmatrix} = j \cdot \begin{bmatrix} a_1(\theta_1) \\ a_2(\theta_2) \end{bmatrix} \quad (28) \\
 &\dots\dots(a_1 \text{ and } a_2 \text{ are real numbers})
 \end{aligned}$$

where the undetermined angle is set to be a variable θ_1 . Regard M_1 as the emerging beam and let it inject into the crystal of length L. The new Jones matrix M_2 is obtained by using Eq. (29).

$$M_2 = e^{-j\phi} \cdot \begin{bmatrix} e^{-j\frac{\pi f}{df_c}} & 0 \\ 0 & e^{j\frac{\pi f}{df_c}} \end{bmatrix} \cdot j \cdot \begin{bmatrix} a_1 \\ a_2 \end{bmatrix} = j \cdot \begin{bmatrix} a_1 e^{-j\frac{\pi f}{df_c}} \\ a_2 e^{j\frac{\pi f}{df_c}} \end{bmatrix} \quad (29)$$

In Eq. (29), df_c is the channel spacing and ϕ is equal to $dn\omega L/2c$. The phase factor $e^{-j\phi}$ can be neglected if interference effects are not important, or not observable. Then use

M_2 to multiply the second half-wave plate ($W_{22.5^\circ} = j \begin{bmatrix} X & Y \\ Y & -X \end{bmatrix}$, X and Y are real numbers) with the angle of 22.5 degree as shown in Eq. (30).

$$\begin{aligned}
M_3 &= W_{22.5^\circ} \cdot M_2 = j \begin{bmatrix} X & Y \\ Y & -X \end{bmatrix} \cdot j \begin{bmatrix} a_1 e^{-j\frac{\pi f}{df_c}} \\ a_2 e^{j\frac{\pi f}{df_c}} \end{bmatrix} \\
&= - \begin{bmatrix} a_1 X e^{-j\frac{\pi f}{df_c}} + a_2 Y e^{j\frac{\pi f}{df_c}} \\ a_1 X e^{-j\frac{\pi f}{df_c}} - a_2 Y e^{j\frac{\pi f}{df_c}} \end{bmatrix} = \begin{bmatrix} E_x \\ E_y \end{bmatrix}
\end{aligned} \tag{30}$$

In Eq. (30), we arbitrarily choose E_x or E_y and square it to obtain the Eq. (31).

$$\begin{aligned}
T_x &= E_x \cdot E_x^* = (a_1 X + a_2 Y)^2 \cos^2 \frac{\pi f}{df_c} + (a_1 X - a_2 Y)^2 \sin^2 \frac{\pi f}{df_c} \\
&= [a_1(\theta_1)X]^2 + \left\{ [a_2(\theta_2)Y]^2 + 2a_1(\theta_1)Xa_2(\theta_1)Y \right\} \cos \frac{2\pi f}{df_c}
\end{aligned} \tag{31}$$

Compare with Eq. (23), the first term needs to equal 1/2 and the coefficient of the second term needs to equal the Fourier coefficient by optimizing the angle of θ_1 . By this way, we can easy to understand the theory of interleaver.

2.3.4 Interleaver Simulation Results & Practical Device Measurement

The lengths of delay-line crystals in the program are determined using Eq. (32).

$$\begin{aligned}
f_c &= m \frac{c}{dnL} \Rightarrow L = \frac{f_c dn}{mc} \\
df_c &= \text{Channel spacing} = \text{FSR}
\end{aligned} \tag{32}$$

In Eq. (32), c is the speed of light; f_c is the central frequency in the range of operation frequencies; m is the order of the birefringent wave plate.

L-2L Interleaver

The found angles for two half-wave plates are 7.7356 and 29.5286 degrees. Figure 2.7 shows the transmission responses of the even and odd channels; the isolation is about 18 dB.

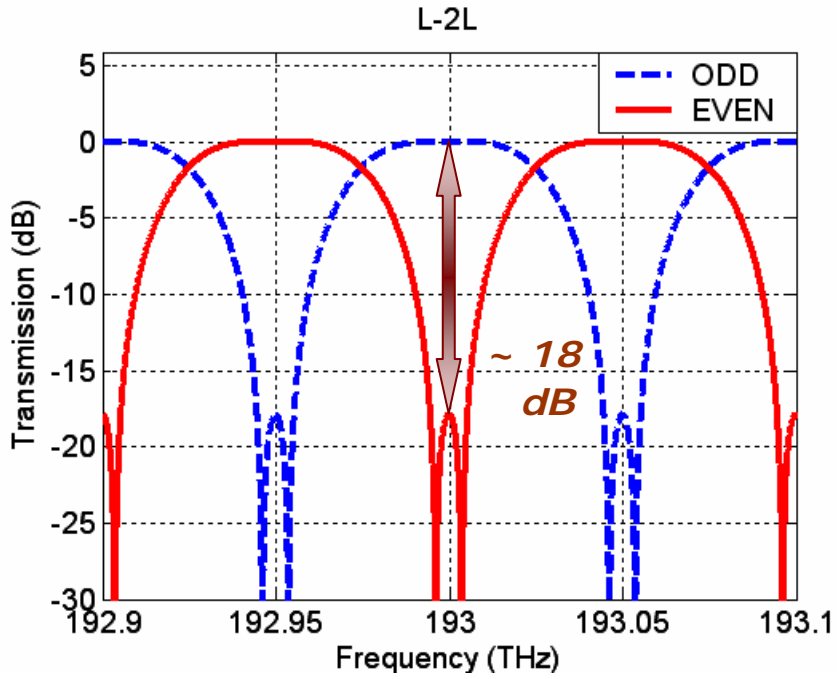


Fig. 2.7 Transmission responses of the even and odd channels.

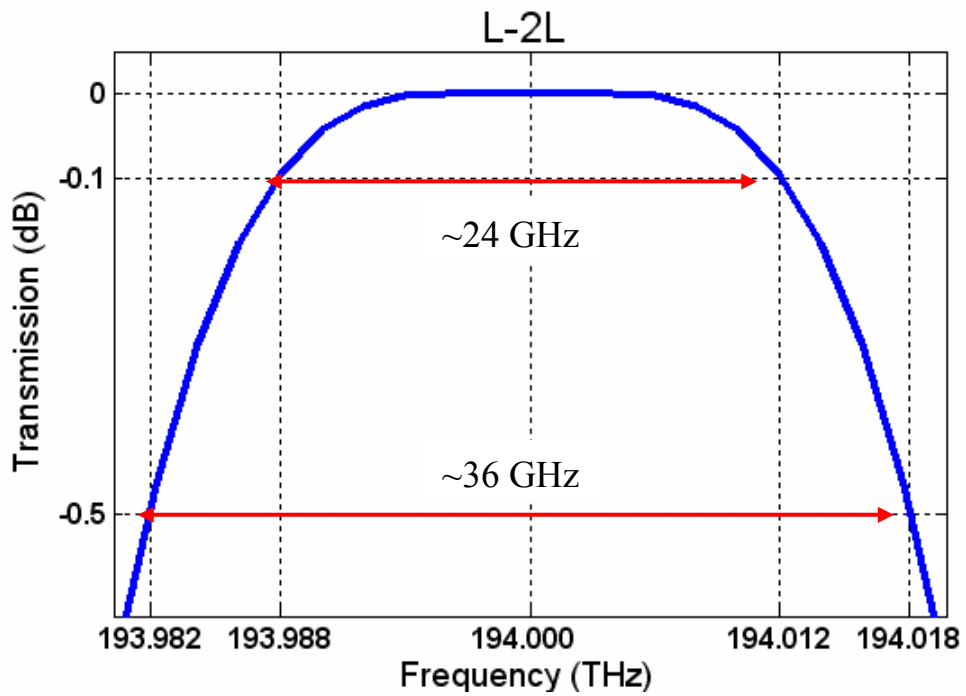


Fig. 2.8 The bandwidth estimations of -0.1dB and -0.5dB for L-2L interleaver.

The ripple is about 0.0026 dB; the bandwidths of -0.1dB and -0.5dB are 24 GHz and 36 GHz, respectively, as shown in Fig. 2.8.

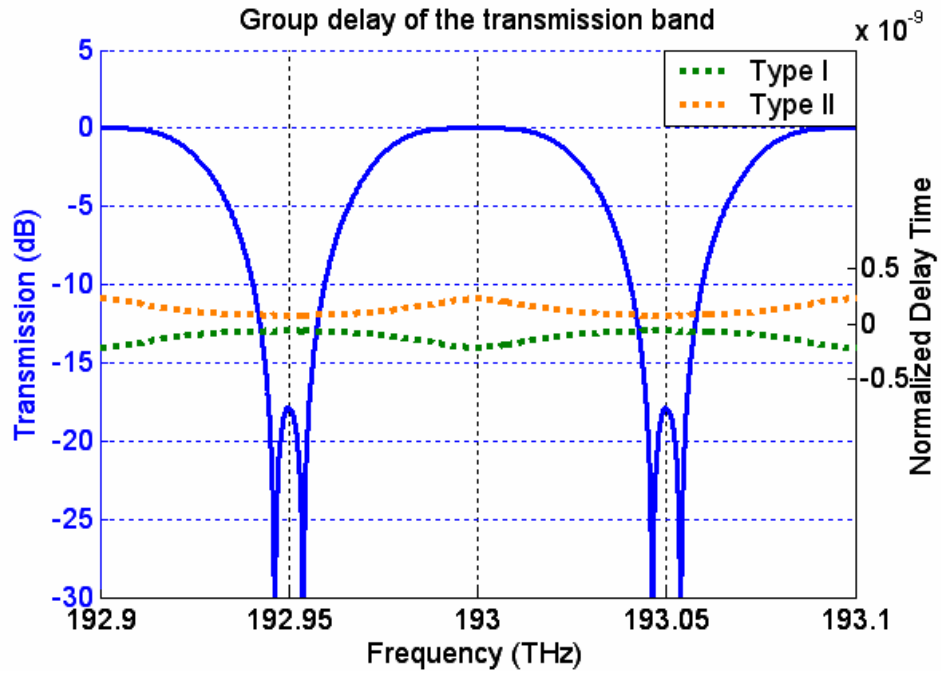


Fig. 2.9 Dispersion compensating interleavers for add/drop node

In Fig. 2.9, the path with the negative group delay is called Type-I here, and another path with the positive group delay is called Type-II. The Type-I and Type-II have the same transmission response.

The corresponding parameters for simulation are given below:

Central wavelength = 193.00 THz;

Difference of index between n_0 and $n_e=0.2138$;

$C = 2.997925 \times 10^8$ m/s;

Channel spacing = 100 GHz;

The interleaver we used is a symmetrical four-port interleaver with two input and two output ports. The detail configuration is shown in Fig. 2.10. It incorporates the birefringent crystal cells; half wave plates (HWP), YVO4 walk off crystals (YWC) and polarization beam splitters (PBS).

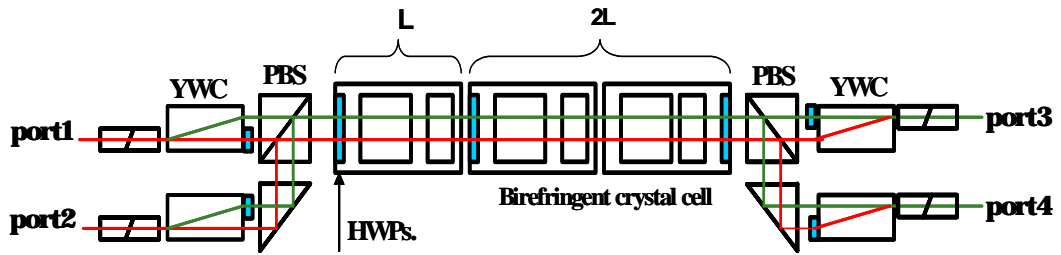


Fig. 2.10 Detail configuration of an L-2L interleaver

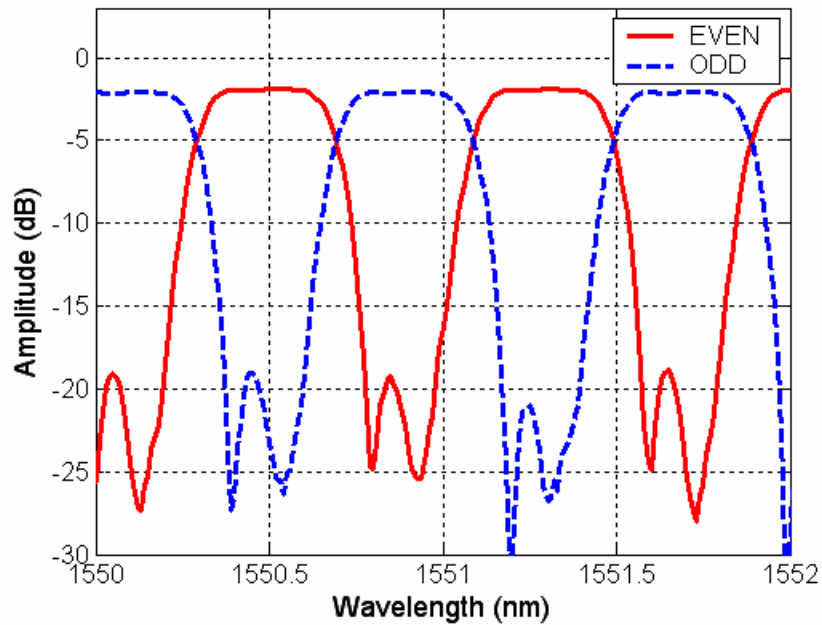


Fig. 2.11. Measured amplitude response of the interleaver for even and odd channels

Figure 2.11 illustrates the measured amplitude response of the interleaver for even and odd channels. The channel spacing of this interleaver is 50-GHz with insertion loss of 2.2-dB and 0.5-dB pass bandwidth of around 36-GHz, respectively. The two mirrored corresponding group delay curves are measure by the channel analyzer (Q7760), shown in figure 2.12(a) and figure 2.12(b).

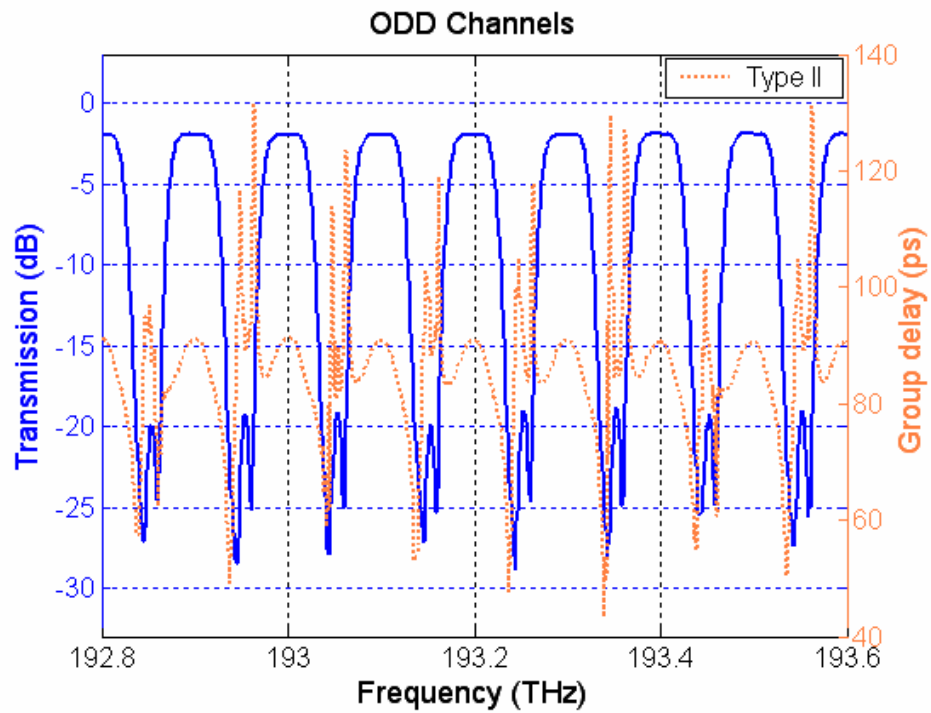


Fig. 2.12(a). Amplitude response and the corresponding group delay of the interleaver for odd channels (type II)

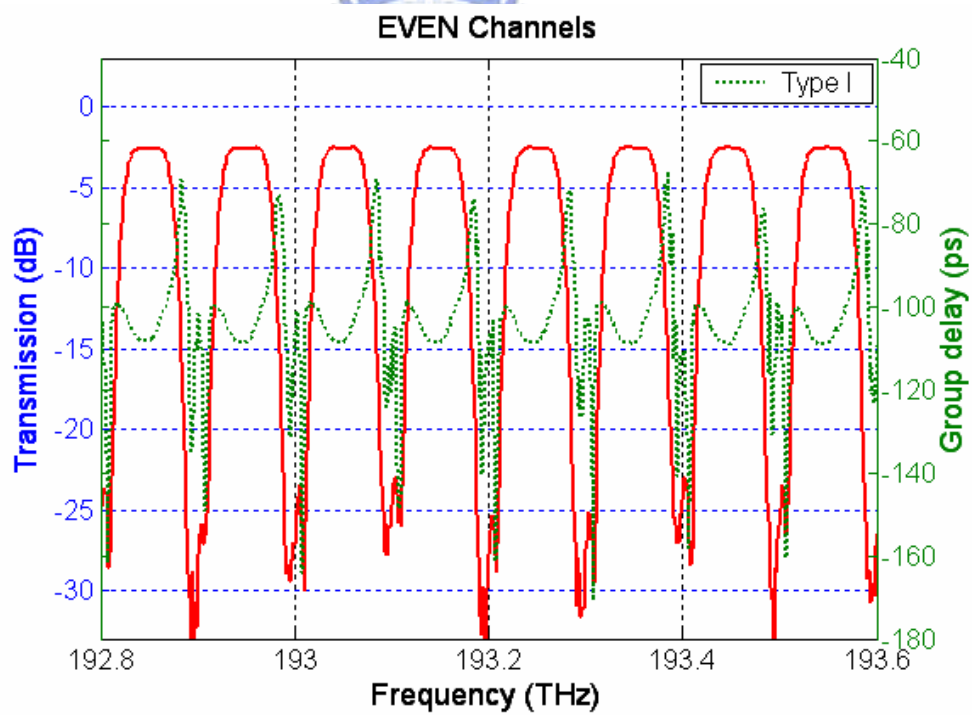


Fig. 2.12(b). Amplitude response and the corresponding group delay of the interleaver for even channels (type I)

2.4 Application of using an Interleaver in bi-directional amplification

We design the interleaver to have complementary wavelength dependent routing characteristics. For example, if λ_1 (odd/west channel) enters port 1, it will be routed to port 3. On the other hand, when λ_2 (even/east channel) goes into port 2; it will also be directed to port 3. A more detail wavelength routing diagram is displayed in Fig. 2.14.

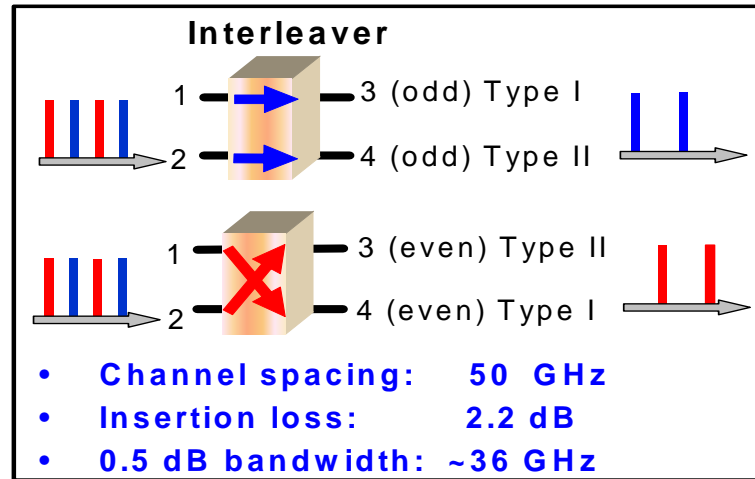


Fig. 2.13. Passband of the interleaver for even and odd channel

Such interleaving property is exploited to route simultaneously both the even channels, which arrive at the interleaver at port 2; and the odd channels, which enter the interleaver at port 1, to port 3. Therefore, the even and odd channels, which propagate in opposite directions, can be transformed into a co-propagating transmission in a single amplification section to achieve unidirectional amplification using a single EDFA, as shown in Fig. 2.15. The proposed innovative interleaving configuration not only supports the use of a single EDFA to achieve bidirectional transmission, but also eliminates the presence of a dead zone in the blue-red splitting technology due to this interleaver is implemented to cover the whole C band (1530 nm to 1560 nm), thus further increases the bandwidth utilization.

The transmission of interleaver we used is shown in Fig. 2.14.

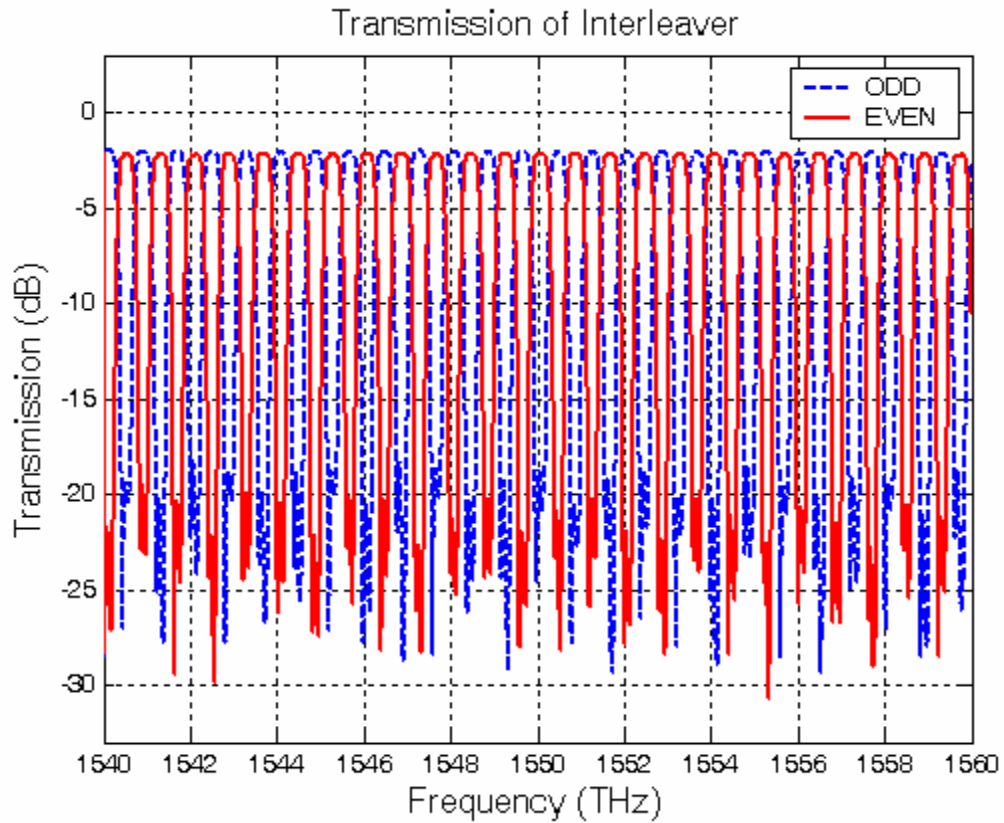


Fig. 2.14. Transmission of Interleaver

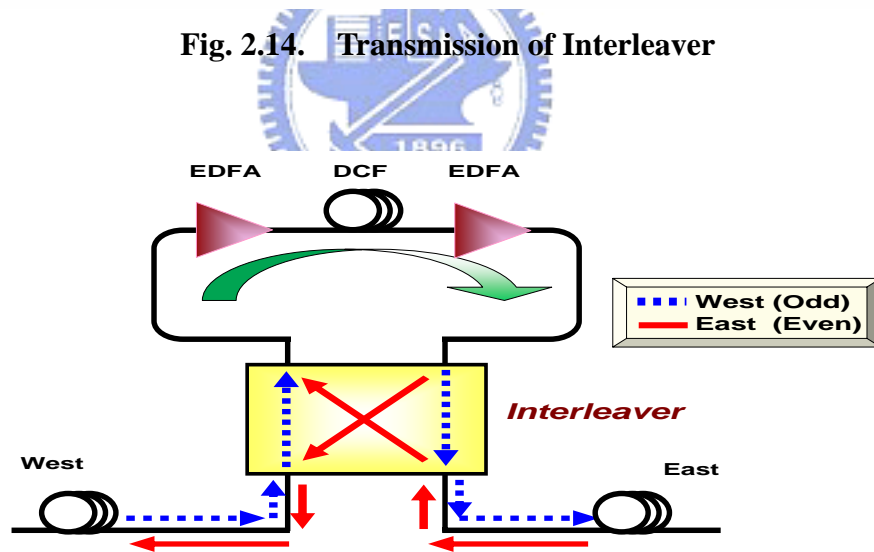


Fig. 2.15. Wavelength re-routing scheme for bidirectional transmission

Along side with bidirectional amplification function, dispersion compensation issue is also considered in this wavelength re-routing scheme. As described in Fig. 2.13, the group delay of routing port 2 to port4 and port 1 to port 3 are a pair of mirrored group delay and vice versa in the case of port 2 to port 3 and port 1 to port 4. The group delay of Type I and Type II

are displayed in Fig. 2.16(a), as well as the group delay after connecting Type I and Type II. Consequently, the wavelength re-routing scheme not only benefits bidirectional amplification but also provides a dispersion compensated environment.

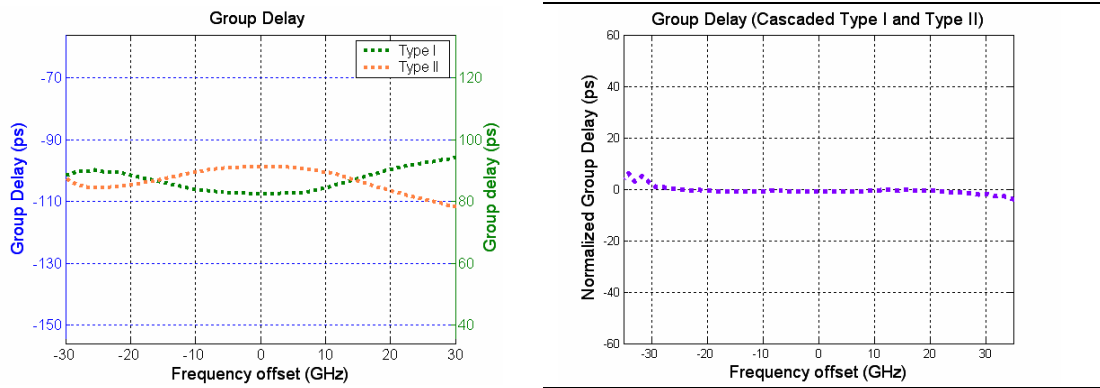


Fig. 2.16 (a) In-band group delay for two types of interleaver, (b) group delay of cascading Type I and Type II.



Chapter 3

Experiment of bi-directional straight line transmission

3.1 Bidirectional Optical Amplifier Configurations

Optical amplifiers are usually equipped with optical isolator, which make them unsuited for bidirectional transmission, in principle. However, it is possible to construct optical amplifiers for bidirectional transmissions. In the following section, we will consider the configuration of bidirectional optical amplifiers.

The simplest configuration for an optical amplifier is obtained by just omitting the optical isolators; since the operation of optical amplifiers is reciprocal. However, when a single EDFA (optical amplifier) is used bidirectionally without optical isolators or filters, interaction between the bidirectional channels may occur. There are at least three mechanisms for this interaction.

- Reflections and Rayleigh backscattering cause crosstalk between bidirectional channels. A bidirectional amplifier will enhance this crosstalk, since it amplified the reflected signal.
- Gain saturation will also cause mutual interaction, since if the signal in one direction saturates the gain, the signal in the other direction will also experience gain saturation.
- Similarly the signal in one direction may influence the noise behavior of the optical amplifier for the signal in the other direction.

The omission of the optical isolators makes the bidirectional amplifier less expensive than a conventional unidirectional amplifier. However, several other configurations have been proposed in literature, see Fig. 3.1

- Ref. [15] demonstrates the use of a unidirectional erbium-doped fiber amplifier

(EDFA) in a circuit, which combines and separates the bidirectional signals with wavelength splitters. The application of WDM makes this bidirectional amplifier configuration insensitive to optical reflections.

- Ref. [16] uses a combination of two wavelength splitters and two optical isolators to have both optical isolation at all wavelengths, and bidirectional transmission.
- Ref. [17], [18] and [19] propose the use of two separate EDFAs to decouple the saturation in the two directions. Here, each EDFA can have optical filters and isolator(s) or circulators.

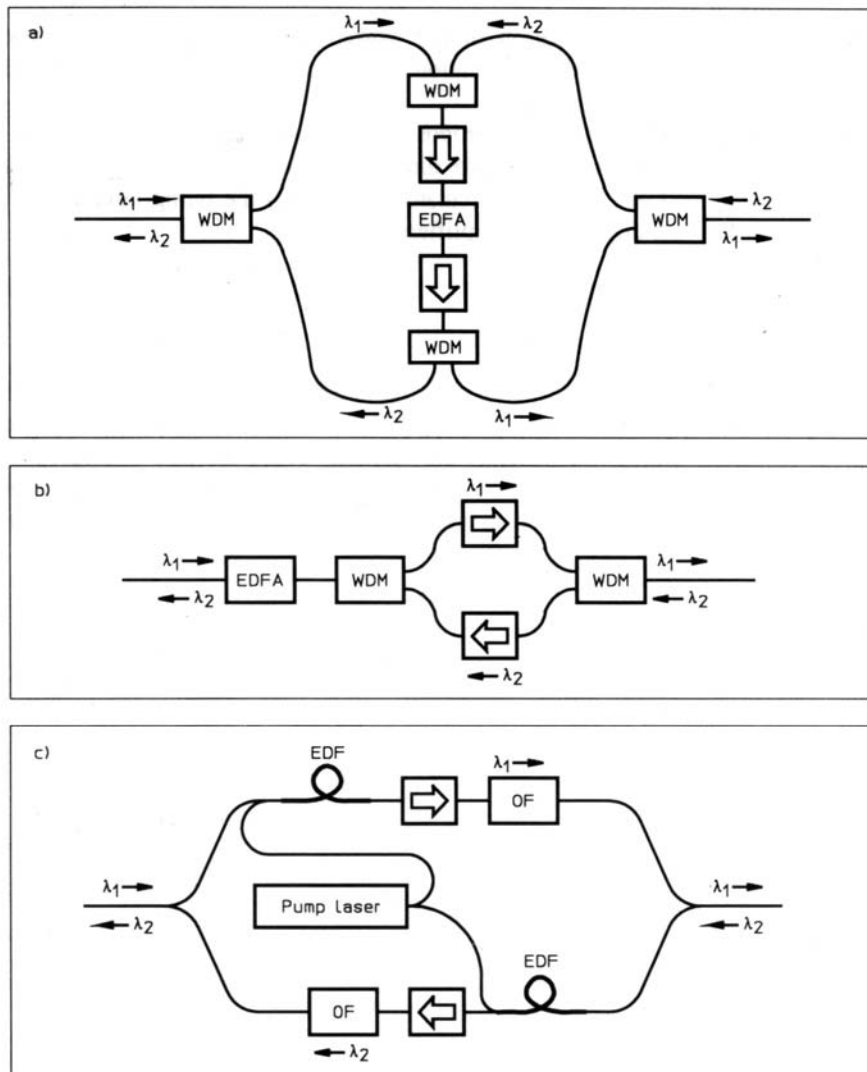


Fig. 3.1 (a) Bidirectional amplification with unidirectional optical amplifier (b) Bidirectional amplifier with optical isolation (c) double optical amplifier with shared pump laser.

3.2 Non-linear effects

The response of any dielectric to light becomes nonlinear for intense electromagnetic fields, and optical fiber are no exception. On a fundamental level, the origin of nonlinear response is related to anharmonic motion of bond electrons under the influence of an applied field. As a result, the induced polarization P from the electric dipoles is not linear in the electric field E , but satisfies the more general relation $P = \varepsilon_0 \{ \chi^{(1)} \cdot E + \chi^{(2)} : EE + \chi^{(3)} : EEE + \dots \}$, where ε_0 is the vacuum permittivity and $\chi^{(j)}$ ($j=1,2,3,\dots$) is j th order susceptibility. To account for the light polarization effects, $\chi^{(j)}$ is a tensor of rank $j+1$. The linear susceptibility $\chi^{(1)}$ represents the dominant contribution to P . Its effects are included through the refractive index n and the attenuation coefficient α .

The nonlinear effects governed by the third-order susceptibility $\chi^{(3)}$ are elastic in the sense that no energy is exchanged between the electromagnetic field and the dielectric medium. Thus, a second class of nonlinear effects results from stimulated inelastic scattering in which the optical field transfers part of its energy to the nonlinear medium. Two important nonlinear effects in optical fiber fall in this category; both of them are related to vibrational excitation mode of silica. These two phenomena are known as stimulated Raman scattering (SRS) and stimulated Brillouin scattering. The fundamental difference is that SBS in optical fiber occurs only in the backward direction whereas SRS dominates in the forward direction. Another nonlinear effect called Rayleigh backscattering (RB) will also deteriorate the bidirectional transmission system. Because any backward scattering will interfere the backward signal directly, the following discussions will focus on SBS and RB effects.

3.2.1 Stimulated Brillouin scattering

Stimulated Brillouin scattering can be understood as scattering of a photon to a lower energy photon such that the energy difference appears in the form of a phonon. The special

characteristics of SBS are the participation acoustic phonons and it only occurs in backward direction. In stimulated Brillouin scattering, the cross section is sufficiently small that loss is negligible at low power levels; however, at high power levels, the nonlinear phenomena of stimulated Brillouin scattering become important.

The physical process behind Brillouin scattering is the tendency of materials to become compressed in the presence of an electric field – a phenomenon termed electrostriction [20]. For an oscillating electric field at the pump frequency, ω_p , this process generates an acoustic wave at some frequency, ω_A . Spontaneous Brillouin scattering can be viewed as scattering of the pump wave from this acoustic wave, resulting in creation of a new wave at the pump frequency, ω_s . Since the scattering process must conserve both the energy and the momentum, the frequency and the wave vectors of the three waves are related by:

$$\begin{aligned}\omega_A &= \omega_p - \omega_s \\ \kappa_A &= \kappa_p - \kappa_s\end{aligned}\quad (33)$$

Where κ_p and κ_s are the wave vectors of the pump and Stoke waves. Using the dispersion relation $|\kappa_A| = \frac{\omega_A}{v_A}$, where v_A is the acoustic velocity, this condition determines the acoustic frequency as Eq. (33):

$$\omega_A = |\kappa_A| v_A = 2v_A |\kappa_p| \sin(\theta/2) \quad (34)$$

Where $|\kappa_p| \approx |\kappa_s|$ was used and θ represents the angle between the pump and scattered waves.

Note that ω_A vanishes in the forward direction ($\theta=0$) and is maximum in the backward direction ($\theta=\pi$). In single-mode fibers, light can travel only in the forward and backward directions. As a result, SBS occurs in the backward direction with a frequency shift

$\omega_B = 2v_A |k_p|$, using $k_p = \frac{2\pi n}{\lambda_p}$, where λ_p is the pump wavelength, the Brillouin shift frequency is given by

$$\nu_B = \frac{\omega_B}{2\pi} = \frac{2\bar{n}\nu_A}{\lambda_p}$$

Where \bar{n} is the mode index. Using $\nu_A = 5.96$ km/s and $\bar{n} = 1.45$ as typical values for silica fibers, $\nu_B \cong 11.1$ GHz at $\lambda_p = 1.55 \mu\text{m}$.

All in all, we control the input powers under 6-dBm injected into the transmission fiber without performance degradation resulting from SBS.

3.2.2 Rayleigh backscattering

A fundamental effect observed in optical fibers is Rayleigh backscattering: light bounces off microscopic defects in the amorphous structure of the glass. These defects (much smaller than the wavelength of the light) scatter the light and give rise to attenuation. Some of the scattered light returns along the fiber. The light scattered from a larger distance along the optical fiber contributes less to the total amount of returning light than scattering near the fiber input, because of attenuation in the fiber.

The magnitude of Rayleigh backscattering is derived by considering a uniformly backscattering fiber of length L . After being coupled into the input of the fiber, a unit energy optical impulse of power $\delta(t)$ propagates in the forward direction. Notice that in this section only light intensities are used, because the different contributions to the Rayleigh backscattering add incoherently. The power propagating in the reverse direction, prior to being coupled out at the same input end, is the backscattered impulse response power

$$h(t) = \begin{cases} be^{-\alpha v_g t} & \text{for } 0 \leq t \leq \frac{2L}{v_g}, \\ 0 & \text{otherwise} \end{cases} \quad (35)$$

Here t is the round-trip transit time of the light out to a point ($z = v_g \cdot \frac{1}{2t}$) along the fiber and back. The fiber parameters above are,

$$\alpha = \text{attenuation coefficient (1/km)}$$

$v_g = \text{group velocity} = c/n_g$ (km/s), where $c \cong 2.998 \times 10^5$ km/s

$n_g = \text{group index}$ (dimensionless)

$b = \text{backscatter parameter} = (v_g/2) \beta_s F$ (Watt/Joule)=(1/s)

$\beta_s = \text{scattering coefficient}$ (1/km)

$F = \text{backscatter capture fraction}$ (dimensionless)

All these parameters are taken to be essentially uniform along the fiber. They depend on fiber type and on wavelength. The parameter b at a point along the fiber is the backscattered propagating power corresponding to a unit incident energy. The parameter F is the fraction of the scattered power that is captured as backward propagating power. It depends on other standard fiber parameters such as the mode-field diameter.

For an input power signal $p(t)$, the backscattered response at the input end is the convolution with the impulse response of Eq. (35):

$$r(t) = \int_{-\infty}^{\infty} h(\tau) p(t-\tau) d\tau = b \int_0^{2L/v_g} e^{-\alpha v_g \tau} p(t-\tau) d\tau \quad (36)$$

Applying this result to the situation of an optical continuous wave, the input power is a steady value $p(t)=p_0$. Substituting this into (36) yields the continuous response $r(t)=r_0$ that depends on the fiber type and length: $r_0(L) = p_0 \frac{bn_g}{c\alpha} (1 - e^{-2\alpha L})$. For short fiber length, the backscatter fraction is

$$B(L) = \frac{r_0(L)}{p_0} \approx \frac{2bn_g}{c} \quad (37)$$

Whereas for long fiber length, the backscatter fraction is

$$B(\infty) = \frac{r_0(L)}{p_0} \approx \frac{bn_g}{c\alpha} \quad (38)$$

This backscatter fraction equals approximately -32 dB for a single mode fiber at 1550 nm. This level can be used as a reference when specifying the reflection of a connector or splice. In general, the Rayleigh backscattering at the facet of a connector or splice is a minor factor

of performance deterioration.

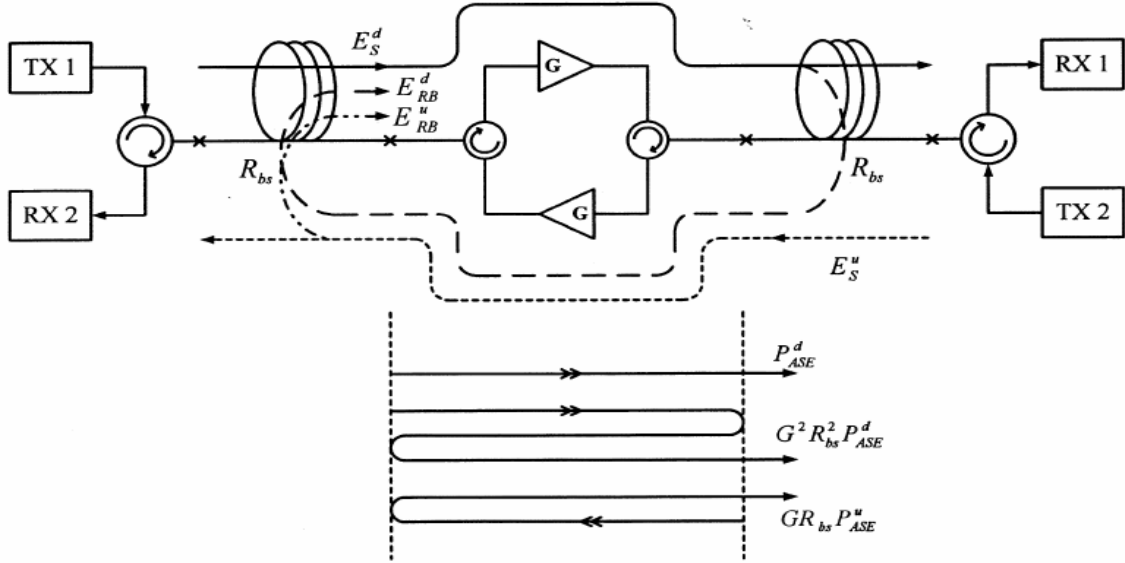


Fig. 3.2. Scheme of crosstalk due to single- and double-amplified RB of signal as well as ASE. P_{ASE} is the power of ASE noise from the EDFA. E_s^d is the downstream signal, and E_s^u is the upstream signal. E_{RB}^d and E_{RB}^u are the Rayleigh backscattered signals of E_s^d and E_s^u , respectively.

However, as illustrated in Fig. 3.2, with the Rayleigh backscattering induced crosstalk, bidirectional amplifier node is susceptible to occurrences of self-oscillation; distributed Rayleigh mirrors are forming optical cavity with enclosed amplifier gain, thus, providing necessary conditions for node lasing. Therefore, under the circulator based bidirectional amplifier, Rayleigh backscattering effect would be an degradation factor not only deteriorates the transmission performance but also limits the gain of the this bidirectional amplifier configuration.

3.3 Experimental setup & results of bidirectional straight line transmission

In order to achieve bidirectional transmission, we build up a transmission system with the utilization of the wavelength re-routing characteristic of the four-port interleaver. The experimental setup is illustrated in Fig. 3.3. We use a dual-stage EDFA with mid-stage

dispersion compensator (DCF) to balance the transmission loss and accumulated dispersion. The eight channel laser sources are grouped into two categories: One range from 1550.52 nm to 1551.72 nm and the other ranges from 1554.54 nm to 1555.75 nm, all of them are on the standard ITU 50-GHz channel spacing grids.

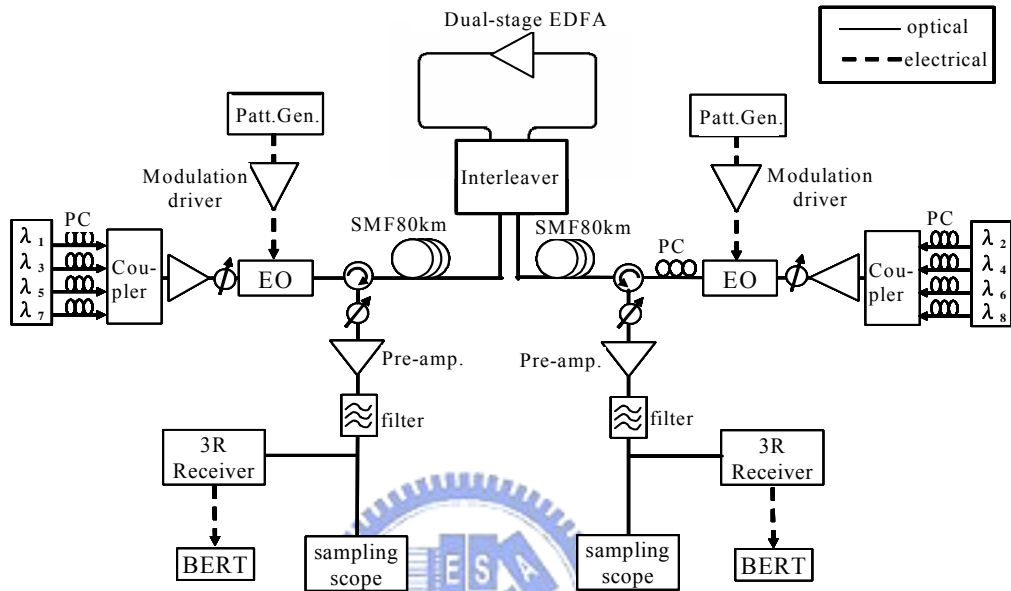


Fig. 3.3. Experimental setup of a bidirectional transmission

Both categories of laser sources were individually modulated by a LiNbO₃ electro-optical (EO) modulator at 10 Gb/s with a pseudo-random binary sequence (PRBS) length of $2^{31}-1$ pattern. The transmission fiber we used were 160-km of standard single mode fiber (Corning SMF-28[®]). Within the dual-stage EDFA, 36-km of Corning dispersion compensation fiber (DCF) was employed to compensate the accumulated chromatic dispersion which caused by 160-km SMF fiber. A polarization controller was used on the east-to-west traffic to ensure that the polarization states between east-even and west-odd channels were orthogonal to reduce the crosstalk induced by the opposite traffics. A 3R receiver of -32 -dBm back-to-back sensitivity at bit error ratio (BER) of 10^{-9} was applied to evaluate the system performance after 160-km transmission. The gains and noise figures of our dual-stage EDFA at all channels are about 23.5-dB and 4.5-dB, respectively. Fig. 3.4 shows the received optical spectrum of the east-even channels after 160-km of transmission.

Since we re-route the bidirectional transmission into unidirectional at the amplification stage using an interleaver, the Rayleigh Backscattering induced noise are diminished significantly. The primary reflection path is showed in the Fig. 3.5. From this figure, we could recognize that the suppression of the unwanted reflection signal at the receiver is dependent on the isolation of the interleaver. Consequently, the optical signals experience much lower NF, compared with the condition of NF larger than 6.5-dB while using a LOA [21]. Therefore, under our proposed method, the OSNR exceed 35-dB are achieved after 160-km of transmission for all channels, whereas in the LOA scheme, the OSNR of all channels are less than 26 dB. A residual crosstalk of 15 and 18 dB on the even and odd channels, respectively, as shown in Fig 3.4(a)~(b). , was observed when the co-propagating channels were interleaved into bidirectional transmissions after amplification. Fig. 3.6 illustrates the BER curves and the corresponding eye diagrams of channel six. After 160-km transmission, both eye diagrams and BER curves indicate that the performance deterioration induced by accumulated ASE noise and dispersion in the bi- and uni-directional transmission systems was similar.

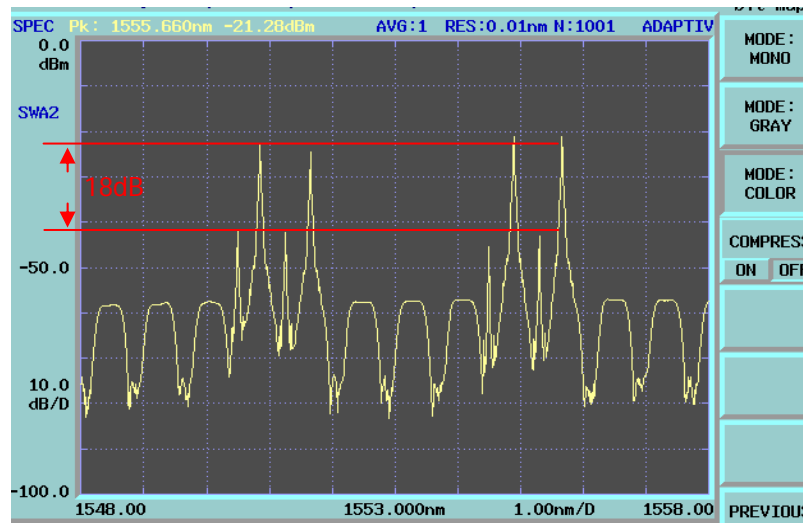


Fig. 3.4(a). Received optical spectrum of the east-even traffic after 160-km transmission

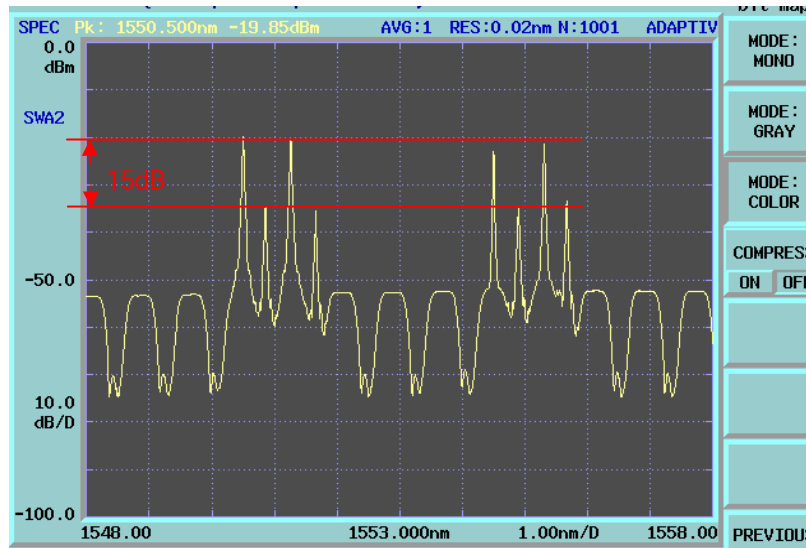


Fig. 3.4(b). Received optical spectrum of the west-odd traffic after 160-km transmission

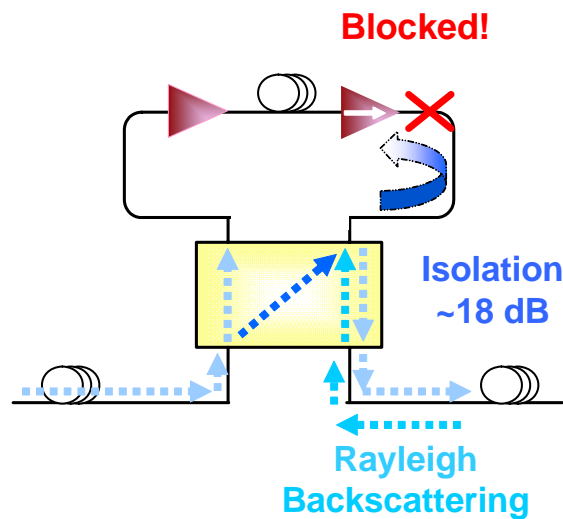


Fig. 3.5. Primary reflection path

In addition, the received power penalty for each channel is shown in Fig. 3.7. We also measure the noise figure and the net gain of our bidirectional amplifier module for each channel showed in Fig.3.8.

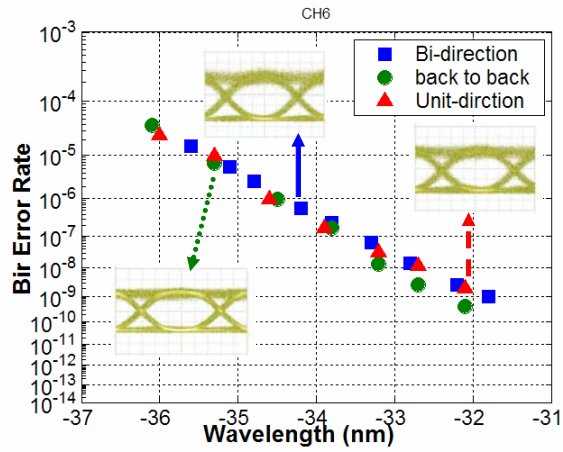


Fig. 3.6. BER curves and corresponding Eye diagrams after 160-km transmission @ CH. 6

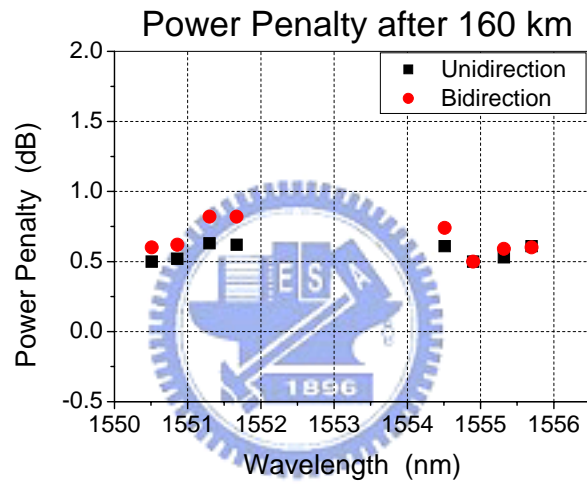


Fig. 3.7. Power penalty of each channel

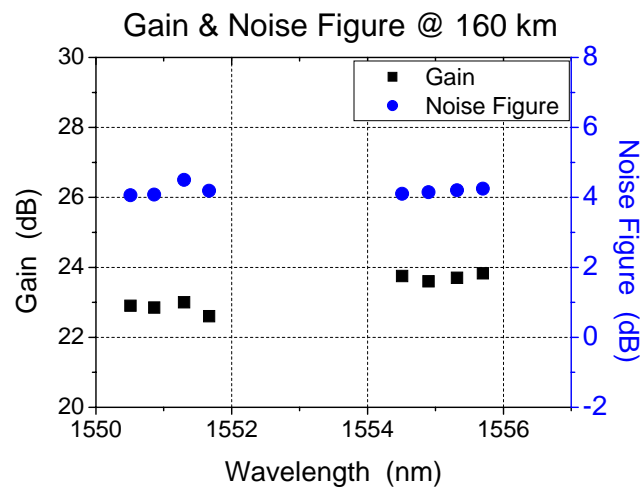


Fig. 3.8. Noise figure and net gain of the proposed bidirectional amplifier

As displayed in Fig. 3.7, all penalties are less than 0.8 dB compared with back-to-back BER curves; the BER penalty variations between bidirectional and unidirectional transmission are less than 0.2 dB at all channels. Furthermore, the maximum noise figure is less than 4.5 dB.

Besides 160-km transmission, we also extend the transmission length to 210 km and apply appropriate length DCF to compensate the chromatic dispersion. The measurement of the received optical spectrum (Fig. 3.9), the power penalty (Fig. 3.11), noise figure and net gain of the bidirectional amplifier (Fig. 3.12) are exhibited as follows. As a result, the maximum power penalty compared with back to back transmission is less than 1.5 dB; the net gain for each channel is about 22.2 ~23dB and the NF is about 6 dB. The BER curves and corresponding eye diagrams for 210km SMF transmission (including of the bidirectional, unidirectional and back to back transmission) are demonstrated in Fig. 3.10.

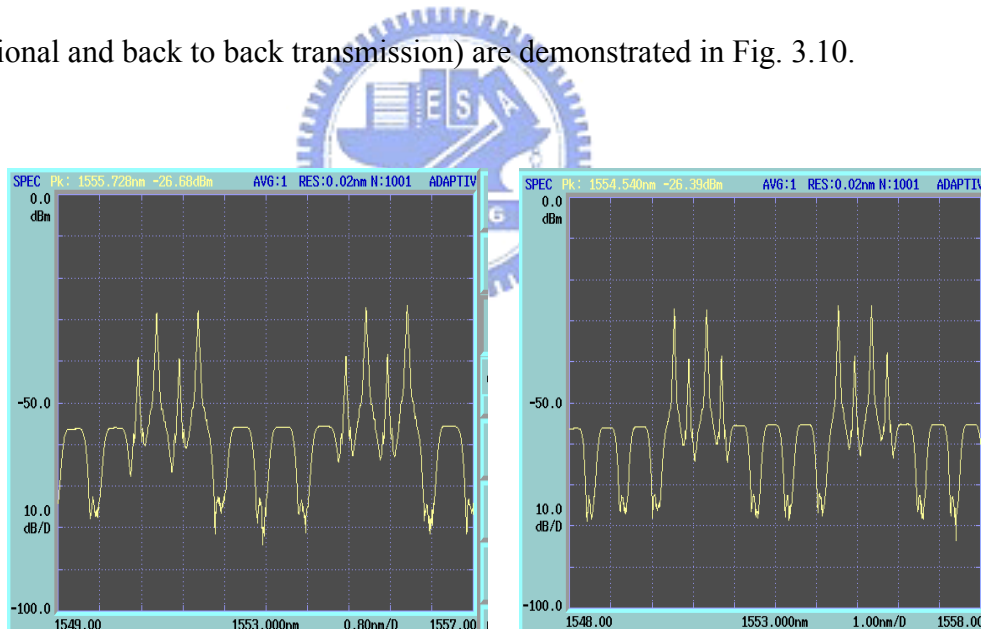


Fig. 3.9. Optical spectrum before the receiver

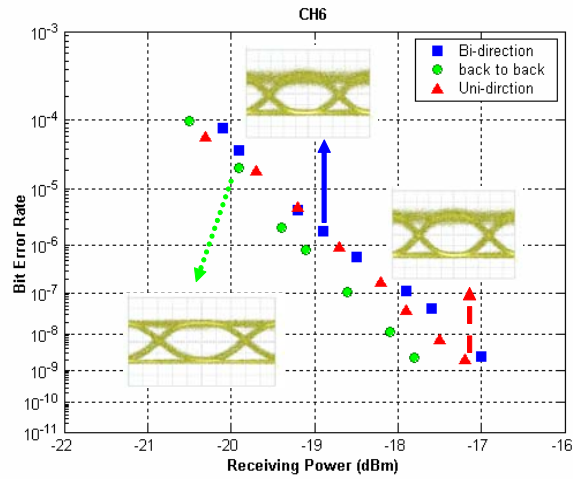


Fig. 3.10. BER curves and corresponding Eye diagrams after 210-km transmission @ CH. 6

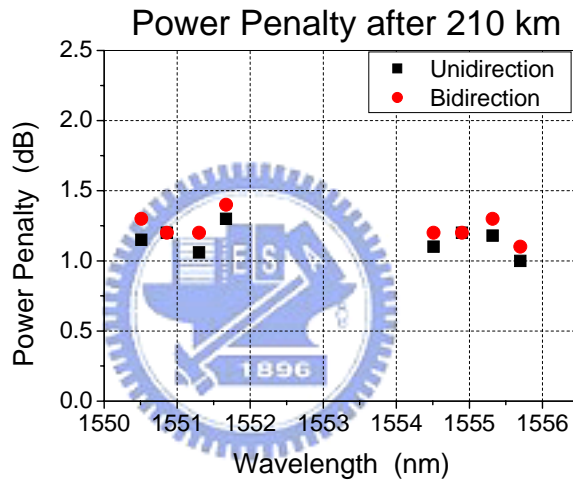


Fig. 3.11. Power penalty of each channel for 210km transmission

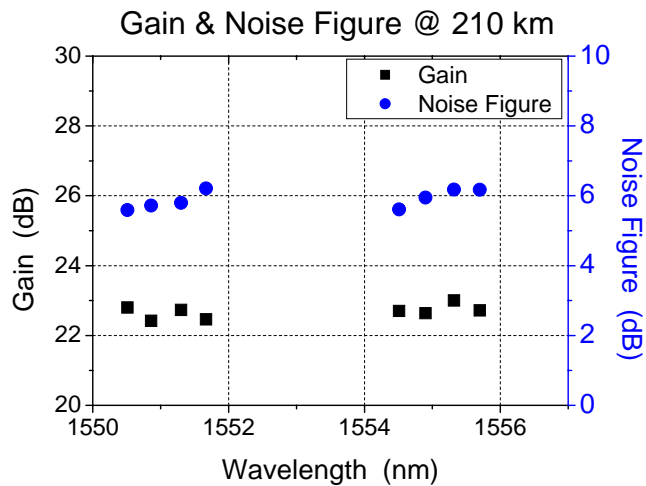


Fig. 3.12. Net gain and noise figure of each channel for 210km transmission

Chapter 4

Experiment of bi-directional loop transmission

4.1 Re-circulating loop transmission

Loop techniques play an important role in the development of long-haul transmission systems by providing a flexible platform using Erbium-doped fiber-amplifier for transmission evaluations. The major function of a circulating loop experiment is to simulate the transmission performance of a long system by reusing or re-circulating an optical data signal through a modest length amplifier chain ranging from tens to hundreds of kilometers. Not only reducing the setup size and complexity but also providing a cost effective way of test could the designers benefit from a recirculating loop. Better still, through circulating loop experiments, valuable information such as system BER, eye diagram shape, dispersion, signal-to-noise ratio, and interchannel interaction of a WDM system could be obtained.

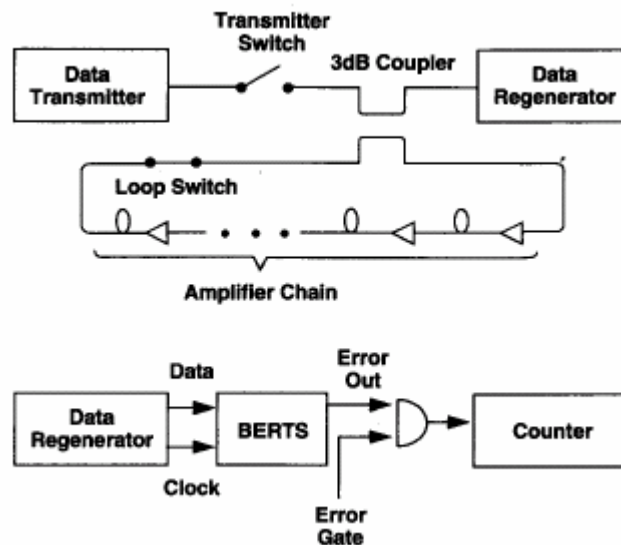


Fig. 4.1. loop transmission block diagram

The loop experiment contains most of the same elements typically found in conventional experiments, for example, an optical data transmitter/regenerator pair, a chain of amplifier/fiber sections, and diagnostic equipment such as a bit error test set (BERTS) (Fig 4.1). In addition, a prerequisite condition for operating a recirculating loop, the power balance

issue, must be concerned. It means that gain and loss in each round trip are equal; otherwise, the system would lead to a consequence that the quality of transmission would degrade severely and might not be able to continue transmitting signals.

4.1.1 Loop time control

Along side with the power balance issue, the loop time control is also a critical issue while constructing a re-circulating loop system. In the loop experiment, optical switch is added to allow data to flow into the loop (the load state) or to allow data to circulate (the loop state), as displayed in Fig 4.2. The basic time unit for the experiment is the round-trip time of the closed loop (showed in Fig. 4.3). With reference to the timing diagram Fig. 4.2 (a), the experiment starts with the transmitter switch on and the loop switch off.

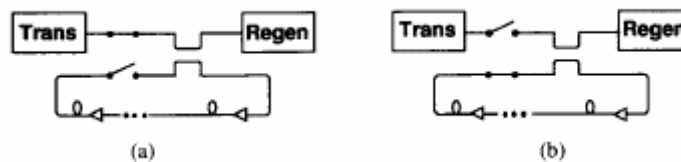


Fig. 4.2. (a) load state (b) loop state

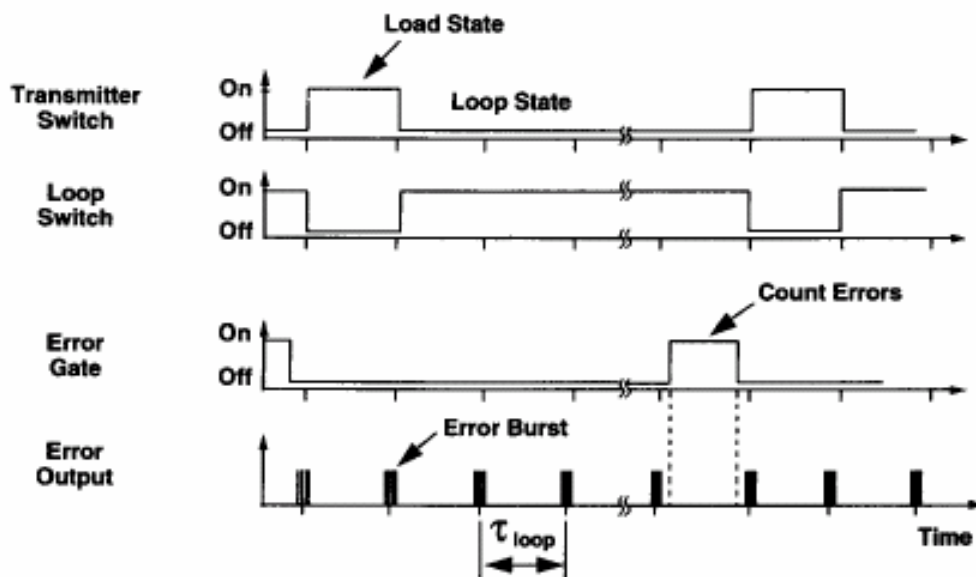


Fig. 4.3. pulse signaling for loop time control

The two switches are held in this load state for at least one loop time to fill the loop with the optical signals. Once the loop is fully loaded with data, the switches change state to the loop state as Fig. 4.2 (b), and the data is allowed to circulate around the loop for some

specified number of circulations. A portion of the data signals are coupled to the receiver for analysis. The data signals are received and re-timed by the receiver and compared to the transmitted signal in the BERTS for error detection. The error signals from the BERTS are combined with the error gate in a logic AND gate so that only the errors in the last circulation are counted. The measurement continues, switching between the load and loop states so that errors can be accumulated over long intervals of time. The BER is calculated as the number of errors detected in the error gate period divided by the total number of bits transmitted during the observation period.

With an unbroken data pattern, the BERTS still detects errors at the boundaries between each loop time, related to the finite speed of the AO switches. During the switch transition from the load state to the loop state, both switches are transmitting some amount of the optical signal. Optical pulses originating from the transmitter will interfere with those pulses returning from the loop, since two pulses have the same wavelength, but random optical phase and polarization. This interference process corrupts the data bits and causes the BERTS to detect bit errors at the transitions.

The circulating loop experiment can be improved through the usage of bit error detectors with fast frame synchronization time (usually referred to the “burst mode”). Because the frame synchronization time of these detectors is much shorter than the loop time, they simplify error counting by de-coupling the strict relationship between the bit rate and the loop time, thus allowing the transmitter to run asynchronous to the loop. Here, the receiver sees broken sections of the transmitted pattern at each circulation because the data words do not fit evenly into the loop. At each border between circulations, the error detector must re-acquire frame synchronization, thus creating a small error burst on the seam. As in the control scheme discussed above, this error burst is removed by gating the error detector and counting only those errors that occur in the middle of the circulation.

4.1.2 Dispersion management

In general, dispersion will cause pulse spreading and power penalties due to the intersymbol interference effect. There are two kinds of dispersion, chromatic dispersion and polarization mode dispersion (PMD). We will pay more attention to chromatic dispersion compensation since it is essential from the practical perspective; the PMD compensation is more complex and has not found a wider application yet, although the situation might change with the introduction of 40 Gbps based transmission systems. Chromatic dispersion causes different wavelengths to travel at different group velocities in single mode transmission fiber. Chromatic dispersion can reduce phase matching, or the propagation distance over which closely spaced wavelengths overlap, and can reduce the amount of nonlinear interaction in the fiber. Thus, in a long undersea system, the nonlinear behavior can be managed by tailoring the accumulated dispersion so that the phase-matching lengths are short, and the end-to-end dispersion is small. The technique has been used in both single channel systems to reduce nonlinear interaction between signal and noise as well as in WDM system.

In-line or all-optical, chromatic dispersion compensation methods can be applied at any point along the light wave path. However, in practice, they are usually employed at inline amplifier sites. Dispersion compensating modules are positioned as a middle stage in in-line optical amplifiers. In our experiment, we use the compensation with DCF's, which are widely used in various transmission systems.

The use of DCF is the most common method since chromatic dispersion can be fully compensated if nonlinear effects are negligible. If nonlinearities are small, compensation can be as a linear process that satisfies the condition.

$$\begin{aligned} D_1(\lambda_c)L_1 &= D_2(\lambda_c)L_2 \\ D_1(\lambda_c) + S_1(\lambda_i - \lambda_c)L_1 &= D_2(\lambda_c) + S_2(\lambda_i - \lambda_c)L_2 \end{aligned}$$

Where D_1 and L_1 are the chromatic dispersion and the length of the transmission optical fiber, respectively, and D_2 and L_2 are related to dispersion and the length of DCF. The

dispersion is fully compensated around 1553.2 nm. The following table listed the parameters for transmission fiber (Corning LEAF) and DCF (Corning DCF) we used in experiments.

Table 1. Parameters of dispersion map for bidirectional loop experiment

Type of fiber	LEAF	Type of fiber	DCF
Length (km)	100	Length (km)	5.02*
Dispersion Coeff. (ps/nm · km)	4.1639	Dispersion Coeff. (ps/nm · km)	-82.9462
Dispersion Slope (ps/km · nm ²)	0.06	Dispersion Slope (ps/km · nm ²)	0.22
Loss (dB/km)	0.2	Loss (dB/km)	0.6

$$5.02^* = 100(\text{km}) \times 4.1639 (\text{ps/nm} \cdot \text{km}) \div 82.9462 (\text{km})$$

The dispersion map of the bidirectional loop transmission experiment is exhibited in Fig. 4.4.

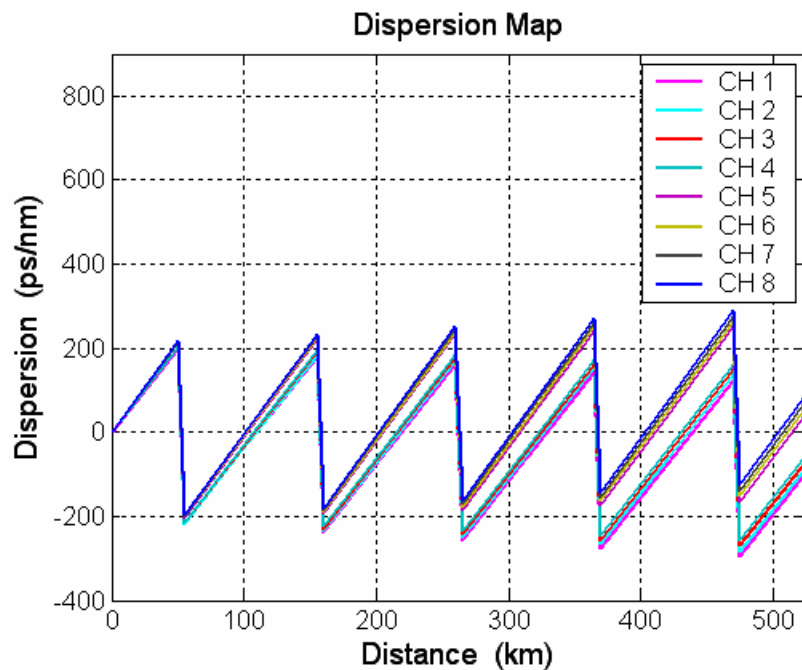


Fig. 4.4. Dispersion map (fully compensated @ 1553.2 nm, Max ΔD in CH 1 equals to 95.5 ps/nm)

4.2 Experimental Setup & results of bidirectional loop transmission

Fig. 4.5 shows the experimental setup for testing long-distance bidirectional transmission using four-port interleavers in a recirculating loop. The eight-channel laser sources are grouped into two categories: One with wavelengths between 1550.52 nm and 1551.72 nm, another with wavelengths between 1554.54 nm and 1555.75 nm; both are on standard ITU 50 GHz channel spacing grids. The even and odd channels stand for two traffic directions – even channels represent east (bond) traffics and odd channels represent west (bond) traffics; they are individually modulated by a LiNbO₃ electro-optical (EO) modulator at 10 Gbps with a $2^{31}-1$ PRBS pattern. A polarization controller is used on the odd traffic to ensure that the polarization states of the odd/west channels are orthogonal to those of the even/east channels, reducing the deleterious nonlinear effects. An interleaver is placed at the input of the recirculating loop to split the odd/east and the even/west channels for bidirectional transmission and reverse-directed traffics (east and west traffics) are combined for unidirectional amplification [31]. The transmission fiber used in the recirculating loop has two spools of 50 km Corning LEAF fiber. A dual-stage EDFA with 5 km of Corning DCF is employed in the mid-stage of the loop to compensate the transmission loss and accumulated dispersion in LEAF fiber. The effective gain and noise figure of the dual-stage EDFA in all channels are around 23 dB and 5.5 dB, respectively. The fully compensated wavelength of this fiber loop is located approximately at 1553.2 nm. The two interleavers in the loop are specially arranged to reduce chromatic dispersion induced by the flat-top transmission band design of the interleaver [32]. A 3R receiver with -32 dBm sensitivity at BER of 10^{-9} is utilized to evaluate the transmission quality.

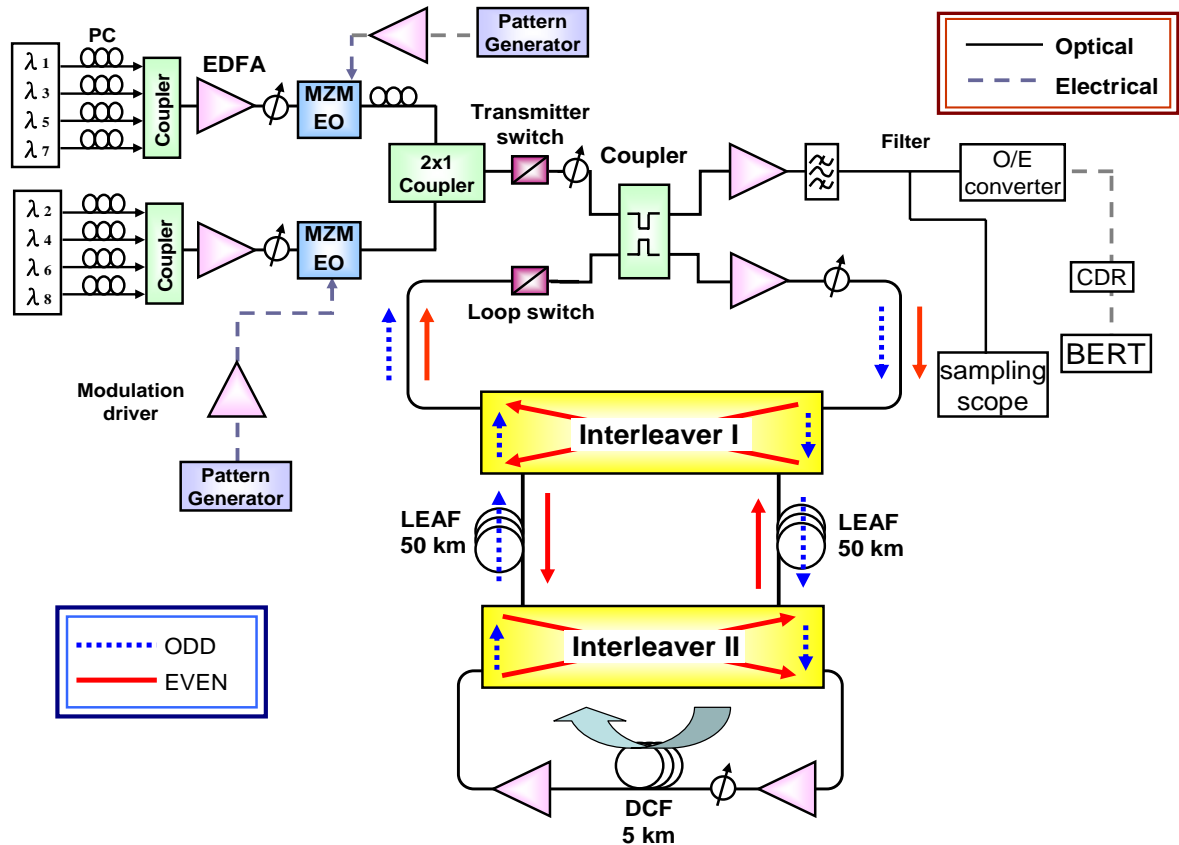


Fig. 4.5. Experimental setup of bi-directional loop transmission

Fig. 4.6 displays the received optical spectrum after 500 km with an OSNR of over 31 dB for all channels with a 0.02nm resolution bandwidth setting on the OSA. This configuration effectively blocks the RB by using only one amplification section for two traffic directions. Fig. 4.7 shows the receiving power penalties of BER equals to 10^{-9} at all channels. All channels had power penalties of less than 2.2 dB and the penalty differential between them is less than 0.36 dB. Fig. 4.8 plots the BER curves and Fig. 4.9(a)~(d) show the corresponding eye diagrams at channel seven, for back-to-back, 100 km, 300 km and 500 km transmissions. The measured power penalties were about 0.4 dB, 1.1 dB and 2 dB for 100, 300 and 500 km transmissions, respectively, at a BER of 10^{-9} with the optimal polarization condition. In the recirculating loop, the polarization controller is used to minimize the polarization effects -- such as polarization dependent gain (PDG) and polarization dependent loss (PDL). The penalties are attributed to ASE accumulation due to the SNR degradation

resulting from high link loss within the amplifier span.

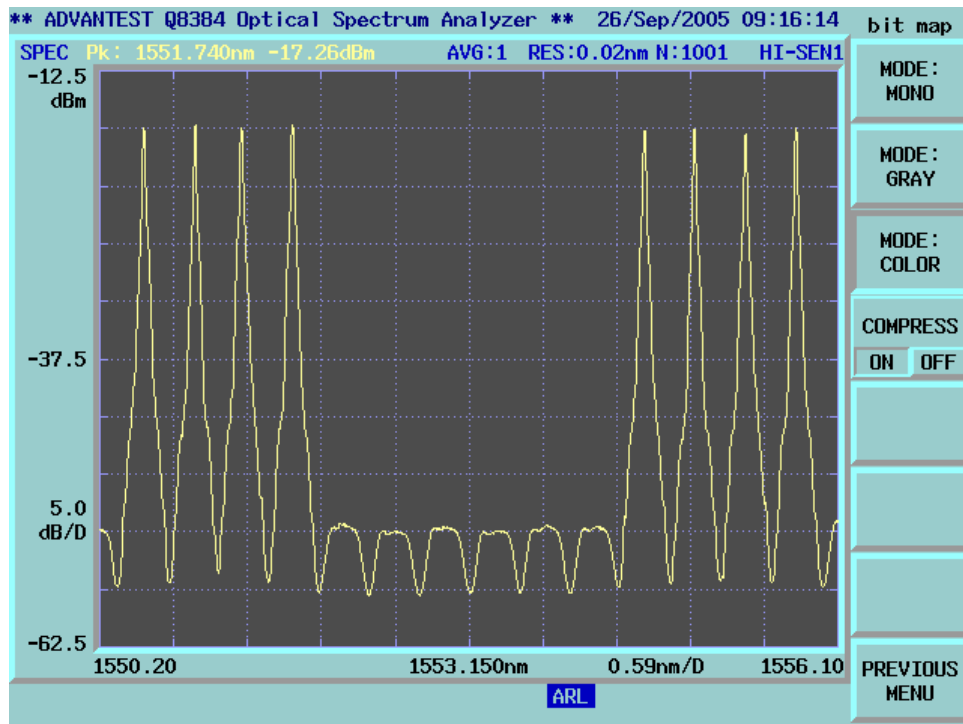


Fig. 4.6. Received optical spectrum after 500 km bidirectional transmission

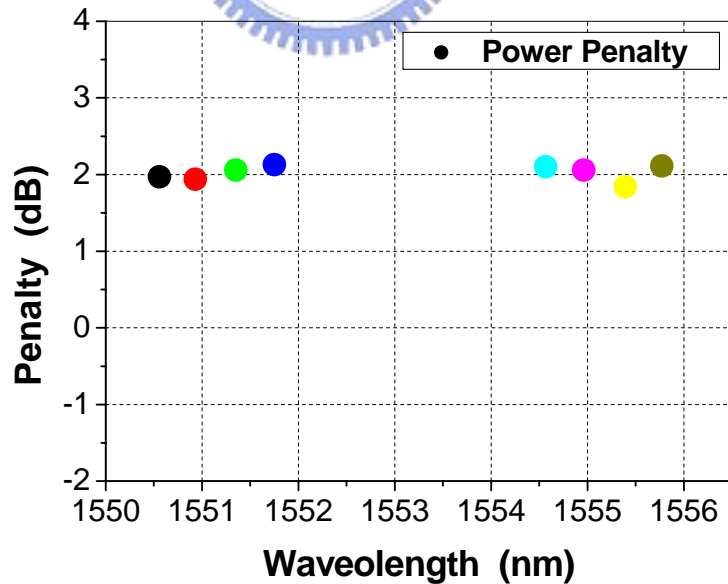


Fig.4.7. Power penalty after 500 km bidirectional loop transmission

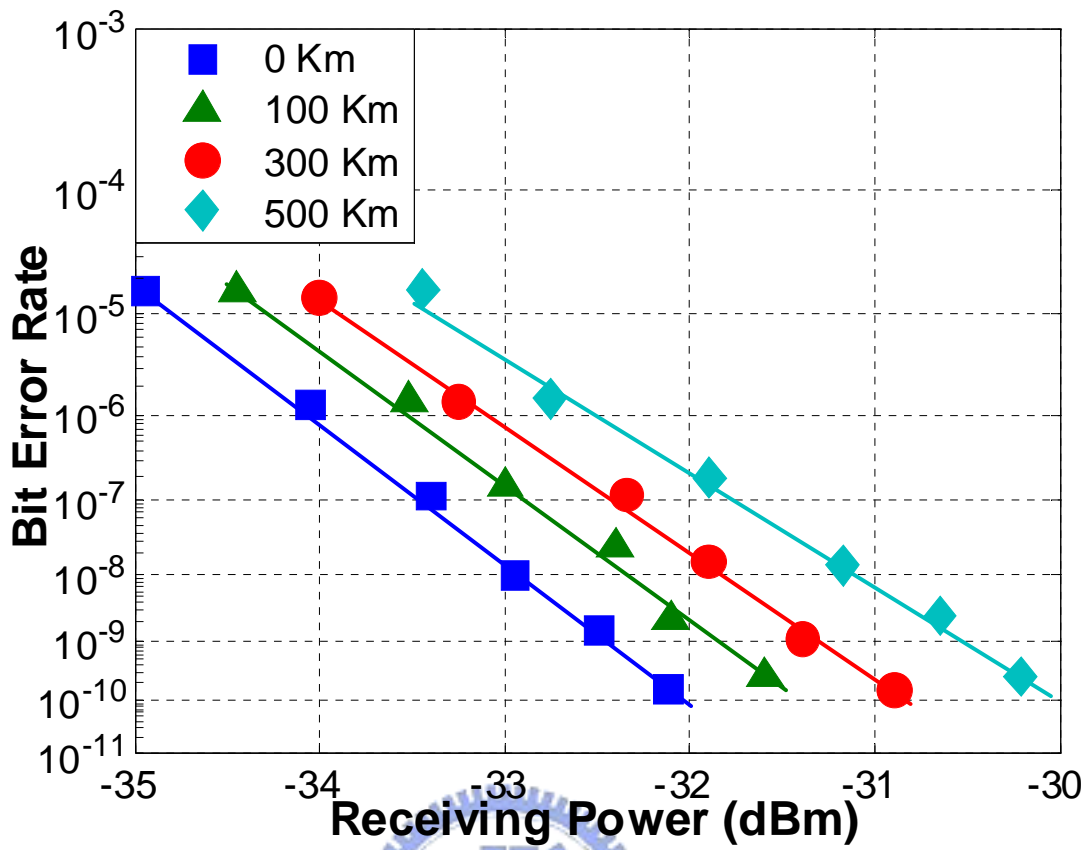


Fig. 4.8. BER curves of Channel 7 after 0 km, 100 km, 300 km, 500 km traffic

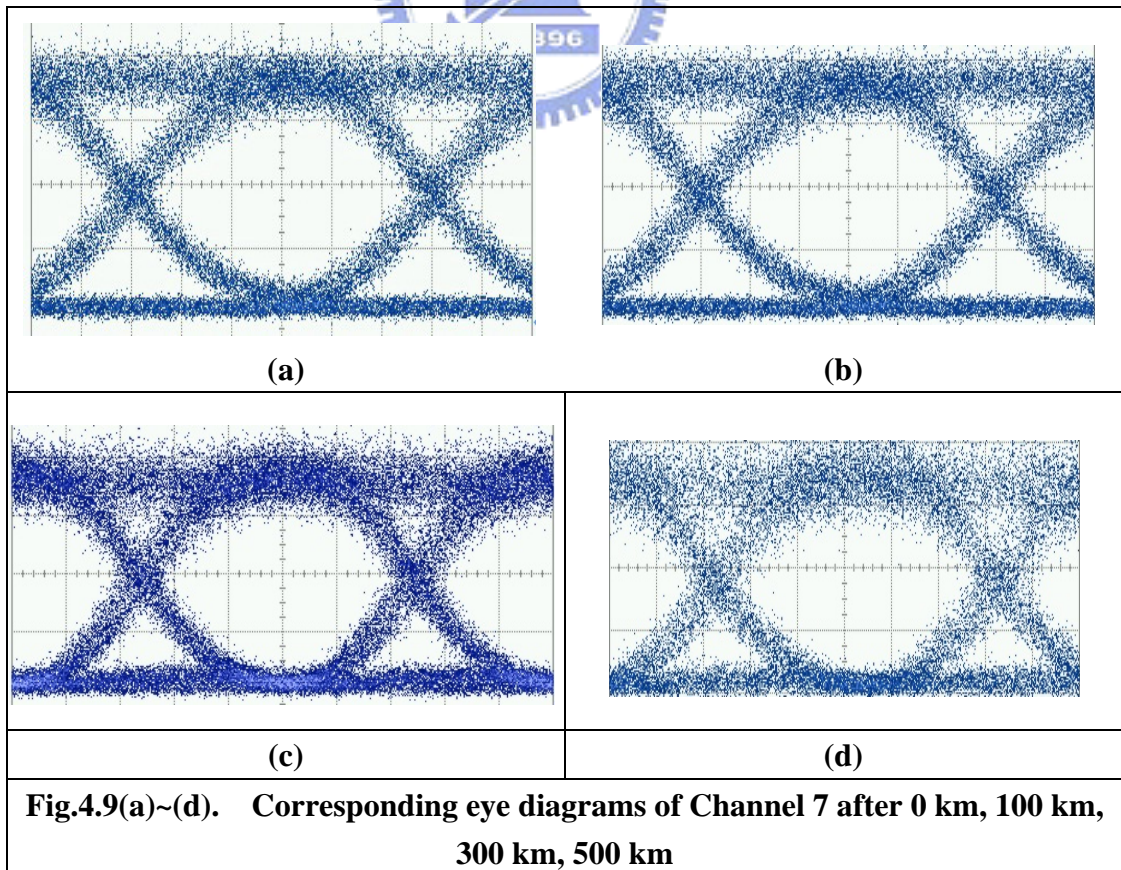


Fig.4.9(a)~(d). Corresponding eye diagrams of Channel 7 after 0 km, 100 km, 300 km, 500 km

In a recirculating loop experiment, if the optical data pattern length time is longer than the sampling window used in taking BER measurement, pattern-dependent errors arise from time to time [34]. An accumulated error measurement can verify the stability and ensure that the appropriate sampling window is used in the recirculating loop experiment. As a result of [34], the error counts accumulate almost continuously when system keeps accurate sampling window. Otherwise, the accumulated errors would be missed for long periods of time, and then would be over-sampled for certain periods of time. Fig. 4.10 plots the measured accumulated errors as a function of time (10-s intervals) at a BER of 2.46×10^{-9} after 100 km and 500 km transmission. This figure demonstrates the robustness of the transmission system for BER measurement. Moreover, the authors believe that this configuration can accommodate more optical channels, 16 or 32 channels, within the C band because this interleaver is implemented to cover the whole C band (1530 nm to 1560 nm).

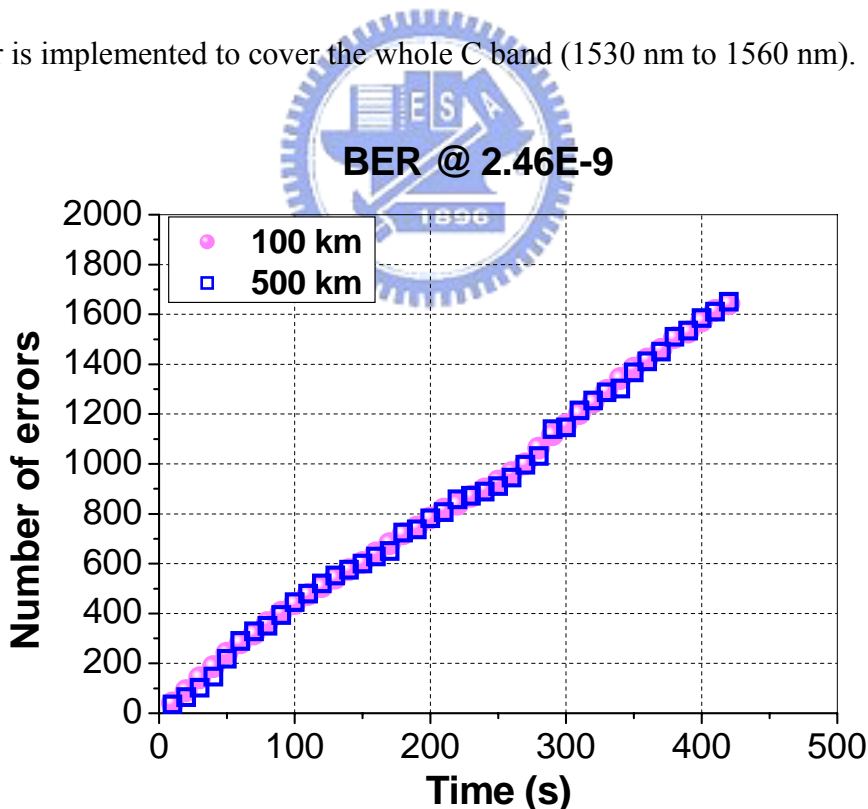


Fig. 4.10. Accumulated Errors after 100 km and 500 km bidirectional transmission at BER = 2.46×10^{-9}

Chapter 5

Simulation of bidirectional transmission systems

According to chapter three and four, we have successfully demonstrated bidirectional transmission system by exploiting four port interleavers. Table II lists the power penalty obtained from the two experiments.

Table 2. Power penalty of bidirectional transmission experiments

Distance \ Configuration	Straight Line	Loop
100 km	-	0.4 dB
160 km	0.8	
210 km	1.5dB	-
300 km	-	1.1 dB
500 km	-	2.1 dB

From the results of experiments, the penalties of “Loop” experiment increase steadily with the transmission distance. However, the mean penalty is 1.4 dB in the “Straight Line” case after 210 km transmission; while the penalty of the “Loop” case is 1.1 dB after 300 km transmission distance. This discrepancy exhibits that “Straight Line” and “Loop” case may not be identical even though they are both bidirectional transmission configurations. This chapter will focus on the simulation for comparing the two schemes.

5.1.1 Analysis of bidirectional loop transmission system

As we know, the recirculating loop is a convenient and economic method to examine the performance for long transmission distance without actually constructing the whole setup. However, in a recirculating loop, some of the concerns in a bidirectional loop system are different from those in a unidirectional loop system. For instance, the loop time control, the setup of the bidirectional recirculating loop, the input noise in EDFA, etc.

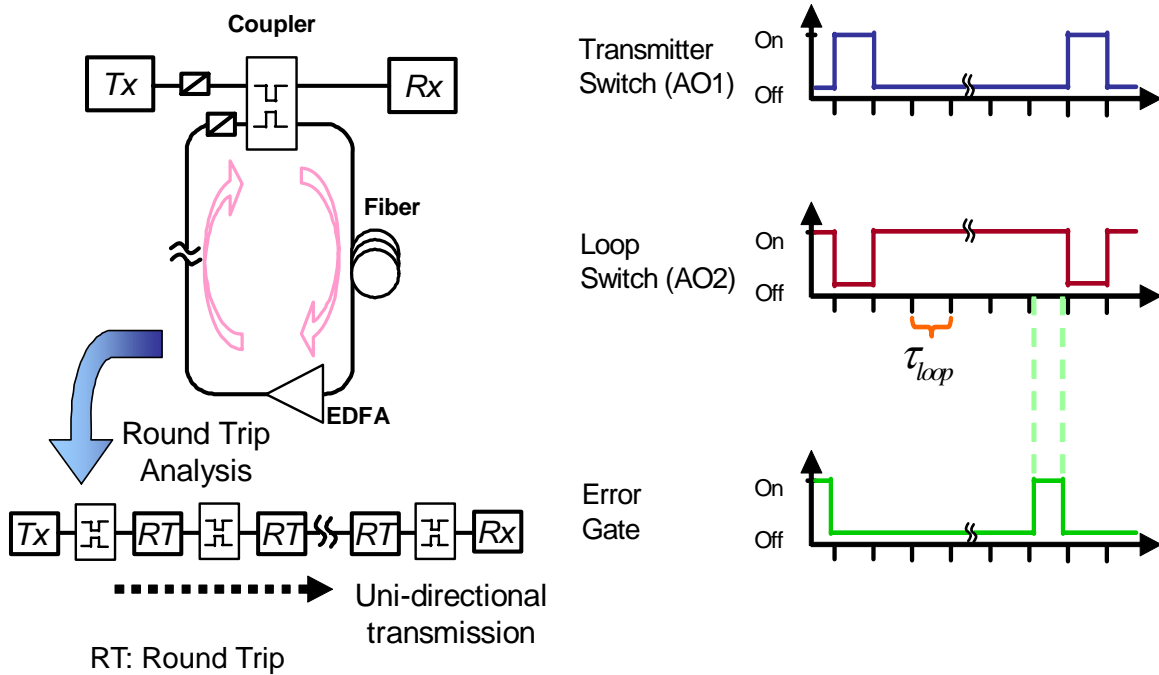
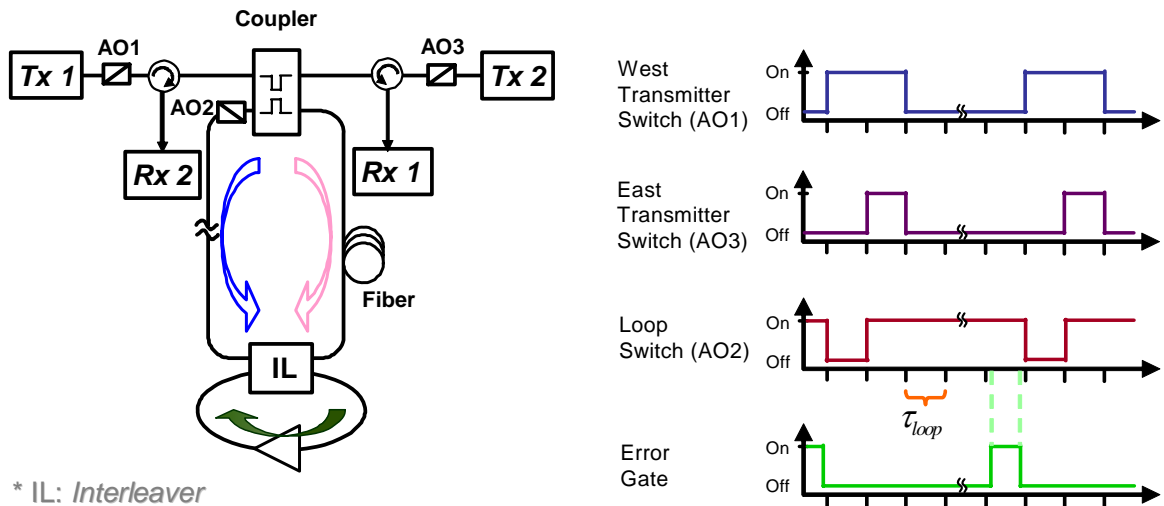


Fig. 5.1(a) Uni-directional loop and corresponding round trip analysis (b) loop time control

In the unidirectional transmission system, as long as the appropriate loop time is executed, all of the concerns are irrelevant whether in loop or straight line system. The performance of a unidirectional loop transmission is approximately the same as that of a straight line transmission, which means the recirculating loop could represent unidirectional straight line system appropriately. On the contrary, due to the lack of the adequate loop time control, it is inappropriate to demonstrate the long distance bidirectional transmission just directly applying the recirculating loop to the bidirectional system. The detail of the structure and loop time control is displayed in the following Fig. 5.2.



* IL: Interleaver

Figure 5.2. (a) Configuration of original bidirectional loop (b) Loop time control of original bidirectional loop

Fig. 5.2(a) seems to be a typical type of bidirectional loop configuration. However, while considering the timing control of such scheme, the lack of proper switching time and the unpredicted power balance issue is inevitable. All of the qualms lead to the consequence that either abandon this configuration or adjust it to be a more practicable structure.

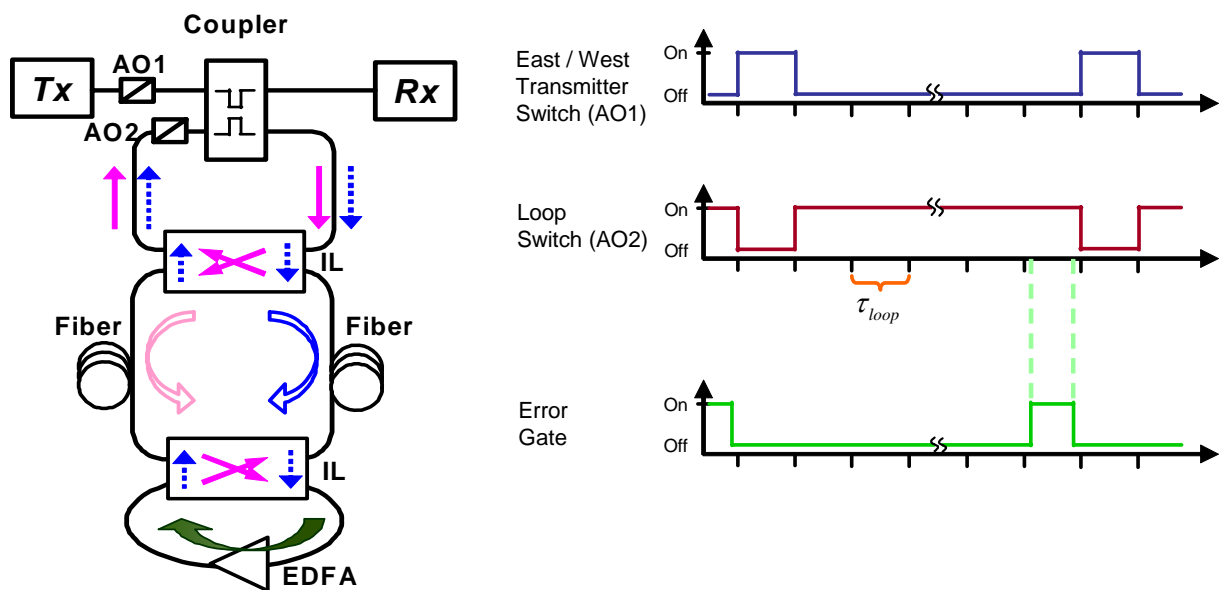


Fig. 5.3(a) adjusted bidirectional loop configuration (b) loop time control

After modifying the loop configuration, as shown in Fig. 5.3, this bidirectional loop scheme seems more achievable. However, the concerns mentioned above, mostly the setup of the bidirectional recirculating loop, the input noise in EDFA, may lead to the consequence that the conditions of a bidirectional loop are not the same as a bidirectional straight line

system. Under this consideration, is bidirectional loop still adequate to stand for bidirectional straight line transmission? The following Fig. 5.4 and Fig. 5.5 depict the differences among bidirectional loop and straight line transmission systems.

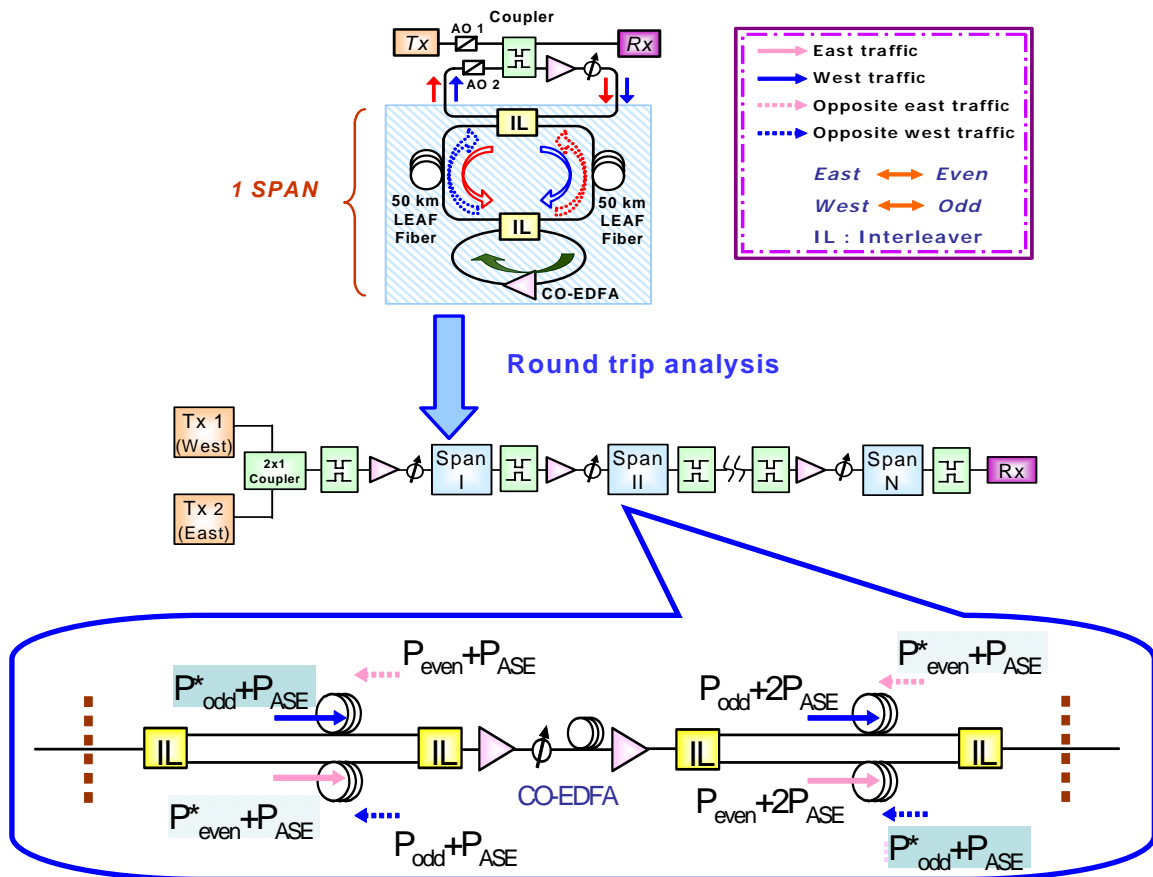


Fig. 5.4 Bidirectional Loop System

From Fig. 5.4, we observe that the “same conditioned” bidirectional traffics co-propagate in the CO-EDFA route. Furthermore, during the forward propagating traffic flow, the opposite signals in transmission fiber (50 km LEAF fiber) are the older/less noisier signals which are ahead of the present signals half of the round trip span, 50 km.

5.1.2 Analysis of bidirectional straight transmission system

As shown in Fig. 5.5, the basic architectures of loop and straight line case are dissimilar. Not only the lack of the extra boost EDFAs within transmission path, but also the traffic flows of the bidirectional signals does the “Straight Line” scheme reveal the differences between the

“Loop” configuration. To be more specific, take the bidirectional traffics input CO-EDFA at span I for example, the west-to-east (odd channel) signal are practically noiseless signals, P_{odd} , which need to be amplified in order to continue propagation, while the east-to-west (even channel) signals, $P_{\text{even}} + (n-1)P_{\text{ASE}}$, are the older and noisier that need to be amplified to complete the transmission. The opposite signals in the transmission fiber are not just older than the present signals for 50 km transmission. It usually concerns with the total transmitted length and at which part of the signal we might be interested. All in all, the conditions of the west-to-east and east-to-west signal flows for straight line case are not the exactly same as those of the loop case.

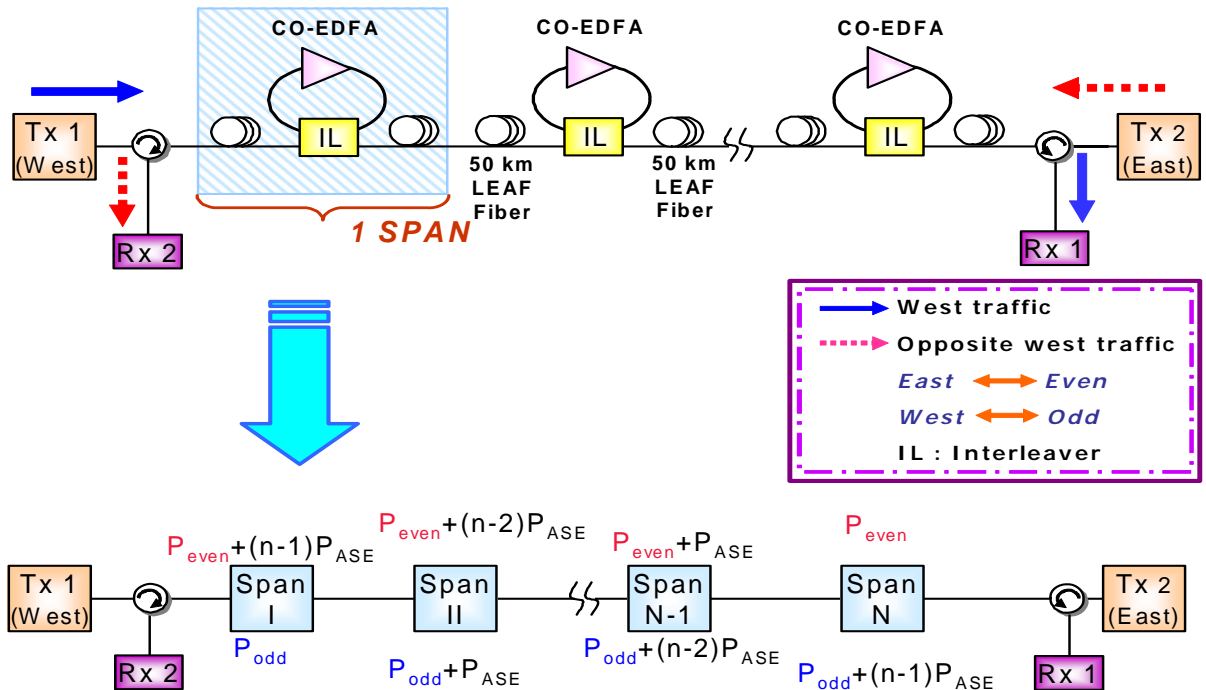


Fig. 5.5 Bidirectional Straight Line System

5.2 Simulation setup

For comparing the two bidirectional systems, straight line and loop system, we ought to build both schemes as many spans as we can. Unfortunately, the lack of the crucial devices, such as Interleavers, obstructs us for doing so. Therefore, we use the simulation tool, VPI, to

simulate both loop and straight line bidirectional transmission structures. To simulate the loop and straight line schemes, we decompose and analyze the signal path in a recirculating loop and in straight line system, separately. The detailed casual relation of bidirectional traffics will be discussed later in Fig. 5.7 ~ Fig. 5.9.

However, some preliminary conditions should we be aware of before starting to simulate and compare the two models. Due to the basic structures of bidirectional loop and straight line are not the same; some of the key factors should be held the same or approximate the same for comparing the two systems.

1. Input power before coupler and circulators, which means the total input power to the whole system.
2. Total power before dispersion compensated fiber.
3. Maxima total power in transmission fiber.

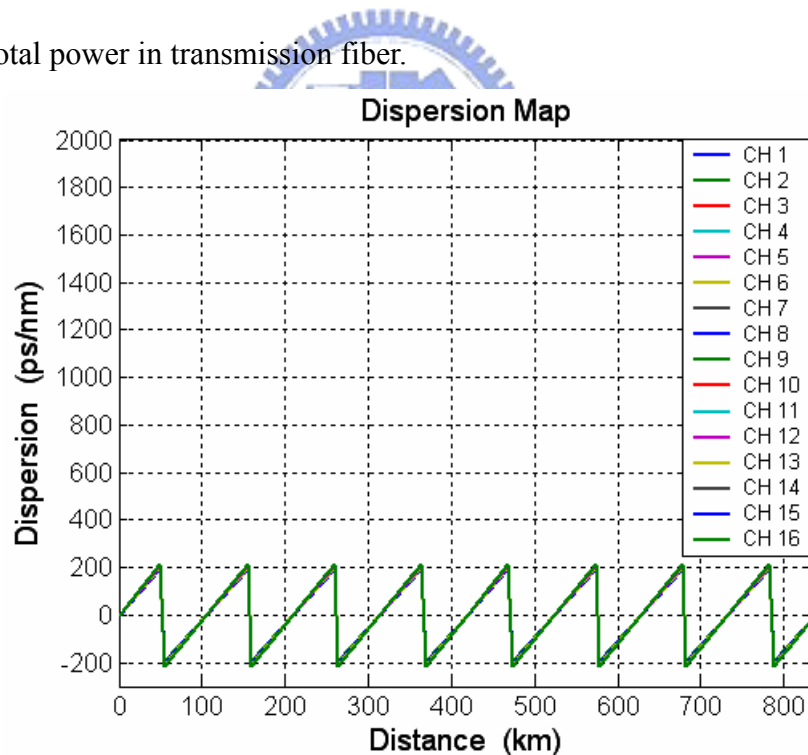


Fig. 5.6 Dispersion map used in simulation

Besides the preliminary conditions, the dispersion management should be taken into account for evaluating both schemes. Generally speaking, for a recirculating loop system, if the dispersion flattened method is not applied, as long as the transmission distance is

elongated, the accumulated chromatic dispersion would be severe in the transmission channel which center wavelength is away from compensated wavelength/frequency. On the other hand, for a straight line system, the dispersion slope and compensated wavelength/frequency vary from one to one DCF. Therefore, the accumulated chromatic dispersion in this circumstance is smoother than that in the loop structure. Nonetheless, the dispersion management is not the crucial discussion in comparing the bidirectional loop and straight line traffics, we apply the dispersion flatten method to eliminated the accumulated dispersion issue. Fig. 5.6 shows the dispersion map for sixteen channels after applying the dispersion flatten method.

5.2.1 Simulation setup of bidirectional loop system

In this simulation, we consider two types of bidirectional transmission, bidirectional transmission using a recirculating loop (bidirectional loop) and the simulated real world bidirectional transmission (the straight line transmission). The setup configuration for bidirectional loop transmission that used in our simulation is shown in Fig. 5.7. We use a four port interleaver, with insertion loss of 2.2 dB and 50/100 GHz channel spacing on standard ITU grid, and a two stage EDFA to function as a bidirectional amplified EDFA in testing the bidirectional traffics. The whole set contains an interleaver and a dual stage EDFA with appropriate length of DCF is so called a CO-EDFA, which main function is a bidirectional amplifier with high gain, low noise figure and elimination of Rayleigh Backscattering characteristics [35]. The sixteen input laser sources are grouped into two categories, west/odd traffic arranges from 1550.52 nm to 1556.15 nm and east/even traffic arranges from 1550.12 nm to 1555.75 nm, each group matches the standard ITU 50 GHz channel spacing grid. The west and east channels are individually modulated by an electro-optical (EO) modulator at 10 Gb/s with a $2^{31}-1$ PRBS pattern.

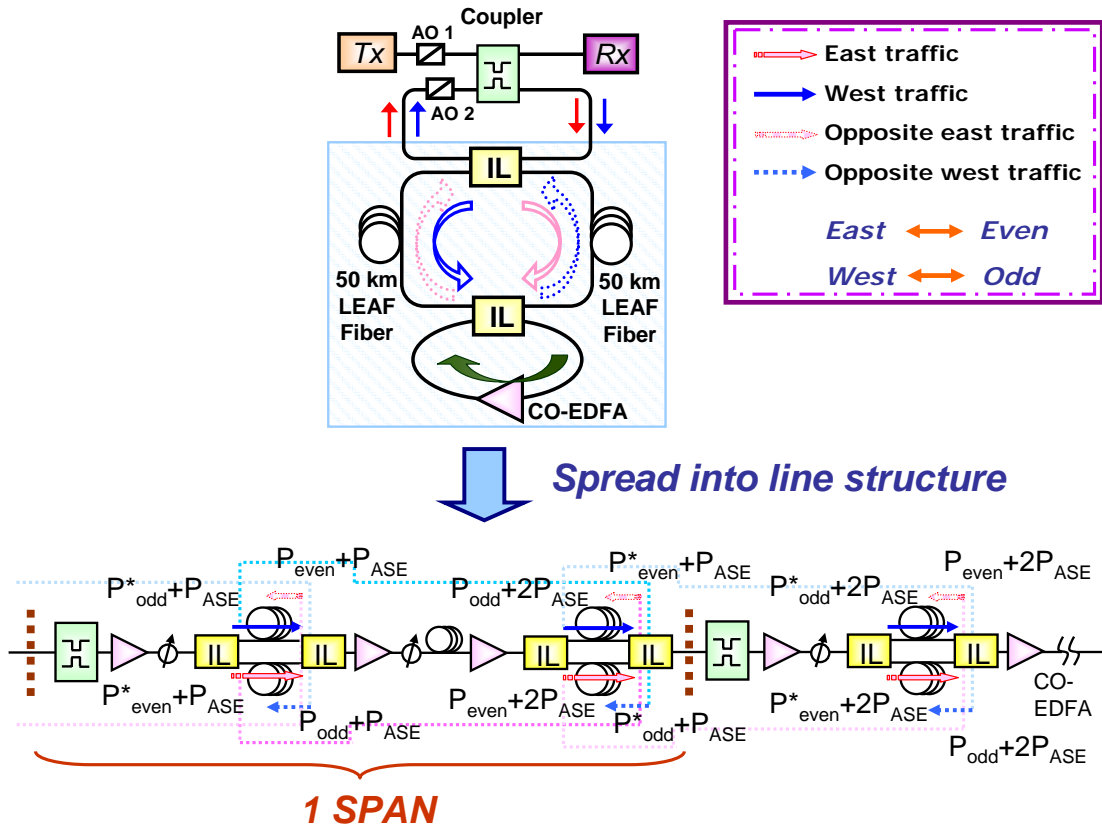


Fig. 5.7 Decomposed bidirectional loop system

The transmission consists of 8×100 -km (50 km /50 km) LEAF fiber, the detail parameters are listed in Tab.3. In the bidirectional loop scheme, with adequate route selection [35], the first Interleaver is used to separate east and west signals for bidirectional traffics; the second Interleaver is used to combine opposite direction signals into uni-directional amplification. A dual-stage EDFA and 4.6-km dispersion compensated fiber (DCF) are employed in the uni-amplification routing for compensating the transmission loss and accumulated dispersion arise from transmission (LEAF) fiber. The chromatic dispersion is assume to be fully compensated at each channel in the two cases, bidirectional loop and bidirectional straight line systems. The noise figure in each amplifier is assumed to be 5 dB. In accordance to the former bidirectional loop experiment [35], the maximum launch power input transmission fiber is +4.1 dBm, whereas the power launched into the DCF is kept low (-5.6 dBm) to avoid introducing nonlinear effects due to the highly nonlinear behavior of this type of fiber. Parameters used in bidirectional loop simulation are listed in Table 3.

Table 3. Parameters used in bidirectional loop architecture.

Number of spans	8	Fiber Length (LEAF)	100 km (50/50)
Dispersion (LEAF)	4.1639	Dispersion slope (LEAF)	0.06
Loss Coeff. (LEAF)	0.2	Nonlinear Coeff. (LEAF)	2.6e-20
Bit rate	10	Max. launch power	+4.1
Power input DCF	-5.6	Fiber Length (DCF)	4.63
Loss Coeff. (DCF)	0.6	Dispersion (DCF)	-90
Dispersion slope (DCF)	-0.06*4.1639/90	Nonlinear Coeff. (DCF)	4.0

5.2.2 Simulation setup of bidirectional straight system

The long distance bidirectional straight line configuration is illustrated in Fig. 5.8.

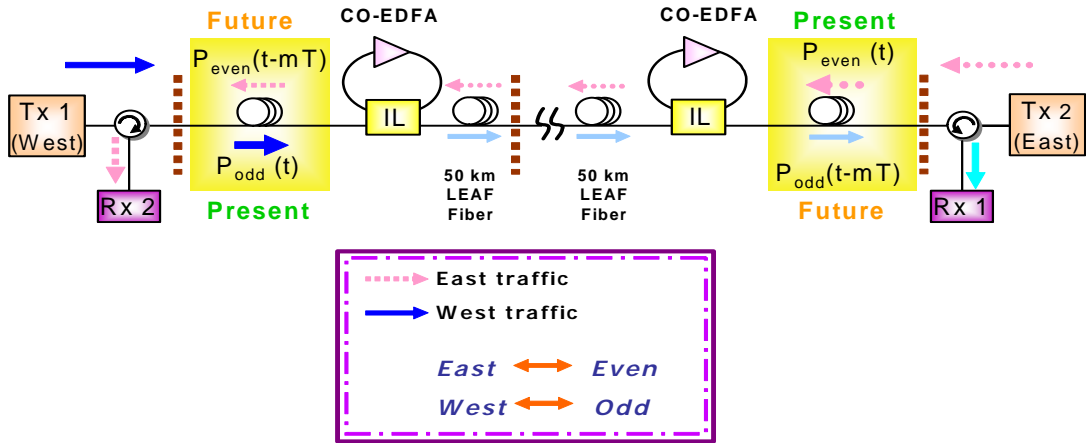


Fig. 5.8 Decomposed bidirectional straight line system

From Fig. 5.8, we observe that “west-to-east traffic” encounters monotonic decreasing amount of ASE within “east to west traffic” during the transmission process, and vice versa. However, constructing the transmission system according to Fig. 5.8 configuration is irrational due to the causal relationship between the west-to-east/east-to-west traffic flows. On the other hand, one cannot take the future incident as present information to manipulate. It’s contradictory to logical operation in our simulation tool, VPI. Therefore, three stages of preparation signals are utilized to simulate the real bidirectional transmission circumstance Fig. 5.9 shows the decomposed bidirectional straight line system as well as some tips we used in the simulation, particularly the causal relationship in the transmission flow is concerned.

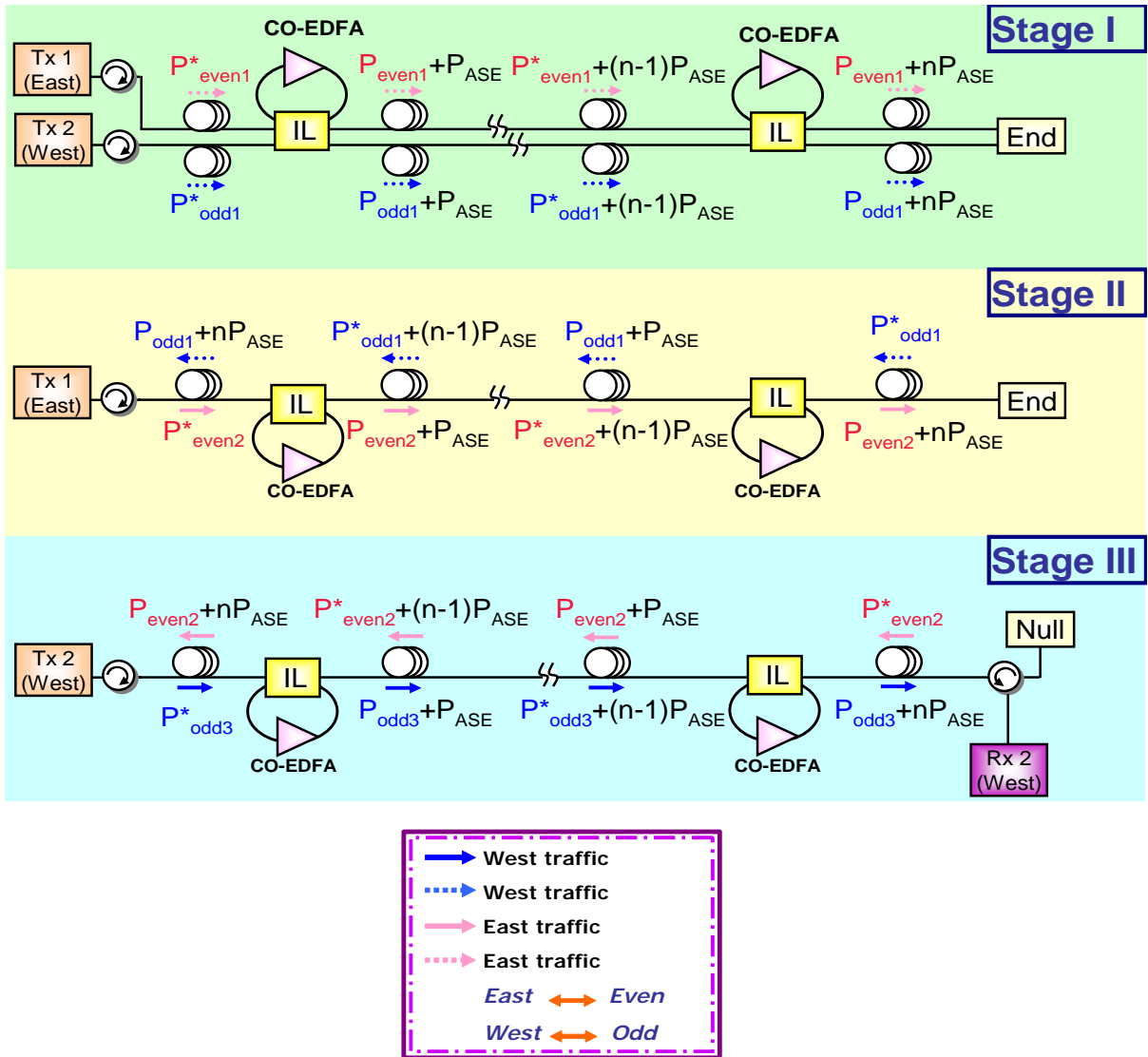


Fig. 5.9 Simulated bidirectional straight line system

The circulators at every input end are used to maintain the same input power at each stage. In stage I, unidirectional signals with different amount of noise are created, these preparation signals could be the opposite input signals for stage II. Stage II focuses on the west-to-east transmission, various opposite signals input to fiber and EDFA are considered. Stage II is a bidirectional system with actual conditions considered, nevertheless, the sources of the opposite data are not generated under bidirectional situation. To simulate the actual bidirectional transmission, not only the various opposite signals should be pondered, but also the opposite signals should be a bidirectional system suffered from different amount of noise in reverse traffic. As a result, a bidirectional transmission, stage III, which opposite signals

originate from a bidirectional system, stage II, is taken into account as a relatively literal bidirectional transmission system.

Considering the optimized setup for straight line structure for comparing with the loop scheme, the maximum launch power input transmission fiber and the power launched into DCF are +4.6 dBm and -5.1 dBm, respectively. Parameters used in simulation are listed in Table I and Table II for loop case and straight line case.

Table 4. Parameters used in bidirectional straight line architecture.

Number of spans	8	Fiber Length (LEAF)	100 km (50/50)
Dispersion (LEAF)	4.1639	Dispersion slope (LEAF)	0.06
Loss Coeff. (LEAF)	0.2	Nonlinear Coeff. (LEAF)	2.6e-20
Bit rate	10	Max. launch power	+4.6
Power input DCF	-5.1	Fiber Length (DCF)	4.63
Loss Coeff. (DCF)	0.6	Dispersion (DCF)	-90
Dispersion slope (DCF)	-0.06*4.1639/90	Nonlinear Coeff. (DCF)	4.0

5.3 Simulation results of bidirectional transmission

The simulation results of two types of bidirectional transmission systems, “Loop” and “Straight Line”, are listed below. Each of the case contains the results such as, the received optical spectrum, the BER curves and the corresponding eye diagrams at channel ten, penalties of all channels at 100-km, 200-km, 400-km, 600-km and 800-km transmission distance, respectively.

5.3.1 Case I: Bidirectional loop system

Fig. 5.10 shows the received optical spectrum after 800 km transmission and an OSNR of 30.5 dB with 0.01-nm bandwidth resolution setting is observed. The BER curves of Channel ten after different transmission distance is shown in Fig. 5.11. A more detailed penalty distribution for sixteen channels after various numbers of loops is depicted in Fig. 5.12. The penalty mean of the sixteen channels at transmitted distance 100, 200, 400, 600 and

800 km, are 0.4, 0.7, 1.5, 2.5 and 3.7-dB, respectively. The descended performance is mainly attributed to the accumulated ASE after long transmission distance.

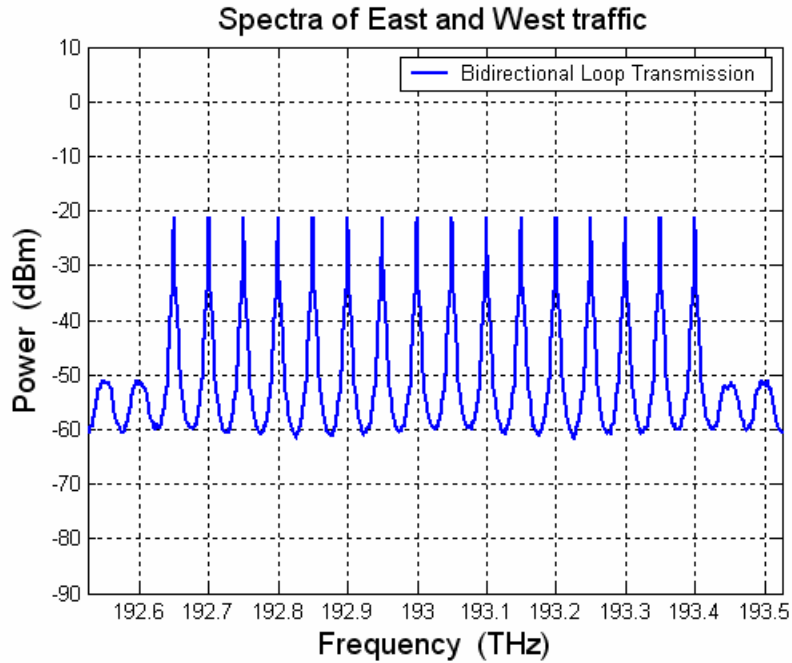


Fig. 5.10. Received optical spectrum after 800 km bidirectional loop transmission

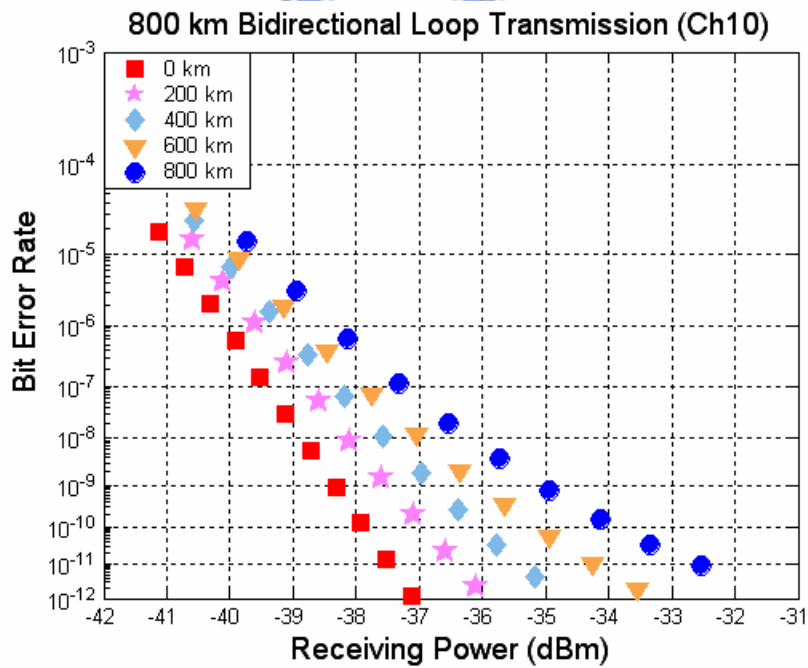


Fig. 5.11 BER curves @ ch.10 after 0, 200, 400, 600 and 800-km bidirectional loop transmission

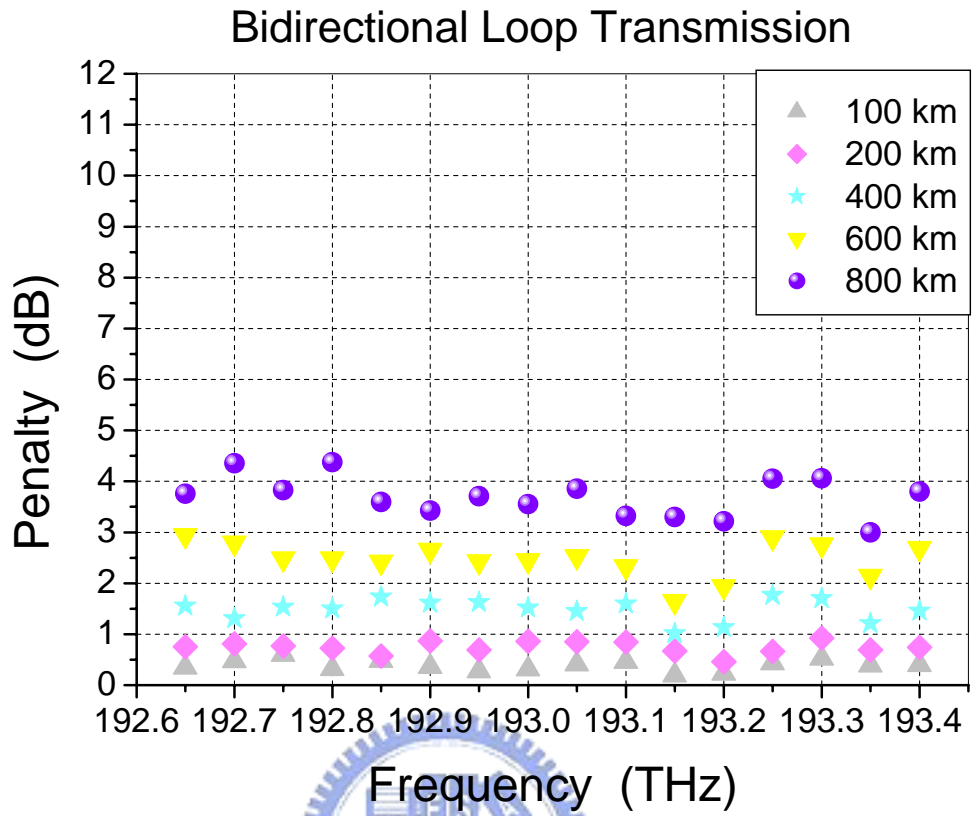
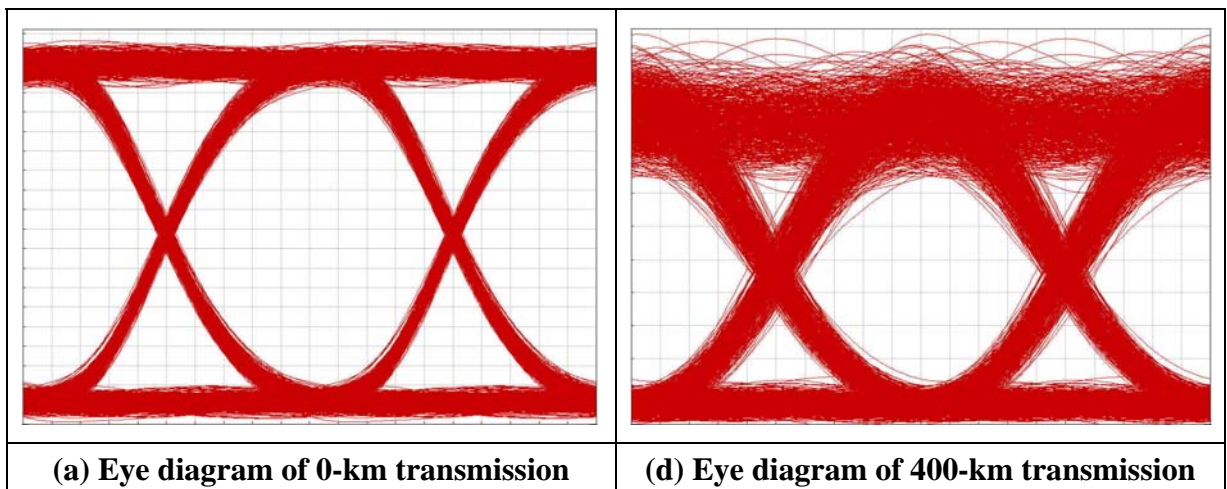
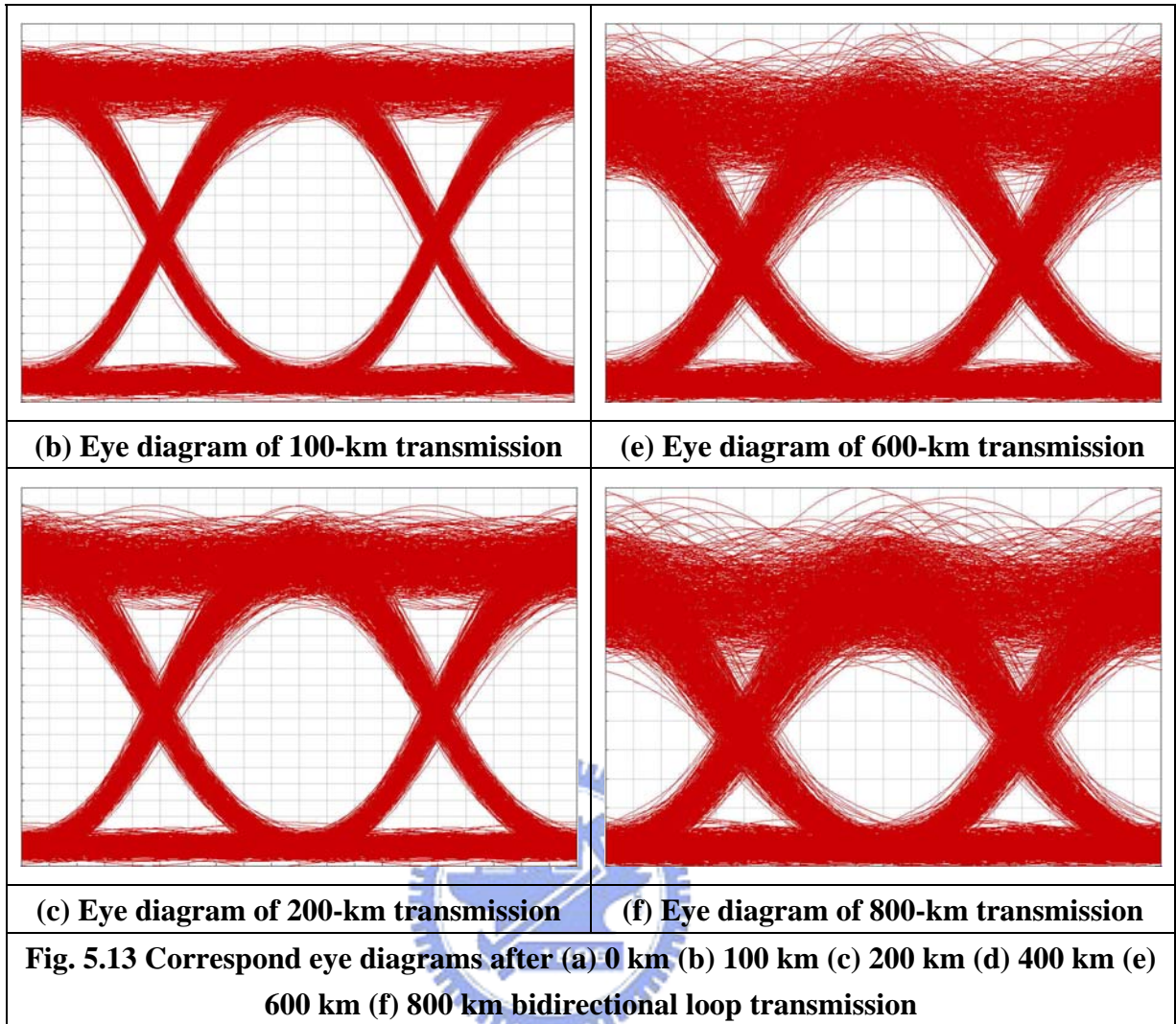


Fig. 5.12. Power penalty distribution of bidirectional loop transmission

Fig. 5.13 (a) ~ (f) demonstrates the corresponding eye diagrams after 0, 1, 2, 4, 6 and 8 loops of bidirectional transmission.





5.3.2 Case II: Bidirectional straight line system

In Fig. 5.14, the optical spectrum after 800 km transmission with an OSNR of 29.5 dB, which bandwidth resolution sets on 0.01-nm, is observed. Fig. 5.15 plots the BER curves at channel ten after different bidirectional traffic length. The detailed power penalty distribution for sixteen channels after several numbers of spans is illustrated in Fig. 5.16. The mean of receiving penalties for sixteen channels at 100, 200, 400, 600 and 800 km transmission length are 0.4, 0.8, 2.1, 4.1 and 7.1-dB, respectively. The performance degradation is due to the accumulated ASE increasing rapidly as long as the transmission distance is extended.

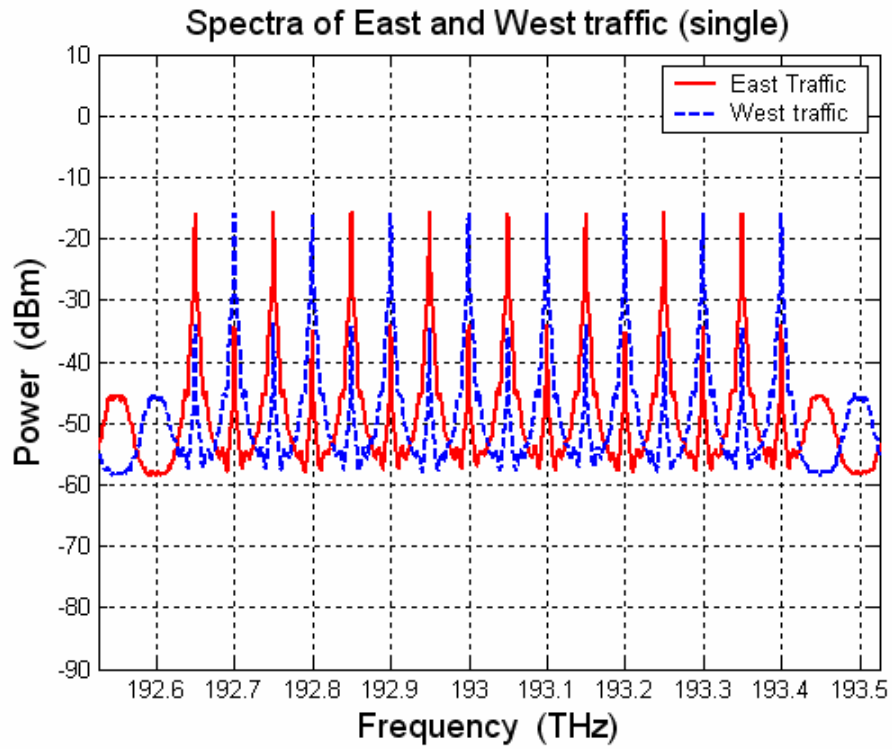


Fig. 5.14. Received optical spectrum after 800 km bidirectional transmission (straight line)

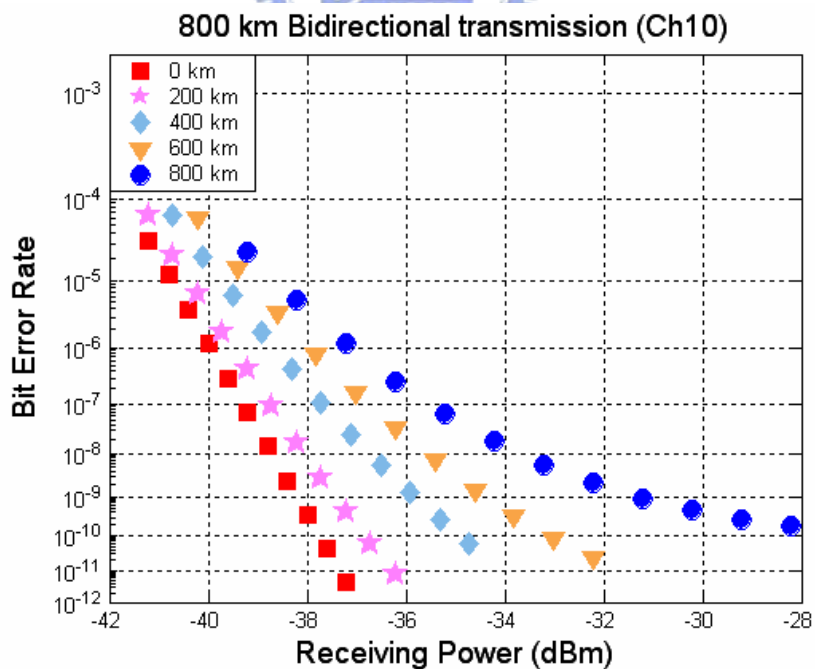


Fig. 5.15 BER curves @ ch.10 after 0, 200, 400, 600 and 800-km bidirectional transmission (straight line)

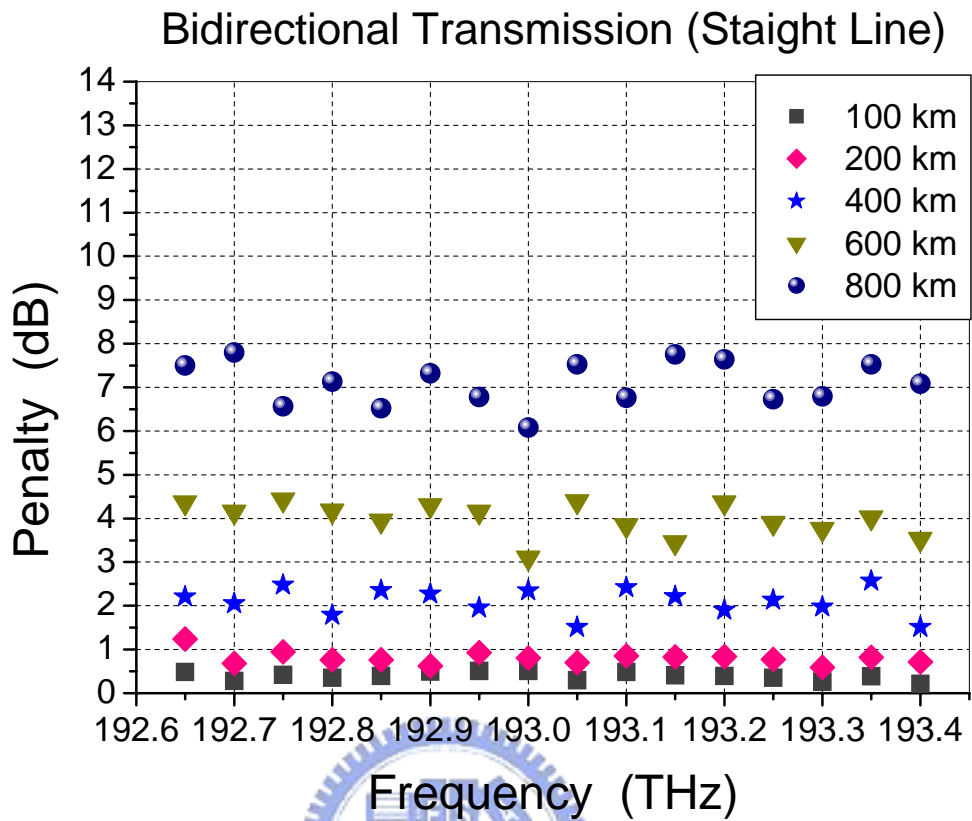
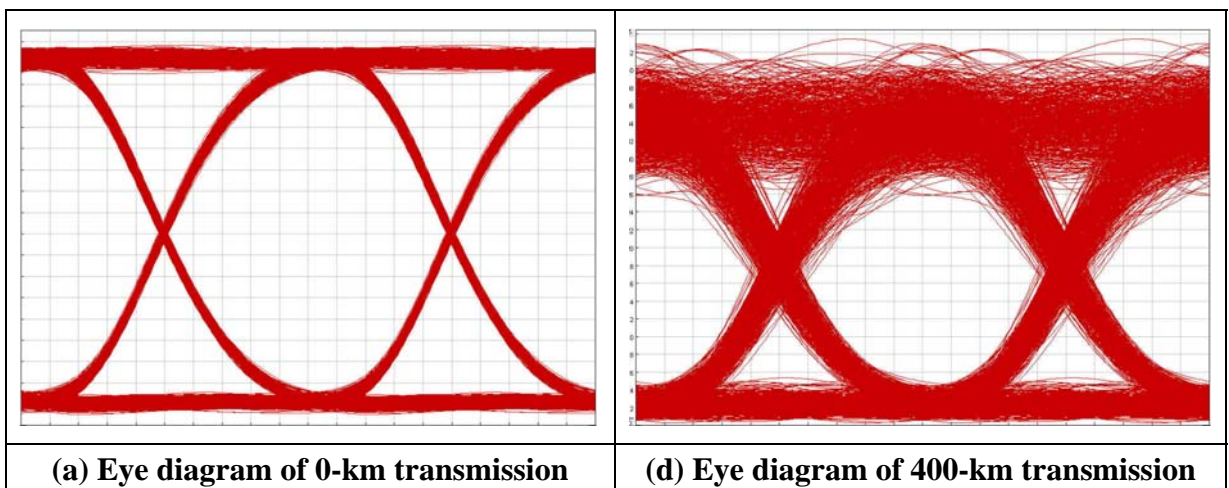
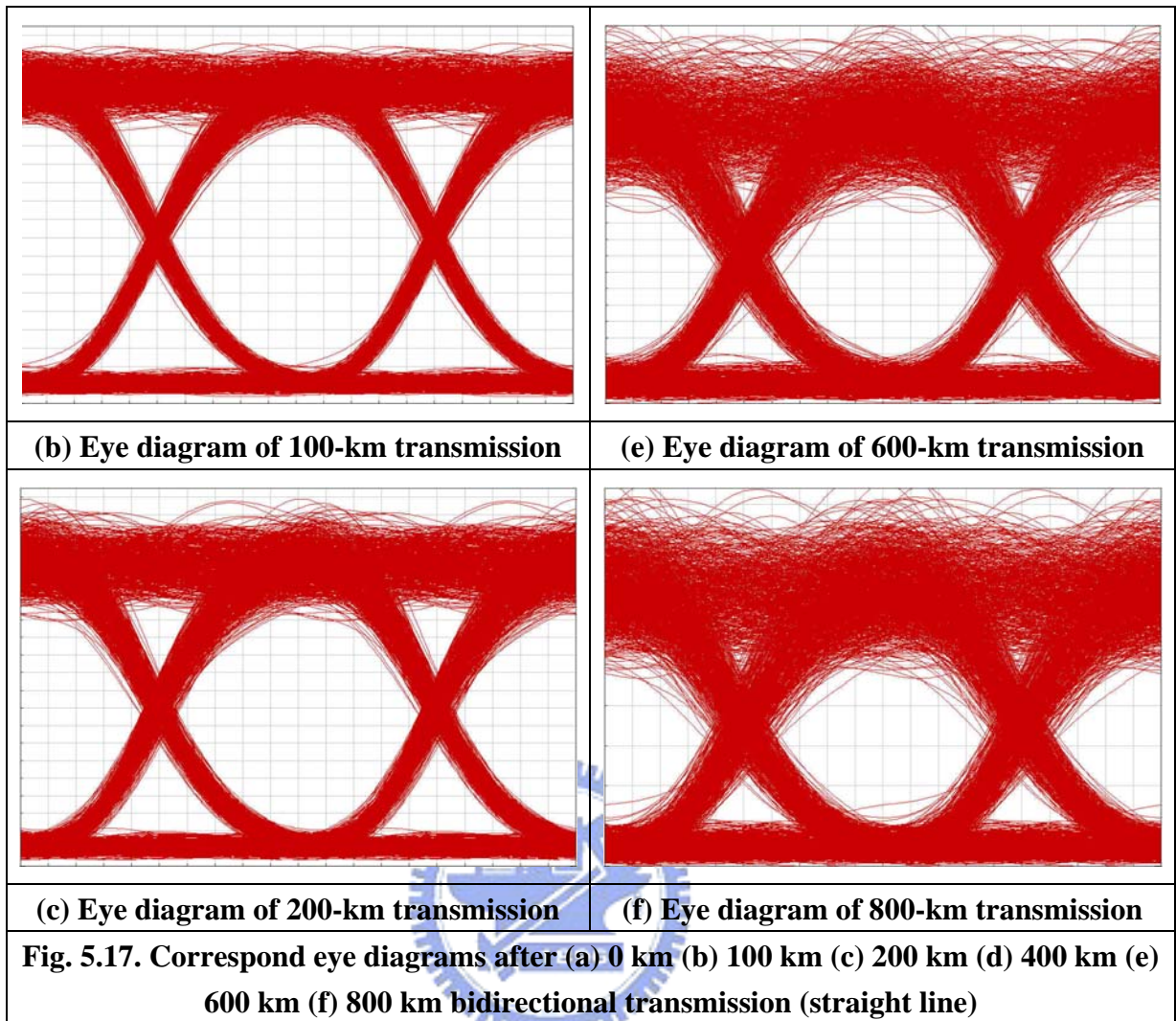


Fig. 5.16 Power penalty distribution of bidirectional transmission (straight line)

Fig. 5.17(a) ~ (f) shows the corresponding eye diagrams after 0, 100, 200, 400, 600 and 800-km of bidirectional transmission.





5.3.3 Comparison of the “Loop” and “Straight Line” cases

Fig. 5.18 shows the BER and corresponding eye diagrams after 0 km and 800 km transmission distance for both cases. Furthermore, a more detail power penalty comparison is exhibited in Fig. 5.19. From simulation results, we obtained the penalty after 800 km bidirectional transmission of “loop” and “straight line” cases are 3.7 dB and 7.1 dB, respectively. The average penalties are represented by symbols and the fitting curves for the two cases are displayed as well. Clearly, from Fig. 5.18, the fitting curve for loop case is a 1st order polynomial function while fitting curve for straight line case is a 2nd order polynomial function. The results manifest that the power penalty difference between the two cases increases along with the transmission distance.

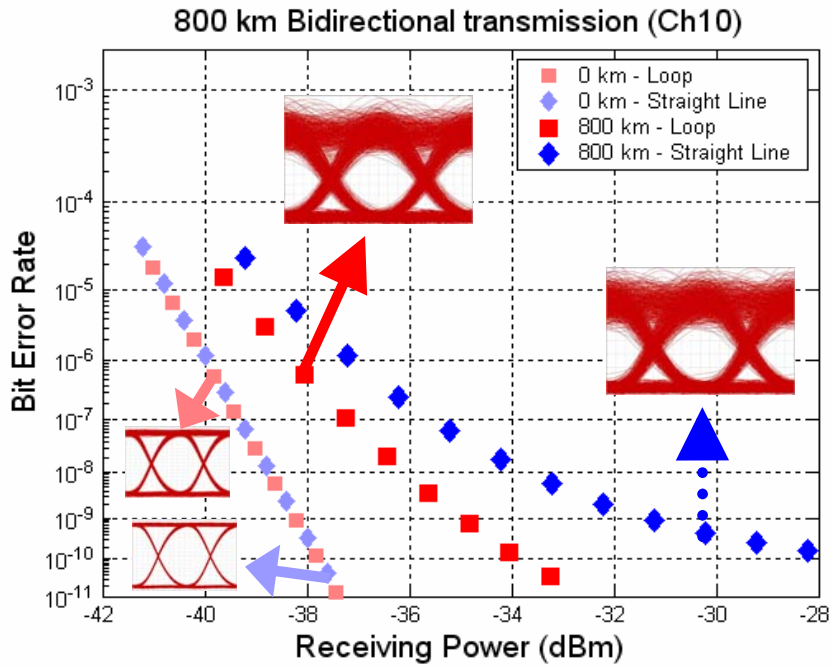


Fig. 5.18 BER curves and corresponding eye diagrams @ ch.10 for “Loop” and “Straight Line” cases after 0 km and 800 km bidirectional transmission.

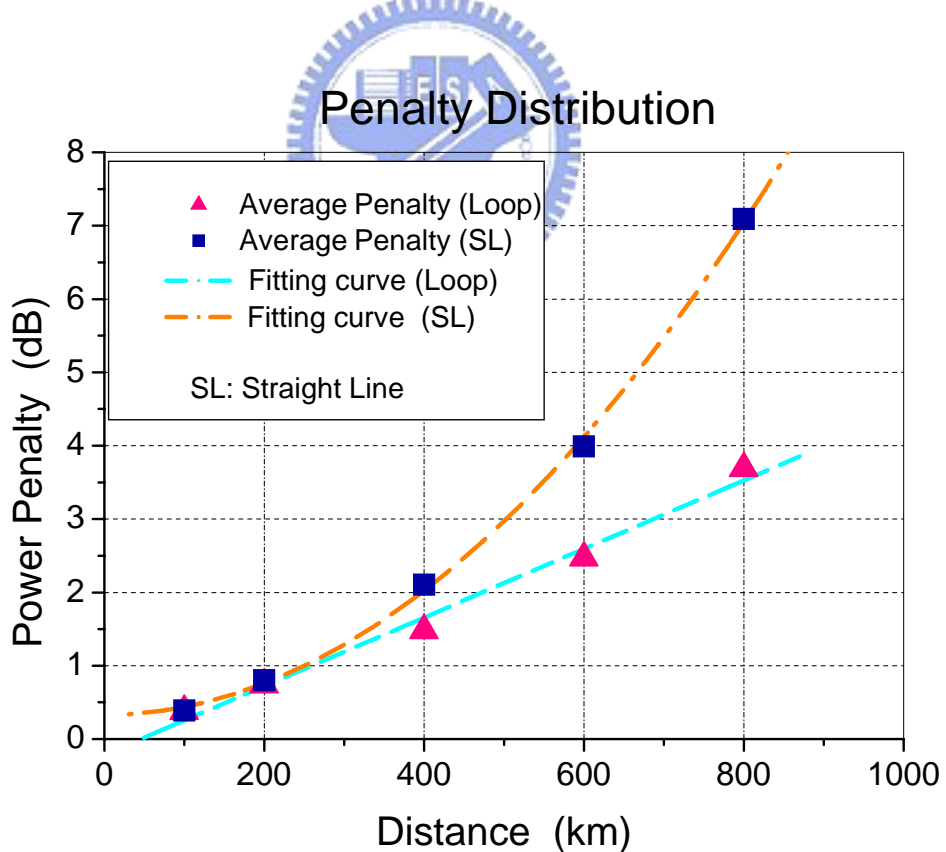


Fig. 5.19. Penalty distribution for “Loop” and “Straight Line” cases.

Nonetheless, due to the different times of passing through interleavers in one round trip, the “loop” case suffers bandwidth narrowing effect more severe than “straight line” case does. In the following simulation, we will simulate an adjusted straight line case that includes the severe bandwidth narrowing effect which we called the “modified straight line” configuration.

5.4 Simulation of modified straight line transmission

The scheme of modified straight line transmission is shown in Fig.5.20 All of the parameters and entire configuration remain the same as in the straight line setup except it includes the same bandwidth narrowing effect as the loop setup does. This concept is achievable with the use of two extra interleavers at the input and output port of co-propagating EDFA. Furthermore, the insertion loss of the extra passed Interleaver is set to zero in order to isolate the narrowing effect from straight line configuration without affecting the optimized system condition.

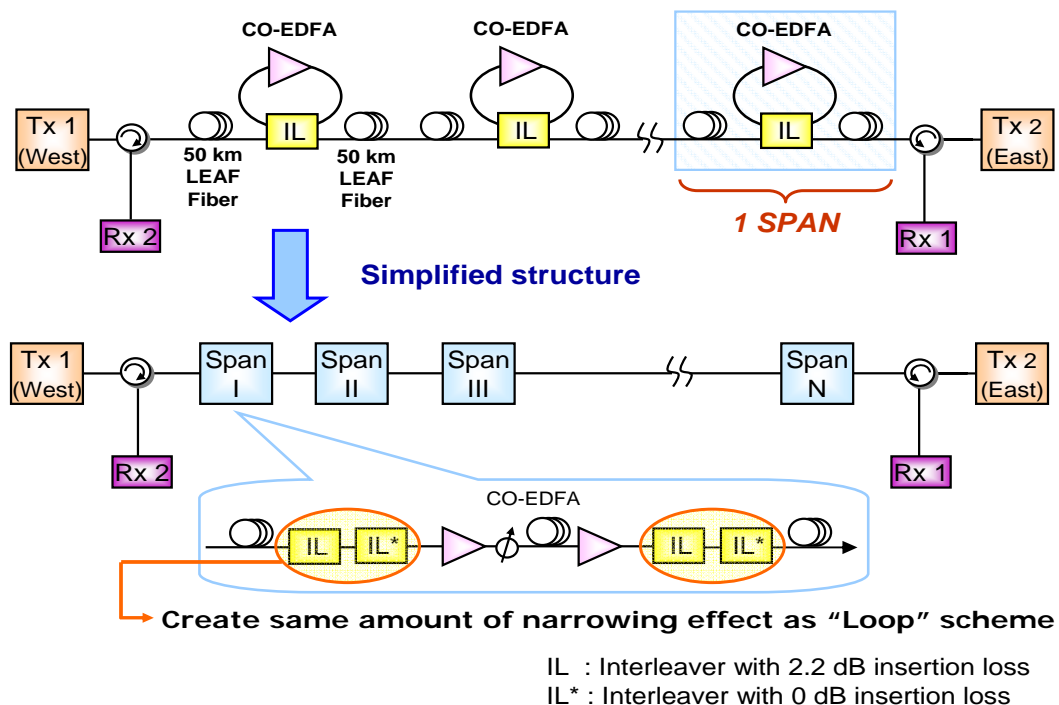


Fig. 5.20 Modified Bidirectional Straight Line System

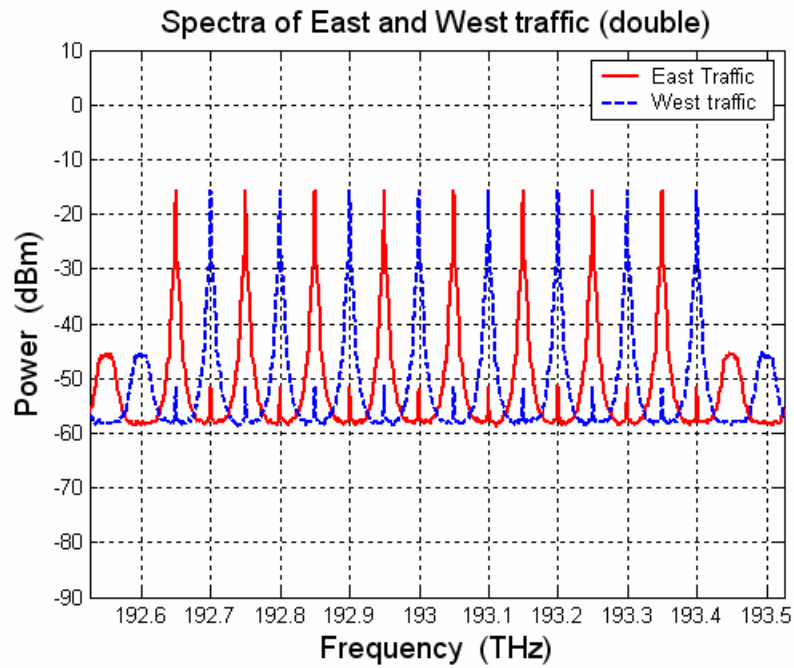


Fig. 5.21. Received optical spectrum after 800 km bidirectional transmission (modified straight line)

After 800 km transmission based on the modified model, the received optical spectrum with an OSNR around 29.5 dB under resolution bandwidth of 0.01-nm is displayed in Fig.5.21. Fig. 5.22 plots the BER curves and corresponding eye diagrams at channel ten after 0, 200, 400, 600 and 800-km transmission length. Fig. 5.23 demonstrates the detailed penalty distribution of every channel after different distance. The average power penalties of all sixteen channels after 100, 200, 400, 600 and 800 km transmission are 0.4, 0.7, 1.9, 3.6 and 6.5-dB, respectively.

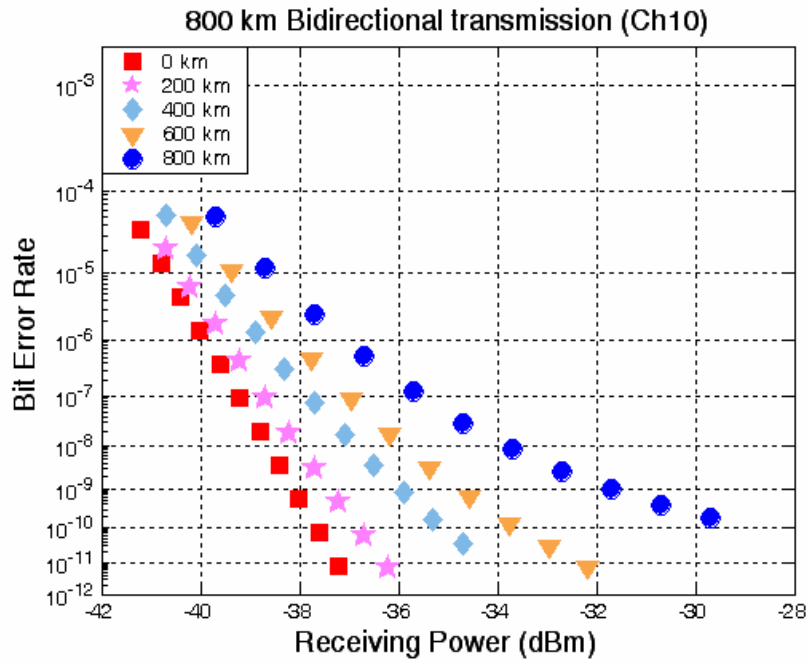


Fig. 5.22 BER curves @ ch.10 after 0, 200, 400, 600 and 800-km bidirectional transmission (modified straight line)

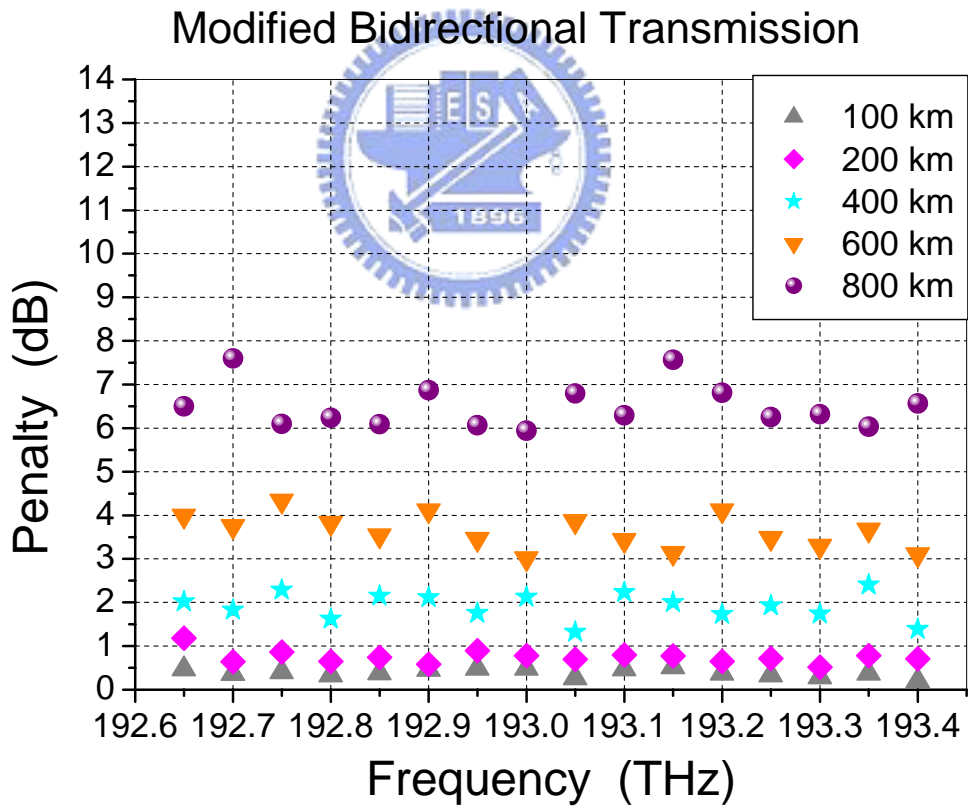
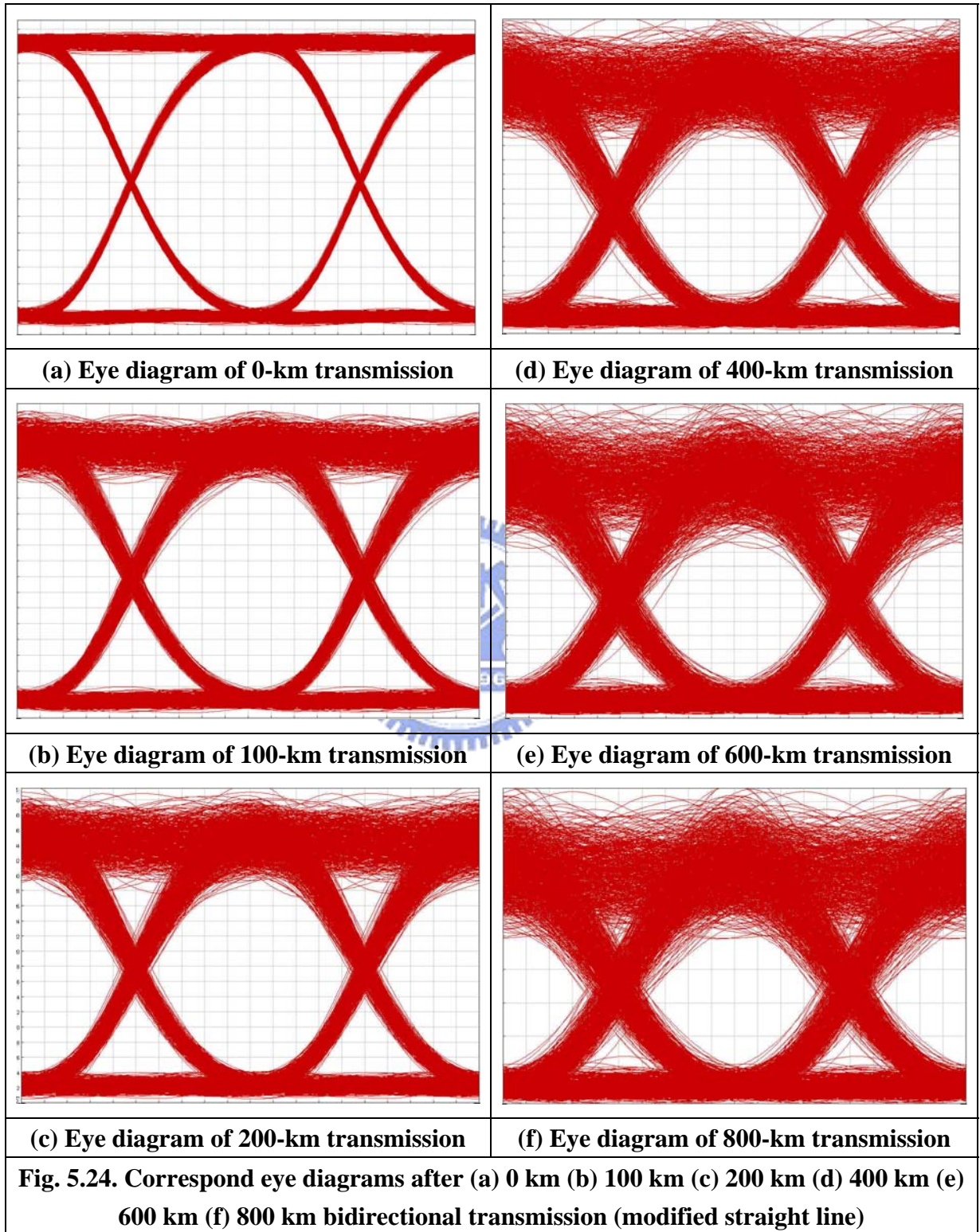


Fig. 5.23 Power penalty distribution of bidirectional transmission (modified straight line)

Fig. 5.24 (a) ~ (f) shows the corresponding eye diagrams after 0, 100, 200, 400, 600 and 800-km of bidirectional transmission.



5.5 Discussion

The comparisons of the three cases are shown as follows. Fig. 5.25 illustrates the BER curves and the corresponding eye diagrams of back to back and 800-km transmission for each case at channel ten.

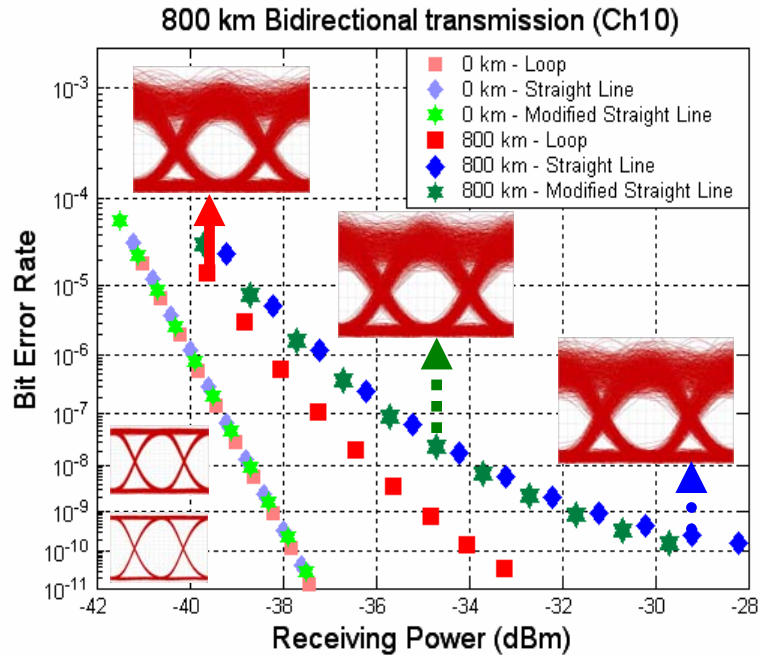


Fig. 5.25 BER curves and corresponding eyes @ ch.10 for case “Loop”, “Straight Line” and “Modified Straight Line”

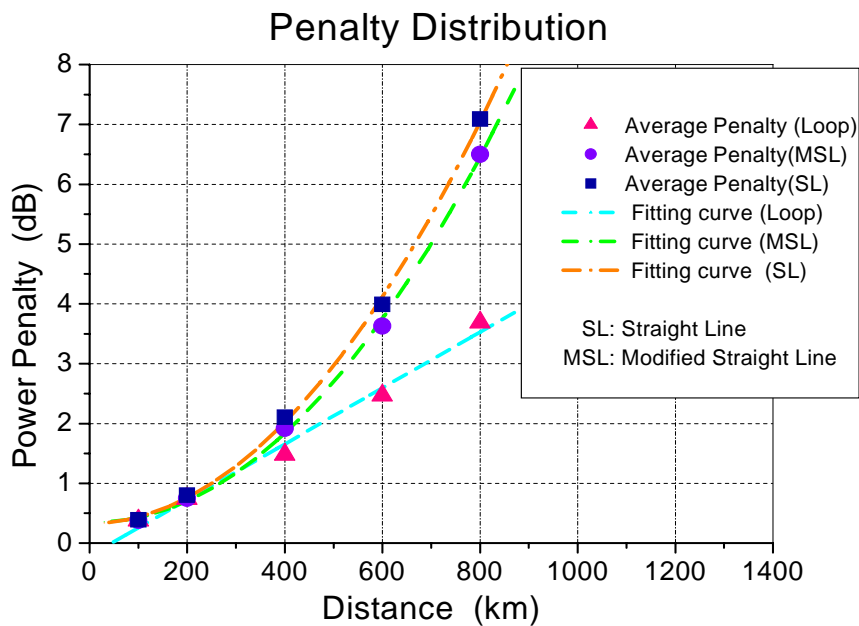


Fig. 5.26 Penalty distribution for case “Loop”, “Straight Line” and “Modified Straight Line”

Fig. 5.26 demonstrates a more generic view of the penalty distribution for three types of bidirectional transmission. The mean penalties for loop, straight line and modified straight line case after transmitted 800-km are 3.7, 7.1 and 6.5 dB, respectively.

According to Fig. 5.25 and 5.26, the simulation results for straight line case and the modified straight line case are practically the same. This simulation results reveal that the longer the bidirectional transmission distance is extended, the more obvious differences between the loop and the straight line case. Not only the received optical spectrum but also the BER curves and the corresponding eyes reveal the straight line case undergoes more accumulated ASE. Therefore, when it comes to evaluate the long distance bidirectional traffic, it may be optimistic to estimate the performance of bidirectional transmission using a re-circulating loop to represent the real bidirectional traffic circumstances.



Chapter 6

Conclusions

We proposed a novel 50 GHz interleaved bidirectional architecture that implements bidirectional amplification using a unidirectional amplification re-routing method. By utilizing such bidirectional amplification technique, we experimentally demonstrated two bidirectional systems: straight line structure and re-circulating loop structure. After two bidirectional experiments, we inspired from the experimental results that bidirectional straight line scheme may not be replaced by bidirectional loop architecture. Finally, with the help of VPI (i.e., an optical simulation software), we simulated the two structures, loop, straight line and even a modified structure of bidirectional straight line scheme, and then compared the simulation results in each case.

In our bidirectional transmission experiments, we first construct a straight line configuration; afterwards, in the second experiment, we build up a re-circulating loop system. By utilizing the complementary wavelength re-routing scheme with a unidirectional amplification routing, the 4-port interleaver enables bidirectional transmission. According to such interleaver-based bidirectional amplifier, we not only benefit from its high gain performance, but also enable its blocking the Rayleigh backscattering. The performance evaluations, measured by system power penalty, of two bidirectional systems, are illustrated in Table 2.

Table 2. Power penalty of bidirectional transmission experiments

Configuration Distance	Straight Line	Loop
100 km	-	0.4 dB
160 km	0.8 dB	-
210 km	1.4 dB	-
300 km	-	1.1 dB
500 km	-	2.1 dB

The discrepancy results show that power penalty of 1.1 dB after 300 km transmission in “Loop” configuration; whereas the penalty after 210 km of straight line scheme is 1.4 dB. The results indicate the dissimilarity between the loop and straight line configurations.

Finally, inspired by the experimental results, we use VPI to simulate two kinds of bidirectional transmission structures -- the “Loop”, and the “Straight Line”. Besides, we also simulated the “Modified Straight Line” configuration, a straight line structure includes the same bandwidth narrowing effect, much like the “Loop” case does. Simulation results of the three cases are listed below; moreover, the experimental results are displayed as well:

Table 5. Simulation and experimental results

Configuration / Distance	Loop	SL	MSL	Exp. SL	Exp. Loop
100 km	0.4 dB	0.4 dB	0.4 dB	-	0.4 dB
200 km	0.7dB	0.8dB	0.7dB	1.4 dB	-
300 km	-	-	-	-	1.1 dB
400 km	1.5 dB	2.1 dB	1.9 dB	-	-
500 km	-	-	-	-	2.1 dB
600 km	2.5 dB	3.9 dB	3.6 dB	-	-
800 km	3.7 dB	7.1 dB	6.5 dB	-	-

According to the above experimental and simulation results, we could come to the conclusion that at short distance bidirectional transmission, either “loop” or “straight line” configuration is appropriate to estimate the performance of bidirectional system. However, if the transmission distance increases, such as 800 km or longer distance, it is over-optimistic to estimate long distance bi-directional transmission performance using a re-circulating loop.

REFERENCE

- [1] C. H. Kim, Chang-Hee Lee, and Y. C. Chung, "Bidirectional WDM Self-Healing Ring Network Based on Simple Bidirectional Add/Drop Amplifier Modules," *IEEE Photon. Technol. Lett.*, Vol. 10, pp. 1340–1342, 1998.
- [2] Ko, S. Kim, J. Lee, S. Won, Y. S. Kim and J. Jeong, "Estimation of Performance Degradation of Bidirectional WDM Transmission Systems Due to Rayleigh Backscattering and ASE Noises Using Numerical and Analytical Models," *Journal of Lightwave Technology*, Vol. 21, pp.938–946, 2003.
- [3] J. L. Gimlett, M. Z. Iqbal, L. Curtis, N. K. Cheung, A. Righetti, F. Fontana, and G. Grasso, "Impact of multiple reflection noise in Gbit/s lightwave systems with optical fiber amplifiers," *Electron. Lett.*, vol. 25, pp. 1393–1394, Sept. 1989.
- [4] S. Radic, S. Chandrasekhar, A. Srivastava, H. Kim, L. Nelson, S. Liang, K. Tai, and N. Copner, "25 GHz interleaved bidirectional transmission over nonzero dispersion shifted fiber," in *Proc. OFC 2001*, Anaheim, CA, 2001, Paper ThF7-1.
- [5] L. D. Garrett, M. H. Eiselt, J. M. Wiesenfeld, M. R. Young and R. W. Tkach, "Bidirectional ULH Transmission of 160 Gb/s Full-Duplex Capacity over 5000 km in a Fully Bidirectional Recirculating Loop", *IEEE Photon. Technol. Lett.*, Vol. 16, pp. 1757–1759, 2004.
- [6] S. Cao, J. Chen, J. N. Damask, C. R. Doerr, L. Guiziou, G. Harvey, Y. Hibino, S. Suzuki, K.-Y. Wu, P. Xie, "Interleaver Technology: Comparisons and Applications Requirments," *Journal of Lightwave Technology*, Vol. 22, Issue 1, Jan 2004.
- [7] Benjamin B. Dingel, "Properies of a Novel Noncascaded Type, Easy-to-Design, Ripple-Free Optical Bandpass Filter," *Journal of Lightwave Technology*, Vol. 19, No. 8. August 1999.
- [8] A. V. Oppenheim, et al., "*Discrete-Time Signal Processing*," 2nd ed., Prentice Hall, 1999.

- [9] Christi. K. Madsen, Jian H. Zhao, et al., “*Optical Filter Design and Analysis: A Signal Processing Approach*,” John Wiley & Sons, Inc. 2003.
- [10] A. Oppenheim and R. Schaffer, “*Digital Signal Processing*,” 2nd. Ed., Englewood, N.J.: Prentice-Hall, Inc., 1975.
- [11] Hermann A. Haus, et al., “*Waves and Fields in Optoelectronics*,” Prentice-Hall, 1984.
- [12] A. Yariv, P. Yeh, “*Optical Waves in Crystals*,” Wiley-Interscience, 2003.
- [13] J. Chen, “Dispersion-compensating optical digital filters for 40-Gb/s metro add-drop applications,” *IEEE Photon. Tech. Lett.*, Vol. 16, pp.1310–1312, 2004
- [14] Gordon E. Carlson, “*Signal and Linear System Analysis*,” John Wiley, 1998.
- [15] S. Seikai, S. Shimokado, K. Kusunoki, “Novel optical circuit suitable for wavelength division bidirectional amplification,” *Electronics Letters*, vol.29, no.14, pp.1268-1270, 1993.
- [16] S. Seikai, S. Shimokado, K. Kusunoki, “2.4-Gbit/s-signal bidirectional WDM amplification by an Er³⁺-doped fiber amplifier,” OFC/IOOC’93, paper TuI4, pp.39-40, 1993.
- [17] C.W. Barnard, J. Chrostowski, M. Kavehard, “Bidirectional fiber amplifiers,” *IEEE Photon. Tech. Lett.*, Vol. 4, no. 8, pp.911-913, 1992.
- [18] J. Farre, E. Bodtker, G. Jacobsen, K.E. Stubkjar, “Design of bidirectional communication systems with optical amplifiers,” *IEEE Photon. Tech. Lett.*, Vol. 4, no. 4, pp.425–427, 1993.
- [19] Y.H. Cheng, N. Kagi, A. Oyobe, K. Nakamura, “622 Mb/s, 144 km transmission using a bidirectional fiber amplifier repeater,” *IEEE Photon. Tech. Lett.*, Vol. 5, no. 3, pp.356-358, 1993.
- [20] R.W. Boyd, “*Nonlinear Optics*,” Academic Press, San Diego, CA, 1992.
- [21] H. S. Chung, J. S. Han, S. H. Chang and H. J. Lee, “Bidirectional Transmissions of 32 Channels 10 Gb/s Over Metropolitan Networks Using Linear Optical Amplifiers,” *IEEE Photon. Technol. Lett.*, Vol. 16, pp. 1194–1196, 2004.
- [22] S.-K. Liaw, K.-P. Ho, C. Lin, and S. Chi, “Multichannel bidirectional transmission using

a WDM MUX/DMUX pair and unidirectional in-line amplifiers,” *IEEE Photon. Technol. Lett.*, Vol. 9, pp. 1664–1666, Dec., 1997.

[23] M. Oskar van Deventer, Jos J. G. M van der Tol and Andrk J. Boot, “Power Penalties Due to Brillouin and Rayleigh Scattering in a Bidirectional Coherent Transmission System,” *IEEE Photon. Technol. Lett.*, Vol. 6, No. 2, February 1994

[24] Jang-won Park and Chang-Hee Lee, “Wavelength interleaved bidirectional add/drop amplifier module,” *IEEE Photon. Technol. Lett.*, Vol. 12, No. 2, February 2002.

[25] Seung-Tak Lee and Chang-Joon Chae, “Low-Cost Bidirectional Optical Amplifier Using a Unidirectional Er-Doped Fiber Amplifier and a Fiber Mach–Zehnder Interferometer”, *IEEE Photon. Technol. Lett.*, Vol. 13, No. 1, January 2001.

[26] Bergano, N. S, C. R. Davidson, “Circulating Loop Experiments for the Study of Long-Haul Transmission Systems Using Erbium-Doped Fiber Amplifiers,” *Journal of Lightwave Technology*, Vol. 13, No. 5, May 1995

[27] Bergano, N. S., F. W. Kerfoot, and C. R. Davidson, “Margin Measurements in Optical Amplifier Systems,” *IEEE Photon. Technol. Lett.*, Vol. 5, No 3, March 1993.

[28] Application Note of Anritsu MP1764A 12.5 Ghz Error Detector

[29] Masataka Nakazawa, “Solitons for Breaking Barriers to Terabit/Second WDM and OTDM Transmission in the Next Millennium,” *IEEE Journal of Selected Topics in Quantum Electronics*, Vol. 6, No. 6, November/December 2000.

[30] P. C. Becker and N. A. Olsson, “*Erbium-Doped Fiber Amplifiers Fundamentals and Technology*,” New York: Academic, 1999.

[31] M.F Huang, J. Chen, K.M. Feng, C.C. Wei, C.Y. Lai, T.Y. Lin and S. Chi, “210-km Bidirectional Transmission System With a Novel Four-Port Interleaver to Facilitate Unidirectional Amplification,” *IEEE Photon. Tech. Lett.*, Vol. 18, pp.172–174, 2006.

[32] K.M. Feng, M.F. Huang, C.C. Wei, C.Y. Lai, T.Y. Lin, J. Chen, and S. Chi, “Metro Add–Drop Network Applications of Cascaded Dispersion-Compensated Interleaver Pairs

Using a Recirculating Loop,” *IEEE Photon. Tech. Lett.*, Vol. 17, pp.1349–1351, 2005.

[33] S. Radic, S. Chandrasekhar, A. Srivastava, H. Kim, L. Nelson, S. Liang, K. Tai, and N. Copner, “Dense Interleaved Bidirectional Transmission over 5×80 Km of Nonzero Dispersion-Shifted Fiber,” *IEEE Photon. Technol. Lett.*, Vol. 14, pp. 218–220, 2002.

[34] A. H. Gnauck, S. Chandrasekhar, A. R. Chraplyvy, “Stroboscopic BER Effects in Recirculating-Loop Optical Transmission Experiments,” *IEEE Photon. Tech. Lett.*, Vol. 17, pp.1974–1976, June 2005.

[35] Ming-Fang Huang; Kai-Ming Feng; Chen, J.; Tse-Yu Lin; Chia-Chien Wei; Sien Chi,, “Wavelength-interleaving bidirectional transmission system using unidirectional amplification in a 5/spl times/100 km recirculating loop,” *IEEE Photon. Tech. Lett.*, Vol 18, Issue 12, pp. 1326-1328, June 2006.

